UNIVERSITY OF CALIFORNIA,
IRVINE

Circuit Dynamics of Emotional Processing: Insights from Human Intracranial Recordings

DISSERTATION

submitted in partial satisfaction of the requirements
for the degree of

DOCTOR OF PHILOSOPHY

in Biomedical Engineering

by

Jie Zheng

Dissertation Committee:
Professor Jack J. Lin, Chair
Professor Gultekin Gualsen
Professor Ramesh Srinivasan
Professor Robert T. Knight

2018

DEDICATION

To

my mom, Yan, my dad, Su, my grandma, Yijun, my fiancée, Jue
and to my pup, Angela Zheng

An experience may be so exciting emotionally as almost to leave a scar on the cerebral tissues.

William James (1842-1910)
The Principles of Psychology (1890)

TABLE OF CONTENTS

LIST OF FIGURES

ACKNOWLEDGMENTS

First, I want to thank my advisor Dr. Gultekin Gulsen for seeing the potentials in me and picking me from a pile of competitive applicants. Without you, I would not have this great opportunity to study at UC Irvine and to meet some many amazing people. Also, thanks for all the suggestions, not only for the science but also for how to be a better “me” in general.

I also want to thank my mentor, advisor and friend, Dr. Jack Lin. Thanks for being patient during my transition from a biomedical engineer to a cognitive neuroscientist. You didn't only feed me with scientific knowledge but also train my skills, especially the critical thinking skill. I appreciate that you always prioritized your time for me whenever I needed your help. Also, thanks for treating me like a family. I enjoy the off-hours spent with you, Xiaomin, Abi and also Toye and I am sure Angela feels the same way.

I also want to thank my collaborator, advisor and friend, Dr. Robert Knight. Although we are not meeting constantly, you are always there supporting me whenever I need your help. Also, I like your funny jokes, your little Spanish greetings in the email and the picture of you with the Photoshopped muscular body. You just make research so much fun.

I want to thank Dr. Kristopher Anderson and also. Dr. Avgusta Shestyuk. for introducing me to the world of computational neuroscience. I learned so much from you. Not only the processing skills, but also all the other small things – the interactions with the patients, the coding style, and the time plan – accelerated my learning curve. I am sure all these will continue helping me adapt to different fields of the career and the life.

I thank my friends from Dr. Gultekin’s lab, Farouk Nouizi, Hakan Erkol, Tiffany Kwong, Jessica Kwong, Alex Luk, Jaedu Cho, Yang Zhang and everyone else. You make the lab day so enjoyable. I will miss the ski trip for sure. Also, I want to thank my friends and also my colleagues, Rebecca Stevenson, Ivan Skelin, Randolph Helfrich, Julia Kam and Anna Jafarpour. I always enjoy the discussion with you, but more beers, more fun!

Also, I thank everyone from the UC Irvine Clinical Team for supporting the cool research we have been doing. I also acknowledge all the patients participated in our research program. Without your generous help, this work could not have been done. I want to thank the special cookie from the cafeteria on the first floor. It amazingly cheered me up every time I felt down.

I want to thank the members of my family who have supported me along the way and I thank my friends, Rachel Qu, Jessica Hsieh, Jessica Kwong who provide much-need distraction. Also, I want to thank my fiancée Jue Hou, and my little puppy Angela Zheng for being the glue that holds my life together.

Also, I acknowledge the financial support from the UC Irvine School of Medicine Bridge Fund and National Institutes of Health (2 R37NS21135).

Curriculum Vitae

Jie Zheng, Ph.D. Candidate

CONTACT INFORMATION

Address	100 Irvine Hall, Irvine, CA 92697
Phone:	(949) 705-8629
E-mail:	zhengj4@uci.edu

RESEARCH FOCUS

My Ph.D. research aims to elucidate the neural dynamics of emotional processing in humans using intracranial recordings of local field potentials and single unit activity. Specifically, I focus on the neural network interactions among three core brain regions: the medial prefrontal cortex, amygdala, and hippocampus. My work has provided new insights into the spatiotemporal dynamics of human behavior by clarifying 1) how this network facilitates emotional information processing and 2) uses prior-knowledge (or schema) to support emotional memory consolidation. I would like to extend this line of research during my postdoc training by using electrophysiological stimulation. The ultimate goal is to combine these mechanistic sights with stimulation-based interventions to develop new therapies for memory deficits and neuropsychiatric disorders.

EDUCATION

INSTITUTION AND LOCATION	Degree	Completion date	Major
Nanjing University, China	B.S.	2013 June	Electrical Engineering
University of California, Irvine	Ph.D.	2018 March	Biomedical Engineering

COMMUNICATION INTERNSHIP

Participant as a script writer in the UC Irvine Science Communications initiative, invited by Sandra Tsing Loh, the host of the 'Loh Down on Science' on National Public Radio.

AWARDS AND HONORS

2017 Public Impact Fellowship

Pubic Impact Fellowships highlight and support doctoral students whose current research has the potential for substantial impact in the public sphere

2017 Graduate Student Award from Cognitive Neurosciences Society

Awarded as one of the ten outstanding graduate students posters with respect to scientific merits and clarity of presentation

2015 Edwards Lifesciences Scholarship

Edwards Lifesciences is the global leader in patient-focused medical innovations for structural heart disease. It awards students in the field of science, technology, engineering and math (STEM) who has dedicated in volunteerism of treating heart disease.

2013 Outstanding B.S. Thesis Award, Nanjing University

2012 Third Prize in Scientific Essay Competition, Nanjing University

2011 First Prize in Creative Thinking Competition, Nanjing University

ARTICLES IN PEER-REVIEWED JOURNALS

Zheng, J., Anderson, K.L., Leal, S.L., Shestyuk, A., Gulsen, G., Mnatsakanyan, L., Vadera, S., Hsu, F.P., Yassa, M.A., Knight, R.T. and Lin, J.J., 2017. Amygdala-hippocampal dynamics during salient information processing. *Nature Communications*, *8*, p.14413.

Zheng J., Lin, J.J., Modulating amygdala-hippocampal network communication: a potential therapy for neuropsychiatric disorders. *Neuropsychopharmacology, 43(1), p.218.*

Mnatsakanyan, L., Vadera, S., Ingalls, C.W., **Zheng, J.,** Sazgar, M., Hsu, F.P. and Lin, J.J., 2017. Language recovery after epilepsy surgery of the Broca's area. *Epilepsy & Behavior Case Reports*.

Ruiz, J., Nouizi, F., Cho, J., **Zheng, J.**, Li, Y., Chen, J.H., Su, M.Y. and Gulsen, G., 2017. Breast density quantification using structured-light-based diffuse optical tomography simulations. *Applied Optics*, *56* (25), pp.7146-7157.

Wan, N., **Zheng, J.**, Yang, Y., Zhuang, J.J., Huang, X.L., Zhu, J.J. and Lu, W.Y., 2013. Microstepping control for the stepper motor in the design of a portable insulin injector. *Journal of Tianjin University of Technology and Education*, *1*, p.010.

ARTICLES IN PROGRESS

Zheng J., Stevenson R.F., Mnatsakanyan L., Hsu F.P., Vadera S., Knight R.T., Yassa M.A., Lin J.J. Frequency-specific amygdala-hippocampal synchrony predicts successful discrimination of emotional memory. *Nature Neuroscience. (in review)*

Stevenson R. F., **Zheng J.**, Mnatsakanyan L., Vadera S., Knight R. T., Lin J. J., Yassa A. Y. Hippocampal CA1 gamma power predicts the precision of spatial memory. *(Submitted)*

Zheng J., Vadera S., Knight R.T., Lin J.J., Amygdala-hippocampus-orbitofrontal dynamics carry over contextual emotion on facial perception. *(in preparation)*

Zheng J., Mnatsakanyan L., Vadera S., Lin J.J., Orbitofrontal cortex integrates amygdala-hippocampal information and guides schema-based emotional categorization. *(in preparation)*

Skelin I., **Zheng J.**, McNaughton B.L., Lin J.J., Sharp wave/ripples reorganize connectivity patterns in cortical networks. *(in preparation)*

ABSTRACTS AND POSTERS

Zheng J., Stevenson R.F., Mnatsakanyan L., Vadera S., Yassa M.A., Lin J.J., Frequency-specific amygdala-hippocampal synchrony predicts successful discrimination of emotional memory. *(International Conference on Learning and Memory 2018)*

Skelin I., Zheng J., McNaughton B.L., Lin J.J., Sharp wave/ripples reorganize connectivity patterns in cortical networks. *(International Conference on Learning and Memory 2018)*

Zheng J., Lin J.J., Orbitofrontal cortex integrates amygdala-hippocampal information and guides schema-based emotional categorization. *(Cognitive Neuroscience Society 2018)* **selected for an oral presentation in the Data Blitz Session.**

Zheng J., Knight R. T., Lin J. J., amygdala-hippocampus-orbitofrontal network dynamics support contextual modulation of facial expression. *(Society for Neuroscience 2017)* **selected as a Dynamic Poster Presentation.**

Skelin I., Zheng J., McNaughton B.L., Lin J.J., Dynamics of sharp wave/ripple-triggered cortical and subcortical high frequency local field potential in humans. *(Society for Neuroscience 2017)*

Zheng J., Stevenson R. F., Harriger D. L., Leal S. L., Vadera S., Yassa A. M., Lin J. J., Depth electrode recording of the amygdala-hippocampal network during mnemonic discrimination of emotional scenes. *(Cognitive Neuroscience Society 2017)* **received Graduate Student Research Award.**

Zheng J., Stevenson F.R., Yassa A. M., Knight R.T., Lin J. J., Category specific phase encoding for facial expressions in the orbitofrontal cortex. *(Society for Neuroscience 2016)*

Zheng J., Riley D. J., Gulsen G., Anderson L. K., Vadera S., Yassa A. M., Knight R.T., Lin J. J., Intracranial EEG of hippocampal-amygdala dynamics during emotional memory discrimination. *(Society for Neuroscience 2015)*

Zheng J., Riley D. J., Gulsen G., Shestyuk A., Anderson L. K., Knight R.T., Lin J. J., Fearful face processing in human engages directional coupling from amygdala to hippocampus. *(Organization for Human Brain Mapping 2015)*

CONFERENCE PROCEEDINGS

Zheng, J., Nouizi, F., Cho, J., Kwong, J. and Gulsen, G., 2015, April. High resolution 3D fluorescence tomography using ballistic photons. In *Proc. of SPIE Vol* (Vol. 9319, pp. 93191V-1).

Zheng J., Rajyaguru R., Riley J., Gulsen G., Hermann B., Lin J.J., 2015, June. Disrupted modular organization of structural cortical network topology in new-onset pediatric epilepsy. *International Society for Magnetic Resonance in Medicine.*

Kwong, J., Nouizi, F., Cho, J., **Zheng, J**., Li, Y., Chen, J.H., Su, M.Y. and Gulsen, G., 2016, March. Diffuse optical tomography with structured-light patterns to quantify breast density. In *Proc. of SPIE Vol* (Vol. 9689, pp. 968942-1).

Kwong, J., Nouizi, F., Cho, J., **Zheng, J**., Li, Y., Chen, J.H., Su, M.Y. and Gulsen, G., 2015, March. Diffuse optical imaging of the breast using structured-light. In *SPIE BiOS* (pp. 93190K-93190K). *International Society for Optics and Photonics.*

Cho, J., Jeon, S.W., **Zheng, J.**, Kim, C.S., Nalcioglu, O. and Gulsen, G., 2014, March. Development of a spectrally resolved fluorescence tomography system using a NIR swept laser and a digital micromirror array based detection system. In *SPIE BiOS* (pp. 89470Z-89470Z). *International Society for Optics and Photonics.*

LECTURE AND PRESENTATIONS

Sep 12th, 2017	Give a TED-style talk at the 'Brews and Brains'
	'Brews and Brains' group translates complex research for a mass audience
June 2nd, 2017	Present at the student seminar from BME Department
2017 – Current	Present at Computational Neuroscience Journal Club from Cognitive Science Department
2016 – Current	Present at Spike Journal Club from Center for the Neurobiology of Learning and Memory
2013 – 2015	Lecture discussion and lab sessions for BME170 (Biomedical Engineering Laboratory), BME130 (Biomedical Signals and Systems) and BME110B (Biomechanics II)

PROFESSIONAL ASSOCIATION

2015 – Current	Society of Neuroscience
2016 – Current	Cognitive Neuroscience Society
2015 – Current	Graduate Association of Biomedical Engineering Students (GABES)
2016 – Current	Graduate Professional Success (GPS) – BIOMED

COMMUNITY SERVICES

2014 – Current Volunteer at Angel Heart International

Angel Heart International is a charity group committed to serving children with congenital heart disease in rural China. We hold fundraisers to raise money for their surgical expense and travel to Lanzhou, physically and mentally supporting them throughout the entire surgery.

2015 – May, 2017 Founder and President for GABES – Professional

GABES (Graduate Association of Biomedical Engineering Students) – Professional seeks to facilitate networking among students, industry, alumni, and the larger Orange County biomedical engineering community. By hosting workshops, speaker series and company tours, we empower the

development of professional skills for graduate students from Biomedical Engineering Department.

ABSTRACT OF THE DISSERTATION

Circuit Dynamics of Emotional Processing: Insights from Human Intracranial Recordings

By

Jie Zheng

Doctor of Philosophy in Biomedical Engineering

University of California, Irvine, 2018

Professor Jack J. Lin, Chair

Swift detection and remembering of salient and emotional stimuli is critical for survival and adaptive fitness. Optimal emotional processing is central to mental health, abnormalities of which are frequently present across all forms of neuropsychiatric illness including major depression, post-traumatic stress disorder, and suicide. Despite the extent of the problem, our fundamental understanding of the neural circuitry underlying emotional processing remains limited, which has hindered therapeutic advances in neuropsychiatric diseases.

Here, we employed intracranial electrodes in drug-resistant epilepsy patients undergoing pre-surgical evaluation to directly record neural signals from the amygdala, the hippocampus and the orbitofrontal cortex, a neuroanatomical circuit core to emotional processing. First, we examined oscillatory activity within the medial temporal lobe during processing of fearful faces compared to neutral landscapes. We found early engagement of the amygdala and unidirectional influence from the amygdala to the hippocampus during processing of fearful faces. In addition, we showed that such modulation is mediated through cross frequency coupling between theta/alpha (4-10Hz) oscillations and high gamma activity

(70-200 Hz). Next, we investigated the oscillatory mechanisms of emotional memory and asked how emotion influences the discrimination of similar mnemonic experiences (e.g. pattern separation). We observed frequency-specific interactions between the amygdala and the hippocampus, with theta (3-7Hz) synchrony facilitating correct mnemonic discrimination and alpha (8-13Hz) synchrony promoting incorrect recognition. Finally, we examined how past context modulates our future perception of facial expression. Using Bayesian decoding techniques, we showed that the high gamma activity is precisely aligned with the phase of theta oscillations, in which the probability densities of the reconstructed time showed that the descending theta phase encodes past context and ascending theta phase represents future face perception. In sum, intracranial recordings have provided critical insights on how oscillations coordinate circuit dynamics in the frontotemporal network to rapidly and flexibly organize emotional information in humans.

CHAPTER 1: Introduction and Significance

1.1 Emotion Perception and Emotional Modulation

1.1.1 Facial Emotion Processing

The recognition of emotional information from facial expression plays a critical role in human communication. It has been the research focus over several decades to a range of disciplines, including psychology, psychiatry and affective neuroscience[1]. Perception of facial emotion can be a simple procedure of feature detection[2] or a complex configuration-based procedure, which requires comprehensive analyses of multiple information including face's gender, identity, emotional expression or other social relevant clues[3]. For instance, happiness can be easily inferred by single facial feature, the smile. On the other hand, discrimination among different types of happiness (e.g. Surprisingly happy versus Smug happy) requires further interpretation of rich information from the face or even the surrounding context. It has been proposed that the emotional processing of faces involve two principal neuroanatomical divisions: 1) occipital and temporal visual neocortex, and 2) subcortical pathway (including amygdala and hippocampus) that bypass visual cortex[1]. Due to the limitation of electrode placement, the studies listed in this thesis are focused on interactions within the subcortical pathway.

Notably, out of all the emotion, facial expressions of fear are processed specially and disproportionately rely on the amygdala[4]. In a rare case, the patient SM with bilateral amygdala damage, she can normally judge age, gender and familiar identity from faces and has little difficulty recognizing most facial expressions, but has severe impairment of fearful face

perception specifically[5]. Evidence from neuroimaging studies has also shown that for fear stimuli (e.g. a fearful face), fast neural responses from amygdala engage in the early processing of salient information, which can occur even prior to awareness[6] and irrespective to subjects' attentional focus[7-9]. Moreover, for efficient emotional learning and environmental adaptation, the amygdala could also trigger associated emotional knowledge via its projections to the hippocampal formation[1]. Evidence from rodent studies have demonstrated a close interplay between amygdala and hippocampus under fear conditioning tasks and indicate a strong modulation from the amygdala to hippocampal encoding plasticity[10-12]. Such directional influence has only been indirectly inferred in humans from behavior[13] and neuroimaging studies[14]. Here we look for direct electrophysiological evidence to support such notion and aim to reveal the oscillatory dynamics between the amygdala-hippocampal circuit during the processing of fearful faces.

1.1.2 Emotional Modulation of Memory

Emotion conveys memory benefits and selectively preserves them from forgetting, which allows the guidance for future adaptation. A typical example is flashbulb memories (a lifetime detainment of detailed and vivid memory of important historical or autobiographical events), which is initially suggested to have a better recollection for emotional events compared to the neutral ones. However, recent studies have pointed out that this enhanced vividness of emotional events may be subjective and are not completely accurate since emotion doesn't enhance memory equally from all the aspects nor for all types of emotional events[15]. Specifically, the emotional modulation of memory is asymmetric, with the central emotional

content (i.e. gist) is enhanced while the memory for peripheral content (i.e. details) is impaired[15,16]. This is consistent with Mather and Sutherland's Arousal-Biased Competition (ABC) model, in which memory of specific stimuli can be either enhanced or impaired based on the competition in favor of high arousal priority. An example of such emotional memory trade-off is the "weapon focus" effect, where eye-witnesses often recall the weapon used in a crime with great detail but fail to encode (or perhaps more quickly forget) peripheral details such as the perpetrator's clothing[17].

Neuroscientists tested such phenomenon by examining the effect of emotional arousal on mnemonic discrimination ability[18], which relies on the hippocampal pattern separation (i.e. the process by which similar episodic memories are stored by non-overlapping neural representations[19,20]). An impaired discrimination ability for emotional stimuli has been found compared to the neutral ones[21], indicating a biased emotional influence on mnemonic discrimination. Moreover, neuroimaging studies have revealed a co-activation pattern between the amygdala and hippocampus, with amygdala activity associated only with emotional valence regardless discrimination accuracy while hippocampal activity co-varied with both emotional valence and discrimination outcomes[22]. These findings suggest that the emotional modulation of mnemonic discrimination might be the results of the influence of the amygdala onto the hippocampus. However, the understanding of the underlying neural mechanism is hindered by the limited ability of non-invasive methods (e.g. surface electroencephalography (EEG), magnetoencephalography (MEG) and magnetic resonance imaging (MRI)) to directly record from the human brain. Here we employ safe and large-scale intracranial electrodes in humans to capture dynamic neural interactions from these regions at an unparalleled spatiotemporal

resolution to further extend the knowledge of such phenomenon to circuit-level understandings.

1.1.3 Context in Emotion Perception

Context influences our emotional perception. This is originally discovered by Soviet filmmaker Lev Kuleshov near a century ago. He found that audiences' emotional perception of an actor's face could be manipulated by different emotional scenes it paired with. In his original experiment, the actor Ivan Mozzhukhin's face is juxtaposed with either a scene of funeral or a scene of a child playing, which results in audience interpretation of Mozzhukhin's emotional disposition as subtly melancholic or happy, respectively[23].

While "Kuleshov Effect" serves as an important editing technique, it also brings interests from psychiatrists and neuroscientists to study the contextual modulation of how we perceive and predict the social world[24]. From an evolutionary perspective, context improves adaptive fitness by constraining search within memory systems to optimize imminent threat forecast[25]. However, this effect can also become maladaptive when inappropriately associating a fearful context with safety or neutral cues. Its persistence can lead to impaired fear extinction[26,27]. Animal electrophysiology[28-30] and human neuroimaging studies[31,32] have shown that the amygdala-hippocampus-orbitofrontal circuit is required for contextual control of fear behavior. The abnormalities of this tripartite network can lead to impaired fear extinction that underlies diverse mental illness including post-traumatic stress disorder, anxiety, and depression[33]. Despite its importance, little is known regarding the circuit dynamics underlying contextual modulation of facial expressions in humans[34]. Here we aim to fill the gap in knowledge by

examining the spatiotemporal information flow of amygdala-hippocampus-orbitofrontal network during the context-face integration.

1.2 Emotion Circuit: Amygdala-Hippocampus-Orbitofrontal Cortex

1.2.1 Anatomy Overview of Tripartite Network

Amygdala anatomical review

Amygdala (means 'almond' in Greek) is the almond-shaped structure located deep and medially within the temporal lobes of the human brain. The amygdala contains about 13 nuclei that have widespread connections with many areas of the brain and can interact with information from every sensory modality. Based on the functional connectivity and the distribution of neurotransmitters[35], nuclei within the amygdala can be distinguished into three major groups: 1) basolateral nuclei (lateral, basal, and accessory basal nucleus), which is typically referred as the BLA, 2) cortical-like nuclei (nucleus of the lateral olfactory tract, bed nucleus of the accessory olfactory tract, anterior and posterior cortical nuclei, and periamygdaloid cortex), and 3) centromedial nuclei (central, medial, and the bed nucleus of the stria terminalis)[36].

Hippocampus anatomical review

Hippocampus (means "seahorse" in Greek) is the seahorse-shaped structure located in the temporal lobe of each cerebral cortex, medial to the inferior horn of the lateral ventricle. It contains two main interlocking parts: the hippocampus proper and dentate gyrus (DG). The hippocampus proper consists of four subfields CA1, CA2, CA3 and CA4, which is the initials of Cornu Ammonis, an earlier name of hippocampus[37]. These four hippocampal subfields curl into

a tight U shape and are distinguished as the narrow area with a single layer of densely packed pyramidal neurons. The hippocampus proper starts with CA1 subfield, which has the major output pathway to the layer III of entorhinal cortex (EC) via the monosynaptic pathway. CA2 and CA3 are often combined together, since CA2 is a small area and the pyramidal cells between two regions are highly alike. CA3 also connected to EC but through the trisynaptic pathway (from layer II of EC to DG and then to CA3 via the perforant path and mossy fiber path)[38,39]. Besides that, CA3 subfield can also receive input from itself via the recurrent collateral network and can project to CA1 via the Schaffer collateral path[39]. CA4 contains mossy cells that receive inputs from granule cells in the DC and sometimes is considered as part of the DG[37]. Due to the relatively large size of electrodes, we couldn't sparse signals from all hippocampal subfields and instead simplify the division as CA1 and DG/CA3 (including CA2, CA3, CA4, and DG).

In addition, it has been noted that the anterior (or ventral) and posterior (or dorsal) portions of the hippocampus have different connectivity with cortical and subcortical areas[37]. Disparate functions have been proposed for these two subregions, with anterior (or ventral) hippocampus mediating anxiety-related behaviors and posterior (or dorsal) hippocampus facilitating spatial navigation[40,41]. Since our tasks contain highly arousal stimuli and our main interests are targeted at the emotional perception and emotional modulation, the analysis in Chapter 2-4 are mainly focused on the anterior hippocampus.

Orbitofrontal cortex anatomical review

Orbitofrontal cortex (OFC) is a part of the prefrontal cortex that consists of Brodmann area 10, 11 and 47 in humans[42]. The name comes from its position, which is right above the orbits where the eyes are located. It has been considered anatomically synonymous with the ventromedial prefrontal cortex[43].

Anatomical connections among three regions

Amygdala and hippocampus are reciprocally connected. The BLA projects to the hippocampus via: 1) indirect connections through the EC, 2) indirect connections through the hypothalamus and medial septum, and 3) direct connections to CA3, CA2, CA1, subiculum, and parasubiculum[44]. On the other hand, the hippocampus projects back onto the amygdala, mostly via hippocampal CA1 to BLA[44,45]. The OFC also has reciprocal connections with amygdala[46,47] and hippocampus[48]. Specifically, OFC is strongly connected with the hippocampus, via the direct pathway from ventral CA1 to medial OFC[49]. The caudal sector of lateral OFC is strongly connected with the amygdala[50], mostly with basal and lateral amygdaloid nuclei[47]. Notably, projections from the dorsal hippocampus to the medial OFC has not been known yet[51].

1.2.2 Functional Cooperation among Three Regions

An extensive body of work[52] has suggested the amygdala-hippocampus-orbitofrontal cortex as the core neural circuit of affective processing, with divergent functions for each region. The amygdala is critical for prioritizing salient information such as emotion[53], valence[54], and motivation[55]. The hippocampus is thought to be important for contextual modulation of fear[56] and emotional memory[57]. The orbitofrontal cortex is important for representing the affective value of goals to predict outcomes[58,59] and is critical for the formation of fear memory to

establish punishment prediction[60]. Indeed, orbitofrontal lesions in nonhuman primates cause enhanced anxiety, fear response and negative bias in decision-making[60,61]. While each region has dissociable functions, recent work in reinforcement-learning models also suggests that overlapping functional roles of these three regions exist[62]. Both the orbitofrontal cortex and the hippocampus form cognitive maps with different emphases. Hippocampus is particularly biased to form associations by linking information into sequences and it has been proposed that these associations provide a predictive map[63]. Orbitofrontal cortex provides a more global cognitive map of the task state or structure by drawing relations between internal and external states to infer rules and outcomes[62]. In addition, overlapping functions have also been found in the orbitofrontal cortex and the amygdala, in which they both encode the value, reward, and decision[64-66]. These findings suggest that emotional processing is not limited to a single region but instead, interactions among this core 'emotional' circuit, anchored by direct and indirect anatomical connections, are critical for appropriate behavior response. Then the key question is how do amygdala, hippocampus, and orbitofrontal cortex cooperate with each other to process emotion? Based on the evidence from rodent studies, a computational model for emotional processing has been proposed, in which the hippocampus and the orbitofrontal cortex cooperate to form cognitive maps that track the causal relationships among stimuli, actions, and outcomes[62]; the amygdala imbues salience and emotion to dynamically interact with hippocampus-orbitofrontal cognitive maps. Therefore, in Chapter 2-4, we aim to testify this hypothesis, look for electrophysiological evidence and build up a unifying model in humans.

1.3 Brain Oscillations and Network Dynamics

1.3.1 Intracranial Electroencephalography

The dawning of the science of electrophysiology

> *"In an era when electricity itself was a young science, and physiology scarcely distinguishable from the anatomy, electrical activity of the nervous system was hardly recognized."*

As Mary Brazier wrote in her book "The History of the Brain: The first half century". The tuning point comes in 1791 when Galvani published his famous Commentary and discovered intrinsic electricity from nerves. It took another fifty years for the scientists to realize these electrical activities from the nervous system could be used as a sign of its function. At that time, intense interests are focused on mapping the motor cortex by stimulating different parts of the brain with electrodes and observing the resulting motions from that. However, Richard Caton, a Liverpool neurosurgeon, used the electrodes to receive the electrical signals from the brain instead of sending electrical signals to it. In the first section of his work, presented in the proceedings of the meeting of the British Medical Association on 24th August 1875, he wrote:

> *"Feeble currents of varying direction pass through the multiplier when the electrodes are placed on two points of the external surface, or one electrode on the grey matter, and one on the surface of the skull…The current is usually in constant fluctuation; the oscillation of the index being generally small, about twenty to fifty degrees of the scale."*

This has been remarked as the original discovery of the electroencephalogram (EEG). But this amazing work was not well recognized until the great German psychiatrist Hans Berger took the

concept further: developed the non-invasive EEG recorded from the scalp and associated robust signal changes with the opening and closure of eyes.

Invention of Intracranial Electroencephalography (iEEG)

In the early 1950s, Wilder Penfield and Herbert Jasper, the neurosurgeons at the Montreal Neurological Institute extended the non-invasive EEG approach to intracranial recordings by placing electrodes directly inside the brain[67]. This is originally designed to identify the cortical regions that generate epileptic seizures. Now it has been widely used as a powerful technique for studying neural dynamics of human brain and linking these electrical features to cognition and disease[68]. It provides a direct measurement of population-level neural activity with high temporal and spatial precision[69]. Compared to the non-invasive EEG, in which electrical signals are spatially smeared when passing through the skull, iEEG can provide functional and anatomical configurations of a distinct neural circuit – the dynamics within and among different brain regions that produce various temporal/spatial/spectral EEG features associated with specific cognitive processes.

1.3.2 Neuronal Oscillations: Local and Global Modes

Clocks tick, bridges vibrate and neural networks oscillate[70]. Oscillatory activities in human were first discovered by Hans Berger using scalp EEG recordings and described as an 8 to 12Hz rhythm. Afterward, different forms of neural oscillations were observed and studied at multiple spatiotemporal scales of the brain across multiple species[68]. As the most prominent feature of EEG, neural oscillations were driven by the synchronization of neural activities and varied in amplitude, timing, and frequency. Although the origin of such periodic brain rhythm

remains unclear[71], countless studies over many decades have suggested oscillatory activity as a mechanism for cerebral integration[72,73] and as a critical "middle ground", linking single-neuron activity to perceptual, cognitive, motor and emotional processes[70,74]. Such integration can exist across a number of anatomical and functional domains with different frequency rhythms associated with each region[75]. The period of oscillations is determined by the physical architecture of the neural network around the implanted electrode. Due to the fact that most neurons are locally connected[76] and their communication speeds are limited by the axon conduction and synaptic delay[77], high-frequency oscillations are usually confined to a small neuronal space, whereas large networks can be recruited via slow oscillations[78,79]. With the cooperation of diverse neuronal oscillations, different brain operations can be carried out simultaneously at multiple temporal and spatial scales[80]. Based on the frequency range, neural oscillations could be divided into two subdivisions: **Local modes** (i.e. high-frequency oscillations) and **Global modes** (i.e. low-frequency oscillations).

Local modes: includes gamma (>30 Hz) activity, which is high in frequency, low in amplitude, and distributed over a limited topographic area. Gamma oscillations are short-lived and typically emerge from coordinated interactions of excitation and inhibition[81]. Simultaneous recordings of single unit activities and local field potentials have demonstrated strong correlations between the power of gamma oscillations and spiking activity[82-84], especially within the high-gamma frequency range (~60-200Hz)[85]. Such correlation is largely attributable to an increased firing rate and more synchronous firing pattern, suggesting that high gamma activity serves as the correlate of local population spiking.

Global modes: include delta (1-3 Hz), theta (4-7Hz), alpha (8-12Hz) and beta (13-30Hz) oscillations, which are lower in frequency, higher in amplitude and span across relatively large brain regions[75]. These slow oscillations can effectively drive postsynaptic cortical neurons by synchronous presynaptic spikes[74] to provide a temporal window for interactions between widely distributed neural assemblies[77]. Moreover, oscillations at different frequency ranges seem to play distinct functional roles. In general, delta oscillations depend on activities of motivational systems and participate in salience detection; theta oscillations are involved in memory and emotional regulation; alpha and beta oscillations are implicated to perform an inhibitory control[75]. Specifically, recent findings have suggested that these four oscillatory systems reciprocally interact, with relative prevalence of alpha/beta oscillations inhibiting behavioral patterns peculiar to the delta and theta activity[86].

1.3.3 Functional and Effective Connectivity

Oscillation-based synchrony is the most energy-efficient physical mechanism for temporal coordination[87,88]. The coupling between neuronal oscillations has been proposed to support inter-regional communications[89]. Here, we summarize three different mechanisms of coupling, coordinated by local and global modes of neuronal oscillations.

Interactions between local modes

In addition to a proxy indicator of local computation[90,91], gamma oscillations have been shown to support inter-regional communication via selective and flexible coupling between different cortical areas[92-96]. Previous studies have demonstrated a potential link between changes in gamma synchrony or gamma coherence across different brain regions and the

diverse cognitive processes in humans[97-99]. However, the ambiguities of which variables are synchronized in gamma coherence measurements remain unsolved. For example, the cross-regional spike-spike coupling at gamma time-scales can be the results of feedforward entrainment of interneurons or the synchronization of principal cells[100-102]. Clarifications of gamma synchronization across distant areas remain a persistent challenge, and strong evidence is still needed to further identify the physiological significance of gamma rhythm in inter-regional communication and neural information transfer[103]. Therefore, in Chapter 2-4, we quantify the network interactions as global-global modes coupling and local-global modes coupling.

Interactions between global modes

Slow frequency oscillations rhythmically open the temporal window, during which the coordinated groups can effectively communicate with each other. Specifically, when both sending and receiving neural assemblies oscillate (i.e. become excitable in a predictable cycle) and phase-locked to each other, communication will be achieved through coherence[89]. However, global phase-locking is often observed in abnormal brain states (e.g. during seizures), which is incompatible with normal cognitive functions. Thus, to achieve cognitive flexibility, the preclusion of communication system is important, in which selective inter-regional synchrony is controlled by the frequency of the coherent oscillations and the relative phase between them. Failures to match in these two variables will lead to the fact that inputs from sending neural assemblies repeatedly miss the excitable window of the receiving group and restrict the communication only to the regions with reliable phase relationship.

Interactions between local and global modes

If the global mode oscillations serve the purpose of integration across diverse cortical areas, they are expected to interact with the local mode oscillations, which implement specific cognitive operations at the local cortical level[75]. In addition, the power density of EEG or local field potential is inversely proportional to frequency (f) in the mammalian cortex[104]. This 1/f power relationship also implies that perturbations occurring at slow frequencies can cause a cascade of energy dissipation at higher frequencies[105]. In other words, widespread slow oscillations modulate faster local events[79,106,107]. Consistent with this theoretical hypothesis, previous studies have shown that transient coupling between low- and high-frequency brain rhythms coordinates activity in distributed cortical areas, providing a mechanism for effective communication during cognitive processing in humans[108]. Moreover, such hierarchical modulation structure might suggest a directional/effective influence. For example, it might reflect the modulation of fast activations in local circuitry by large-scale networks operating in lower frequencies (top-down integration), or a bottom-up mechanism for propagation of local activation to other cortical regions[109,110].

CHAPTER 2: Amygdala-Hippocampal Dynamics Support Salient Information Processing

2.1 Introduction

Swift detection of social, emotional, or threatening stimuli is critical for adaptive fitness in humans. When we interact with each other, emotionally salient stimuli, such as fearful facial expressions, provide ecologically relevant signals that focus our attention towards perceptually relevant information. Thus, recognizing motivationally salient information constitutes an important social and biologically meaningful incentive and plays a key role in guiding our interpersonal behavior[111]. Successful detection of and response to motivationally important stimuli have been shown to rely on activities within two brain structures – the amygdala and hippocampus. In particular, the amygdala is critical for prioritizing salient information such as emotion[53] , valence[54] and motivation[55]. The hippocampus is thought to be important for contextual modulation of fear[56], emotion judgment[112], and emotional memory[57] - all operations that are critical for remembering motivationally salient stimuli. Further, rodent studies have shown that manipulating amygdala function alters the hippocampal processing of salient information[10-12]. However, there is no direct electrophysiological evidence for amygdala-hippocampal connectivity in humans and thus their directional relationship is unknown.

We addressed this question by presenting dynamic salient (fearful faces) and neutral (landscapes) stimuli to patients with medication resistant epilepsy and recorded direct brain signals from intracranial depth electrodes in both the amygdala and hippocampus. We examined the local activities for both regions by tracking the stimulus induced high gamma activities (70-150Hz) and indexed amygdala-hippocampal functional connectivity as the phase

locking values between inter-regional theta/alpha (theta = 4-7Hz, alpha = 8-12Hz) oscillatory synchrony, which is ubiquitous in the human hippocampus[113] and amygdala[114]. Further, we investigated the directional influence of these responses using Granger Causality and Phase Slope Index analysis. Consistent with the model that rapid detection or prioritization of salient information in the amygdala[115] influence subsequent hippocampal mnemonics processing[10-12], we hypothesized that during salient information processing: 1) high gamma activities in the amygdala would occur earlier than in the hippocampus; 2) stronger low frequency oscillatory synchrony would facilitate inter-regional communications when compared to neutral conditions; 3) amygdala would exert directional influence on the hippocampus rather than the reverse.

2.2 Materials and Methods

Participants. Data were obtained from nine patients (four female, five male, age 24–58, see APPENDIX A) who had stereotactically implanted intracranial depth electrodes (Integra or Ad-Tech, 5 mm inter-electrode spacing) placed at the University of California, Irvine, Medical Center to localize the seizure onset zone for possible surgical resection. The institutional review boards of University of California at Berkeley and at Irvine approved the research, and written informed consent was obtained from each subject before testing. Electrode placement was exclusively guided by clinical needs, and the patient selection was solely based on magnetic resonance imaging (MRI) confirmed depth electrode placement in the amygdala and hippocampus. Recordings were conducted from four patients (subjects 1–4) with depth electrodes localized ipsilateral and five patients (subjects 5–9) contralateral to or outside of the seizure onset zone. There were no seizures recorded in any of the epochs, and any epochs with

interictal epileptiform activity were removed from the analysis. Comparable results (e.g. high gamma, phase locking values and phase amplitude coupling) were observed in all nine subjects, and there were no differences in the magnitude of effects between recordings from electrodes ipsilateral and contralateral to the seizure focus.

Behavioral task. Participants watched silent movie clips on a laptop computer placed on the service tray at a comfortable distance in front of them. We employed dynamic fearful faces as a form of aversive stimuli, rather than static facial expressions, to provide participants with temporal cues that mimic real-life social exchanges[116]. The total length of the task was about 7 minutes, consisting of alternating 9 blocks of landscapes and 8 blocks of fearful faces (approximately 24 seconds/block, see Figure 1.1a). During the experiment, participants viewed 70 landscapes and 71 fearful face clips (clip duration: 2.8 ± 1.3 s; mean ± s.d.). Within each block, movie clips were shown continuously without breaks.

Electrode localization. MRI scans. Electrodes were localized in each participant using co-registered pre-implantation and post-implantation structural T1-weighted MRI scans. The pre-implantation scans were all 1 mm isotropic. The post-implantation scans were either 1 mm isotropic (subjects 1, 5, 6, 8 and 9) or 0.75 x 0.75 x 7 mm (subjects 2–4 and 7). For each participant, the post-implantation scan was registered to the pre-implantation scan using a six-parameter rigid body transformation (three rotations and three translations in x–z directions), implemented in Advanced Normalization Tools (ANTs http://stnava.github.io/ANTs/)[117].

Anatomical masking. For determining exact electrode locations, we used a high-resolution anatomical template (0.55 mm) developed in our laboratory with manual tracings of

hippocampal subfields and amygdala nuclei. This template has been used in past studies[21,118,119]. Regions of interest (ROIs) in the medial temporal lobe included the DG/CA3, CA1, subiculum, entorhinal cortex, perirhinal cortex, parahippocampal cortex, BLA, central nucleus of the amygdala (CeA), and the cortical nuclei of the amygdala (CORT)[120,121]. Segmentations for hippocampal subfields followed our previously published protocols[122]. Briefly, the segmentation included DG/CA3, CA1 and subiculum, and procedures followed closely the atlas of Duvernoy[120], in which the subfields are defined along the anterior-posterior axis of the hippocampus. Amygdala segmentation procedures were based on Entis et al.[123], but were modified to define three regions: BLA, CeA and CORT. To label these sub-regions of the amygdala, three key points were identified: (1) the medial tip of the alveus (up to the optic tract); (2) the most lateral point of the entorhinal sulcus; and (3) bottom of the circular sulcus. These three points are easily observable and provide a reliable landmarking system for segmenting the amygdala sub-regions. After identifying these points, lines were drawn to connect the three points to each other, creating four quadrants (basomedial and basolateral were combined to form the basolateral complex).

Labeling individual participant scans. The labeled high-resolution anatomical template (resampled to 1 mm isotropic) was aligned to each individual's pre-implantation scan using ANTs Symmetric Normalization[124], such that the labels could be applied to each participant's MRI. This allowed for visualization and accurate identification of electrode locations using anatomical labels in each participant's space. Each electrode location was determined by selecting the center of the electrode artifact and identifying the region of interest that

encompassed the center. Cases where electrodes were on the border between ROI's or between grey matter and white matter, were noted as such.

Data collection and preprocessing. Intracranial EEG data were acquired using a Nihon Kohden recording system (256 channel amplifier, model JE120A), analog-filtered above 0.01 Hz and digitally sampled at 5000 Hz. All the data were analyzed in MATLAB combined with open source toolboxes and customized scripts. After the acquisition, neuronal recordings were band-pass filtered from 0.1 Hz to 350 Hz using a zero phase delay finite impulse response filter with Hamming window and then down-sampled to 2000 Hz for subsequent analyses. A regression method[125] was used to filter 60 Hz noise and its harmonics. All hippocampal and amygdala electrodes were re-referenced to the nearest electrode located in white matter. A neurologist with subspecialty training in epilepsy manually inspected all EEG signals to identify and remove segments with interictal epileptiform discharges as well as excessive noise, including broadband electromagnetic noise from hospital equipment. To avoid potentially biasing the results, the neurologist was blinded to the electrode location and stimulus conditions associated with EEG signals. These preprocessing steps were performed prior to the further analysis listed below.

Electro-oculogram and perisaccadic high gamma activity. To investigate the possibility of eye-movement-related contamination of our results, one subject (S9) was recorded along with a free head fixation eye tracker (SensoMotoric Instruments, Inc. RED 250 mobile) and EOG recordings. The eye tracker, connected to the laptop with Universal Serial Bus (USB), was placed at the inner edge of the presentation laptop. Before the task, the eye tracker was calibrated using the iView RED-m software. Timing between the eye tracker recording and the video clips

was synchronized through an E-Prime script. After averaging the velocity of the eyes in the X and Y dimensions from the eye tracker data across clips, two-sample t-tests were performed for each data point to test for significant differences in patterns of eye movements between conditions that could affect the results. In addition to the eye movement analysis, we estimated the time course of high gamma activity (HG) in the vertical and horizontal EOG. Again, two-sample t-tests were performed for each data point to test for significant differences between conditions. As a third test to investigate the contribution of ocular activity to our findings, we used ICA (Bell-Sejnowski ICA algorithm)[126], implemented in the EEGLAB toolbox for Matlab on the EOG combined with white matter re- referenced amygdala and hippocampal activity to compute the weights of contributions from each channel of data to each independent component. Any components composed of mostly EOG activity were removed from the data by zeroing those components and re-projecting the remaining components into the channel space. All analyses were then re-run with this 'corrected' data.

Saccades were detected through a velocity-based algorithm[112]. The velocity of eye movement was estimated as the first derivative of the Euclidean distance between eye positions at successive sample points. A threshold was set at the 99th percentile of velocities and saccades were marked at the time points of the peak velocities that surpassed this threshold, with a minimum spacing of 200 milliseconds between saccade events. High gamma (70–180 Hz) activity in hippocampal and amygdala contacts was then epoched based on these events. After baseline correction (-200 ms to 0 ms), two-sample t-tests were performed for each data point to determine significant differences between conditions. To further investigate the possibility that PAC analyses could have been influenced by EOG activity, we calculated the

PAC using the gamma-range component of the EOG signal and low-frequency phase from the hippocampus and amygdala (the same analysis as described in the Methods 'Phase-amplitude coupling' section). We observed no significant PAC pattern between the amygdala or hippocampus and the EOG HG signal, which indicates that there was no appreciable influence from potential eye movement artifacts on the PAC analysis.

Power spectral density (PSD) and subject-specific low-frequency band. PSD was estimated using Welch's method (pwelch.m in Signal Processing Toolbox from MATLAB) wherein the PSD was estimated for each subject separately using 1 s time windows with a 50% overlap. The slope of the power spectrum was estimated using the linear regression approach in a semi-log space, where the power P at each discrete frequency f was estimated from the frequency itself using the following formula:

$$P_f = f'\beta + \varepsilon$$

where f' is a two-column matrix composed of the discrete frequency bands of interest and a column of ones; β is the regression coefficient (the slope of the model), and ε is the error term. In intracranial power spectra, β is typically negative, which is important given that task-related increases in neural activity result in a broadband upward shift within the high gamma range[127]. To characterize spectral dependence between the amygdala and hippocampus in a narrow band, we selected the subject-specific low-frequency band based on the PSD plots. Specifically, the value of exponent x in the power-law relation $P \sim \frac{1}{f^x}$ was obtained by fitting a straight line to the experimentally measured PSD. Then the distances between the PSD and the fitting curve

were calculated at each frequency point. The subject-specific band was defined as the farthest points from the fitting curve within the low-frequency range with a bandwidth of 4 Hz.

Frequency decomposition. Data from amygdala and hippocampus were first filtered into subjects' specific low frequency bands (see Figure 1.1c Amygdala: $x_{Amy\theta}$ = 6.0 ± 0.49 Hz; hippocampus: $x_{Hipp\theta}$ = 6.5 ± 0.16 Hz; mean ± s.e.m.) and high gamma (x_{γ}, 70-180 Hz) using a two-way, zero-phase lag, least-squares finite impulse response filter to prevent phase distortion (eegfilt.m function in EEGLAB toolbox[128]). The length of the filter in points was determined by the specific frequency, cycle number (usually 4-5 cycles) and sampling rate. The center frequency of each frequency bin was spaced apart by 0.1 of the lower frequency band and the bandwidth varied by multiplying the fractional bandwidth index 0.3 with the center frequency. For example, for the frequency bin centered at 10 Hz, the next center frequency was 10*0.1+10 = 11 Hz and the bandwidth was 10*0.3*2 = 6 Hz. Since we chose adaptive rather than fixed bandwidths, the bandwidths within low frequency range were sufficiently narrow to define a meaningful phase while the bandwidths within higher frequency range were broad enough to fit the sidebands caused by the assumed modulating lower frequency band[129]. We then applied the Hilbert transform (hilbert.m function in Signal Processing Toolbox from MATLAB) to estimate the amplitude ($a_x[n]$) and phase ($\theta_x[n]$) for both bands, which yields a complex time series:

$$S_x[n] = a_x[n]e^{i\phi_x[n]}$$

where $\mathrm{a_x[n]}$ represents the instantaneous analytic amplitude and $\mathrm{\phi_x[n]}$ is the instantaneous phase.

Event-related potentials. The ERPs were calculated individually for both the amygdala and hippocampus separately. The LFP signals were first low-pass filtered at 30 Hz using the same filter parameters as described in Methods ('Frequency decomposition' section). Then the filtered signals were segmented into epochs, and the ERPs were calculated by averaging across these epochs within each condition. After baseline correction by subtracting the mean baseline (-500 ms to 0 ms) value from all data points, two-sample t-tests were performed for each data point to determine significant differences between conditions.

High gamma activity. To investigate the time course of high gamma activity within the amygdala and hippocampus, we extracted the banded signal and averaged the results within each region. Specifically, the time series of high gamma amplitude were divided into 2-second epochs, including 0.5 seconds of averaged baseline period (Figure 1.1a Black screen) and 1.5 seconds from the start of each movie clip. The amplitude data at each time point was first z-score normalized to the entire trial time-series. Then the computed z-scores were then baseline corrected by subtracting an average of pre-stimulus baseline data points (the 0.5s baseline period). This allows us to eliminate the positive skew typically observed for high gamma amplitude values[130]. We then statistically compared the event-related high gamma amplitude changes between the neutral and the aversive conditions using a cluster-based permutation test, computing statistics at the cluster level and correcting for multiple comparisons[131]. First, all the trials from the two experimental conditions were randomly shuffled, and the means of each condition were subtracted 1000 times to create a null distribution of differences between conditions. T-scores were then computed for each null difference time series by comparing it to the entire distribution of null difference time series at every time point. Then, all t-scores

corresponding to uncorrected p values of 0.05 or less were formed into clusters with any neighboring such t-scores. The sum of the t-scores in each cluster is the "mass" of that cluster and the most extreme cluster mass in each of the 1000 sets of tests were recorded and used to estimate the distribution of the null hypothesis. Finally, clusters were obtained from the true data, and the percentage of null cluster masses greater than each true data cluster mass was taken as the corrected p value for that cluster. Onsets and offsets of the significant high gamma activity for each condition were computed by taking the first and last time sample that passed a threshold of $p < 0.05$. Time-to-peak was defined for aversive and neutral conditions as the latency of the maximum amplitude in the high gamma range across all trials within each condition during the range of time where a significant difference between the two conditions was found.

Phase locking value (PLV). To quantify the inter-electrode low frequency phase coupling, phase differences were calculated for each electrode pair (i, j) using the phase time series $\phi_x[n]$ obtained from equation 1.1. The frequency range covers the low frequency peaks from both amygdala and hippocampus (identified in the power spectrum density plot from Figure 1.1c) with a bandwidth of 4 Hz. The phase difference between these two temporal courses $\phi_{\theta ij}[n]$ indexes the coherence between each electrode pair and is expressed as the Phase Locking Value index (Equation 1.2). PLVs range between 0 and 1, with values approaching 1 if the phase differences between the electrodes vary little across time.

$$PLV = \frac{1}{N} \left| \sum_{n=1}^{N} e^{\phi_{\theta i,j}[n]} \right| \quad (1.2)$$

The filtered data were segmented into one-second windows and then separated according to task condition before computing a PLV for each electrode pair and condition. Relative increases (or decreases) in PLV in response to fearful faces vs. landscape scenes were assessed by subtracting the two PLVs for each electrode pair. To test the significance of differences between two conditions and, at the same time, maximally eliminate the influence of ERPs, we did a two-step approach as described below. We first permuted trials and computed the 99th percentile threshold within each condition. Only the electrode pairs with PLVs passing above the threshold for both conditions were selected for calculating the PLV difference. Then the statistical significance for each electrode pair was estimated using a cluster-based permutation test, in which a null distribution was created by randomly assigning trials (i.e., one-second windows) into two conditions, computing the relative PLV differences between conditions, and repeating this procedure 1000 times. The observed data were then compared to this null distribution to estimate a p value. The results were depicted as hive plots to visualize the magnitude of the PLV and the associated p values among pairs of electrodes[132].

To test the regional specificity of this phase coupling effect, an ANOVA analysis with pairwise comparisons was conducted to test differences between hippocampal sub-regions using the R statistic toolbox. First, the Shapiro-Wilk test (function Shapiro.test) was conducted to test whether the data were approximately normally distributed. Second, the homogeneity of variances was tested using Bartlett's test (function Bartlett.test). Then the pairwise comparison was computed using the function pairwise.t.test. In addition, to further address the continuous consistency of the phase relationship between the amygdala and hippocampus, the PLV spectra were created as a function of frequency (1 to 30 Hz) for all BLA and hippocampal electrode

pairs averaged across all subjects for each condition and the difference was calculated by subtracting neutral from aversive condition and z-score normalized. A 5th order spline interpolation was implemented (spapi.m in Curve fitting toolbox from MATLAB) to smooth the curve of PLV difference spectra.

Phase amplitude coupling (PAC). Based on the previous phase coupling analysis, we analyzed the phase amplitude coupling between the amygdala-hippocampal electrode pairs that exhibited the most significant PLV in each patient. To extract the directionality information from these electrode pairs, the relationship between lower-frequency (1-30 Hz; delta, theta, alpha, beta) phase from electrode i and higher frequency (30-250 Hz; including high gamma) amplitude from electrode j was examined individually for each condition by calculating the circular linear correlation between the instantaneous phase of low frequency oscillations and the instantaneous phase of high frequency activities[133].

$$\rho_{\phi_a} = \sqrt{\frac{r_{ca}^2 + r_{sa}^2 - 2r_{ca}r_{sa}r_{cs}}{1 - r_{cs}^2}} \qquad (1.3)$$

Where $r_{ca} = c(cos\phi_{\theta i}[n], a_{\gamma j}[n])$, $r_{sa} = c(sin\phi_{\theta i}[n], a_{\gamma j}[n])$ and $r_{cs} = c(sin\phi_{\theta i}[n], cos\phi_{\theta j}[n])$ with $c(x, y)$ equal to the Pearson correlation between x and y, $\phi[n]$ equals to the instantaneous phase from modulating signal, and $a[n]$ equals to the instantaneous analytic amplitude from modulated signal. To compare the significance of the difference between correlation coefficients ρ_1 and ρ_2, we applied Fisher's z-transform to normalize correlation coefficients such that $z_\rho = \frac{1}{2}\log\left(\frac{1+\rho}{1-\rho}\right)$, and calculated the difference $\Delta\rho_z = z(\rho_1) - z\,(\rho_2)$[134]. The permutation test described for the previous analyses was also

used here to create a null distribution of PAC differences between two conditions for each electrode pair. Then the z-PAC was defined as the z-score of the real difference in PAC between the two conditions based on the distribution of phase-amplitude coupling values obtained from these null distributions with the positive value indicates PAC increase in the aversive condition vs. neutral condition.

Phase-amplitude coupling with time lag. As the communication between the modulating and modulated signal builds, the carrier oscillation is likely to appear first in the modulating signal. In other words, immediately preceding the synchronization between two signals, the 'driver' signals should be predictive of the 'receiver' signal. To probe the direction of functional coupling and to further explore how the neuronal dynamics in low-frequency and gamma bands interact, we examined the PAC magnitude as a function of the time lag between modulating and modulated signals. A diagram of the data processing steps is shown in Supplementary Fig. 12. The cross-regional PAC was calculated using the same algorithm as outlined in the PAC analysis section but with different time lags (in 10 ms intervals for the total duration range of ±200 ms) by shifting one signal relative to the other one.

Power spectral density (PSD) of the high gamma envelope. The goal of this step was to identify rhythmic fluctuations present in the higher-frequency power time series. We tested the assumption that if the power time series within the higher-frequency band are synchronized with a lower-frequency oscillation, the power time series will not be constant over time but instead will fluctuate at the specific lower oscillation frequency[135]. For example, if a signal banded at 80 Hz is synchronized with a 6 Hz oscillation, the power time series of the 80 Hz

might itself oscillate at 6 Hz. To test this hypothesis, we first selected the subject-specific high-frequency band centered at the frequency with the strongest PAC and bandwidth of 40 Hz. Then, the PSDs of the selected high-frequency bands were calculated using the same methods as described in Methods ('Power spectral density and subject-specific low-frequency band' section).

Theta-trough locked averaging of time–frequency plot. A theta-trough locked time–frequency averaging plot for a single subject was created to demonstrate the oscillatory features of the underlying signal5. To create the tracing in the lower panels of Supplementary Fig. 9 (see APPENDIX A), the raw signal from the amygdala/hippocampus was first filtered within subject-specific low-frequency band (5.8–9.8 Hz for this subject) using the same FIR filter parameters as described in the Methods ('Frequency decomposition' section). By applying the Hilbert transform, the phase at each time point was extracted from the filtered data within $(-\pi, \pi]$, where π radians corresponded to a theta trough and 0 radians corresponded to a theta peak (cosine phase). Then, the signal was segmented into 1 s epochs centered at the theta troughs, which were identified as the local minima of the phase less than $(-\pi + 0.01)$ and the theta-trough locked ERP were generated by averaging across all epochs. For Supplementary Fig. 9 upper panel (see APPENDIX A), a set of normalized instantaneous power time series from the hippocampus/amygdala was constructed, with center frequencies ranging from 1 to 250 Hz. To facilitate comparisons between different frequency bands, the band-pass filtered signals within the specific frequency range were first normalized by subtracting the temporal mean and dividing by the temporal s.d. The normalized instantaneous power time series were generated by applying the Hilbert transform and taking the square of the extracted amplitude time series.

These power series were then segmented into the epochs centered on the corresponding theta trough (Supplementary Fig. 9 lower panel, see APPENDIX A), P values for each time point in each frequency band were calculated using the non-parametric permutation test described in Methods ('High gamma activity' section).

Phase slope Index (PSI). As an index of dominant unidirectional interaction[136], PSI indicates the direction of coupling between two systems. Given a pre-specified bandwidth parameter, it reflects the change of phase difference between neighboring frequency bins, weighted with the magnitude of the coherence. Based on the assumption that independent sources do not contribute to the imaginary part of the cross-spectrum, the PSI is defined as:

$$\widetilde{\Psi_{\iota,J}} = Im\left(\sum_{f\in F} C^{*}_{i.j}(f)C_{i,j}(f+\delta f)\right), F = (v-\frac{\beta}{2}, v+\frac{\beta}{2}) \qquad (1.4)$$

where $C_{i,j}(f) = \frac{S_{i,j}(f)}{\sqrt{S_{i,i}(f)S_{j.j}(f)}}$ is the complex coherence, $S_{i,j}(f) = \frac{1}{N}\sum_{n=1}^{n=N} z_i(f,n)z_j^{*}(f,n)$ is the cross spectrum between two time series, v is the center frequency of the targeted frequency range, and Im denotes the imaginary part. We use β as the bandwidth for which the phase slope is calculated and choose it to be 8 times of the frequency resolution δf [137]. For example, when calculating directionality for a phase modulation centered at 8 Hz rhythm with a 1 Hz frequency resolution, a phase slope estimated between 4 and 12 Hz is reasonable ($\beta = 4\,Hz$). To understand interaction and directionality between the signals involved in cross frequency coupling, we segmented the phase of modulating signal and the power envelope of modulated signal into N epochs and used them as inputs to calculate the PSI for both aversive and neutral conditions. As the interactions between modulating and modulated signals require

certain amount of time, and if the speed at which these waves travel is similar, the sign of the PSI informs about which signal is temporally leading the other one. In other words, when the phase differences between the 'sender' and 'recipient' signal increase with the corresponding frequencies, a positive slope of the phase spectrum is expected. By performing the PSI analysis with a sliding window of 100 ms, spaced at 25ms (75% overlap), we were able to track the switching of the directionality between two signals at each time point. To assess the statistical significance of PSI, we applied the analogous non-parametric approach as described above by randomly shuffling the trials within a condition. Then the PSI null distribution was created at each time point, and the 99.5th percentile threshold was defined for each condition separately.

Granger causality. To further investigate interactions between brain regions, we computed spectral Granger causality using the Multivariate Granger Causality (MGVC) Matlab Toolbox[138]. Granger causality represents how much introducing past measurements from a first time series can decrease the variance of the prediction error for a second time series at the current time point. Spectral Granger causality extends this analysis to the frequency domain[139]. The time-domain data was first low-pass filtered at 85 Hz and then down-sampled to 250 Hz before fitting to an autoregressive model and computing spectral Granger causality. The model order m was determined by the Akaike information[140], which is a tradeoff between sufficient spectral resolution and over-parameterization. Model orders were estimated for each patient and varied from 7 to 13. The Granger index was computed using the first 1500ms from each clip as trial realizations. To further address whether this directionality was task specific, the null hypothesis distributions of spectral Granger causality for each condition were created by randomly swapping clip segments between channels. The spectral Granger causality was

considered significant if they exceeded the 99% confidence interval of this null hypothesis distribution. To further test whether the Granger causality is significantly different between conditions, the null difference time series were computed by subtracting the Granger time series from the aversive condition and the ones from neutral condition, which were calculated by randomly flipping the segments between conditions. Then for each frequency point, there were two Granger values as the upper or lower range of the 99% confidence interval, where 98% of the null Granger difference time series were either less or greater than these values. It shows a greater Granger for aversive condition compared to the neutral one if the real difference line is above the upper confidence interval while the neutral condition has a stronger Granger if the real difference line is below the lower confidence interval.

2.3 Results

2.3.1 Experiment design and electrode localization

We recorded oscillatory activity in local field potentials (LFPs) from nine human participants with intracranial depth electrodes implanted into the amygdala and the hippocampus. Electro-oculogram (EOG) electrodes and an eye tracker were used for one subject to evaluate the potential influence of saccadic muscle movements on neural signals. We examined neuronal responses while individuals watched aversive movie clips containing blocks of dynamic fearful faces and neutral movie clips of landscapes (Figure 2.1a). We employed dynamic fearful faces as a form of aversive stimuli, rather than static facial expressions, to provide participants with temporal cues that mimic real-life social exchanges[141]. The localization of depth electrodes was determined based on co-registered pre- and post-implantation

magnetic resonance imaging (MRI), as well as registration to a high-resolution anatomical atlas, labeled with medial temporal lobe regions of interest. Localization of each electrode was performed in a semi-automated manner, guided by the anatomical atlas and visually checked by an experienced rater (S.L.L.). In all subjects, there were two to three depth electrodes located in the BLA and one to three electrodes located in the hippocampus (dentate gyrus (DG)/CA3 or CA1, Figure 1.1b and Supplementary Fig. 1, see APPENDIX A). A three-dimensional rendering of the amygdala and hippocampus showed that for all subjects, the electrodes were located in the basal aspects of the amygdala and the anterior hippocampus (Figure 1.1c).

2.3.2 Local power and event-related potentials

Neuronal networks typically demonstrate activity in several oscillatory bands that cover both low- and high-frequency spectra with distinct roles in neuronal communication21. Whereas high gamma band activity is a spatially precise measure of local neuronal population spiking16, temporal synchronization of low-frequency phase is thought to mediate inter-regional communication[142]. Therefore, we first determined the spectral specificity of low- and high-frequency oscillations in LFP. The power spectral density (PSD) plots revealed that each subject had a specific frequency peak in the theta/alpha and high gamma frequency ranges (Figure 2.1d). These peaks are thought to reflect coherent oscillatory processes[143]. We then band passed the raw LFP signal to extract separate frequency components. These analyses showed that the low frequency of the amygdala and high gamma band power envelope of the hippocampus tended to co-occur in time during the aversive condition (Supplementary Fig. 2, see APPENDIX A). Additional analyses demonstrated that event-related potentials (ERP;

Supplementary Fig. 3, see APPENDIX A) and ocular muscle activity (Supplementary Figs 4 and 5a,b, see APPENDIX A) did not contaminate the neural signals used in subsequent analyses.

2.3.3 Amygdala and Hippocampus High Gamma Activities

We explored the temporal profile of the oscillatory response to fearful faces vs. landscapes. Electrodes localized in the amygdala (BLA) and hippocampus (DG/CA3 + CA1) with high resolution MRIs as shown in Figure 2.1c were included in the analysis. We then focused on the temporally resolved changes in high gamma amplitude and examined the coordinated timing of amygdala and hippocampus neuronal responses during the processing of aversive compared to neutral stimuli (Figure 2.1d). The onset time was defined as the earliest time point at which two conditions showed a significant difference in high gamma amplitudes; the peak time was defined as the temporal latency of the maximum magnitude of differences in high gamma amplitudes for each condition. The average high gamma amplitude across trials was higher for the aversive relative to the neutral condition after 123 ± 18 ms (mean ± standard error of the mean, s.e.m.) in the amygdala and after 241 ± 22 ms in the hippocampus post-stimulation onset (onset time, t-test, $p < 0.05$). Similarly, high gamma amplitude peaked earlier in the amygdala compared to the hippocampus (amygdala: 493 ± 31 ms vs. hippocampus: 641 ± 42 ms; peak time, t-test, $p < 0.05$). These findings indicate that the amygdala and hippocampus are both engaged in the early stages of salience processing, with amygdala activation preceding hippocampal activation.

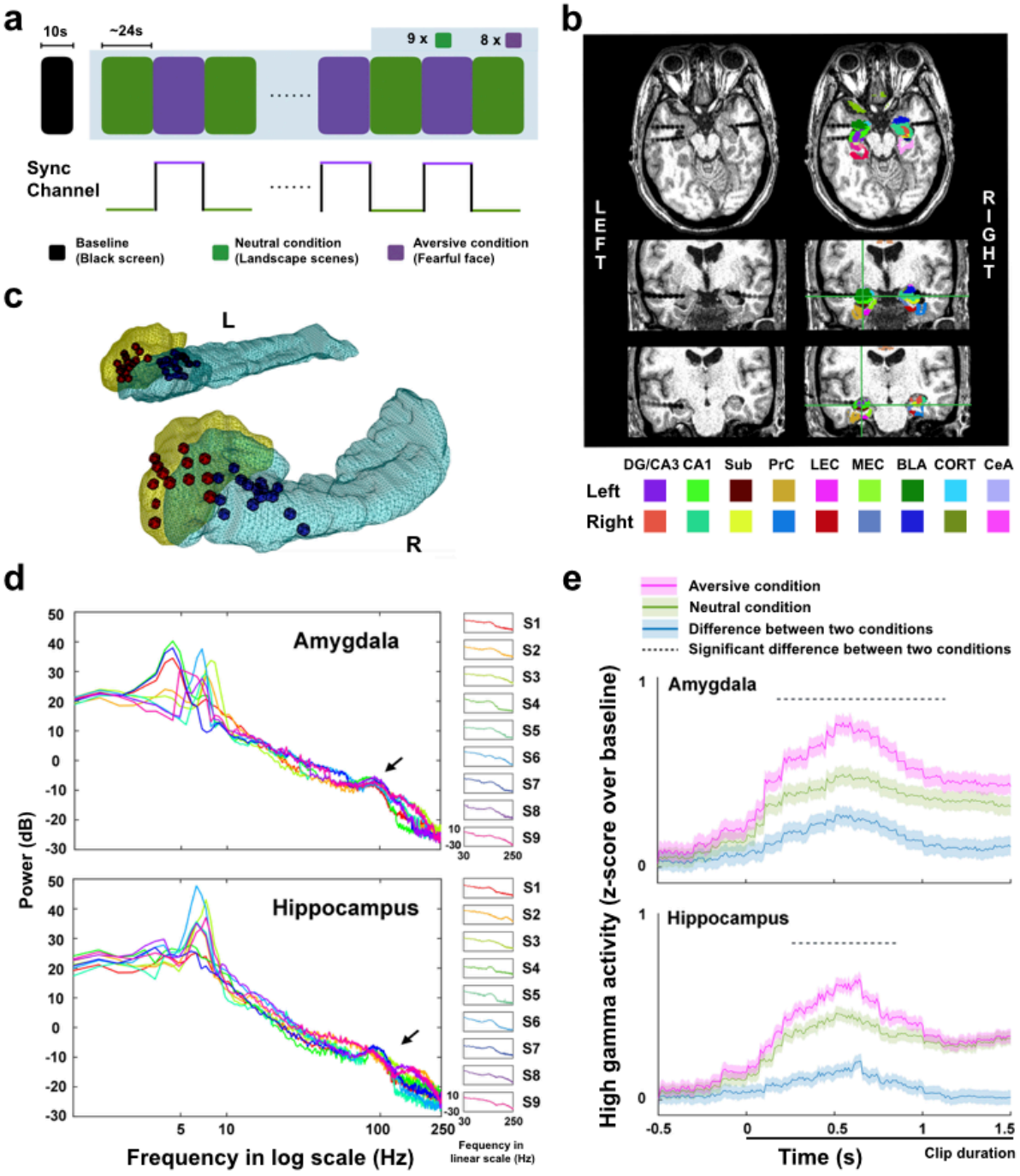
a
10s
~24s
9 x
8 x
Sync Channel
Baseline (Black screen)
Neutral condition (Landscape scenes)
Aversive condition (Fearful face)
b
LEFT
RIGHT
DG/CA3 CA1 Sub PrC LEC MEC BLA CORT CeA
Left
Right
c
L
R
d
Amygdala
Hippocampus
Power (dB)
Frequency in log scale (Hz)
Fequency in linear scale (Hz)
S1
S2
S3
S4
S5
S6
S7
S8
S9
e
Aversive condition
Neutral condition
Difference between two conditions
Significant difference between two conditions
Amygdala
Hippocampus
High gamma activity (z-score over baseline)
Time (s)
Clip duration

Figure 2.1 Task, electrode locations, power spectral density, and high gamma activity. (a) Participants watched silent movie clips consisting of alternating blocks of neutral (landscapes) and aversive stimuli (fearful faces). (b) Example MRI and template for a single subject. 1-3: Electrodes were localized in each participant using co-registered pre-implantation and post-implantation structural T1-weighted MRI scans. 4-6: A high-resolution template of the hippocampal subfields and amygdala nuclei was aligned to each participant's pre-implantation scan to visualize electrode locations in subject-specific anatomical space. Regions of interest (ROIs) in the medial temporal lobe included the dentate gyrus (DG)/CA3, CA1, subiculum (Sub), perirhinal cortex (PrC), lateral and medial entorhinal cortex (LEC, MEC), parahippocampal cortex (PhC), basolateral amygdala (BLA), central nucleus of the amygdala (CeA), and the cortical nuclei of the amygdala (CORT). Each electrode location was determined by selecting the center of the electrode (indicated by cross-hairs) and determining which ROI best encompassed the center of the electrode. (c) Electrode localization of all subjects, rendered onto a three-dimensional amygdala and hippocampus model based on the high-resolution template. Red dots indicate electrodes in the amygdala; blue dots denote electrodes in the hippocampus. (d) Power spectral density (PSD) in log scale for amygdala (upper panel) and hippocampus (lower panel). Peaks within theta (4-7 Hz)/alpha (8-12 Hz) and high gamma range (70-180 Hz) were consistently observed through all subjects. The black arrow denotes the power increase in the high gamma range, which is also shown for each individual subject on a linear scale (30-250 Hz) in the small plots. (e) High gamma amplitude (70-180 Hz), averaged across participants (± s.e.m. shown as shading around the mean trace) and locked to stimulus onset, is shown for electrodes located in the amygdala and hippocampus (DG/CA3 + CA1). Dotted lines represent significant differences between fearful face and landscape conditions (permutation test, see methods).

2.3.4 Amygdala-Hippocampal Low Frequency Phase Coupling

Given the distinct high gamma temporal profiles of the amygdala and hippocampus, we then investigated whether these two regions interact through low frequency phase coupling. The inter-regional coordination was examined with phase locking values as a metric of effective connectivity between electrodes targeting the amygdala (red) and hippocampus (blue, Figure 2.2). The three most medial electrodes targeting the amygdala and four most medial electrodes targeting the hippocampus were included in the phase coupling analysis. Note that this selection criterion was agnostic with regard to the experimental conditions (i.e. aversive vs. neutral) and the magnitude of phase coupling. Due to individual differences in the frequency of the event-related low frequency band[144], we first selected a specific band for each subject centered on the low frequency peak in the power spectrum density plot (Amygdala = 6.02 ± 0.49 Hz; hippocampus= 6.51 ± 0.16 Hz, mean ± s.e.m., Figure 2.1d) with a bandwidth of 4 Hz.

We characterized the timing relationships of the low frequency phase among all electrode pairs for each subject and calculated the phase locking value within and between the aversive and neutral conditions. Within each condition, amygdala-hippocampal phase locking values were significantly increased compared to the null distribution (all $p < 0.05$, permutation test, Supplementary Fig. 6, see APPENDIX A). We next tested differences of phase locking values across conditions and found enhanced phase locking values between the low frequency phase of BLA and the low frequency phases of DG/CA3 as well as CA1 hippocampal subfields while viewing aversive compared to neutral movie clips (all $p < 0.05$, permutation test, Figure 2.2).

To validate the role of low frequency phase coupling in coordinating amygdala-hippocampal network communication during processing of motivationally salient information, we examined the phase locking value spectra of the most significant phase coupled electrode pairs (denoted by an asterisk in Figure 2.2). Across all subjects, the phase locking value increased when viewing aversive fearful faces compared to neutral stimuli (main effect: $F(1,67) = 8.88$, $p = 0.004$) and peaked in the low frequency band for BLA-CA1 and BLA-CA3 compared to BLA- parahippocampal and BLA-subiculum electrode pairs (Supplementary Fig. 7a, see APPENDIX A). Further, the magnitude of low frequency PLV varied among hippocampal sub-regions ($F(3,67) = 2.88$, $p = 0.042$) with the highest PLV observed for the BLA-CA1 electrode pairs. The phase coupling between BLA and CA1/CA3 were significantly greater than the other hippocampal sub-regions (t-test, $p<0.05$; Supplementary Fig. 7b, see APPENDIX A). These findings indicate that the amygdala and CA1/CA3 regions of the hippocampus exhibit strong low frequency synchrony during processing of aversive stimuli.

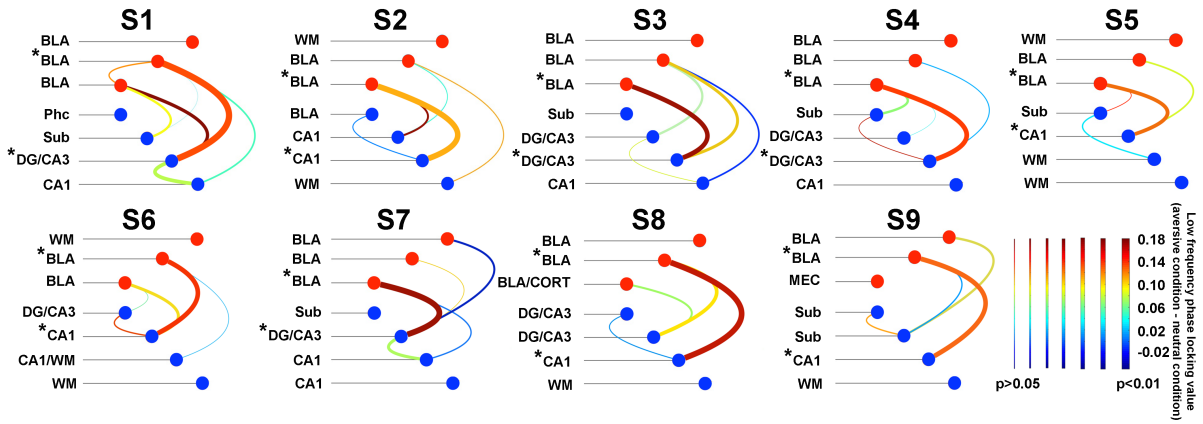

Figure 2.2. Differences in amygdala-hippocampal low frequency phase coupling. Low frequency phase coupling differences (aversive - landscapes) for pairs of electrodes targeting the amygdala (red dots) and hippocampal subfields (blue dots), depicted with hive plots. Differences in the phase locking values (PLV) between aversive and neutral conditions are presented in color, with warmer colors indicating a greater magnitude of the contrast. Significance levels derived from permutation testing are indicated by the thickness of lines connecting each electrode pair. Asterisk represent electrode pairs with the most significant PLV that were used for directional coupling analyses in Figure 2.3 and 2.4.

2.3.5 Amygdala-Hippocampal Phase-Amplitude Coupling

On the basis of the strong low-frequency phase coupling between the amygdala and hippocampus across all subjects, we then examined the directional influence of these responses with phase-amplitude coupling (PAC) across the two structures. To accomplish this, we again restricted our analysis to the most significant low-frequency phase coupling electrode pairs from the PLV analysis. Given that the electrodes with significant local PAC are more likely to engage in inter-regional coherence[145,146], we first found that PAC within both the amygdala and the hippocampus was increased when viewing aversive stimuli compared with neutral stimuli (Supplementary Fig. 8, see APPENDIX A). We then examined the directional PAC between the amygdala and hippocampus in the aversive condition compared with the neutral condition (Figure 3.3a). We found that the HG amplitude in the hippocampus was phase locked to the amygdala low- frequency rhythms (all $P < 0.01$, permutation test, Figure 3.3a). The stronger

coupling between the amygdala low-frequency phase and the hippocampus HG power was also observed in the theta trough-locked averaging of time–frequency plot in the aversive condition ($P < 0.05$, Supplementary Fig. 9a, see APPENDIX A), while this modulation was nearly absent when examining the reverse direction (for example, HG amplitude in the amygdala phase locked to the phase of hippocampal low-frequency activity (Figure 3.3a and Supplementary Fig. 9b, see APPENDIX A).

We also examined whether the PAC varied as a function of the time lag between low-frequency and HG signals. We posited that an amygdala to hippocampus directionality would result in a conduction delay[142], which would translate to a relative phase shift between low-frequency and HG oscillations (Supplementary Fig. 12, see APPENDIX A). Specifically, an earlier phase of amygdala low-frequency oscillations entraining hippocampal HG would result in the strongest PAC. We found that in the aversive condition, PAC between low frequency of the amygdala and HG of the hippocampus peaked around zero time lag (-13.15±2.92 ms versus hippocampus to amygdala directionality 13.52±22.83 ms), with 7 out of 9 subjects demonstrating that the amygdala low-frequency was leading the hippocampal HG (Figure 3.3b, denoted by "+" near the red line, Pearson's χ^2-test = 6.73, $P = 0.035$). In contrast, PAC between amygdala HG and hippocampus low-frequency was lower and failed to demonstrate a consistent peak at any time lag.

Since spectrally broad transients such as evoked activity can produce spurious PAC results[147], we examined the spectral specificity of the modulated HG activity from the PAC results. To identify the rhythmic low-frequency fluctuation of the higher- frequency power time

series, we determined the center frequency of the HG signal from the PAC and filtered the raw signal within the HG band to extract the analytic amplitude of the signal (that is, envelope), which was then subjected to the PSD analysis. All subjects showed individual narrow-band low-frequency (4–12Hz) peaks in the gamma envelope, thus supporting oscillatory properties of a separate low-frequency modulating signal in the HG band (Supplementary Fig. 10, see APPENDIX). To examine the potential influence of eye movements on the PAC results, we ran an independent component analysis (ICA) on the EOG combined with white matter referenced amygdala and hippocampal activity in one participant (subject 9)[126]. Components composed of EOG activity (three components, based on mixing weights, Supplementary Fig. 4f, see APPENDIX A) were removed from the raw intracranial data and all analyses were re-run with this 'cleaned' data. The observed PAC effect remained significant after ICA correction (Supplementary Fig. 11, see APPENDIX A). Further, there was no significant PAC between EOG channels and the amygdala as well as the hippocampus (Supplementary Fig. 5c,d, see APPENDIX A). These findings indicate that eye movement contamination did not contribute to the original results.

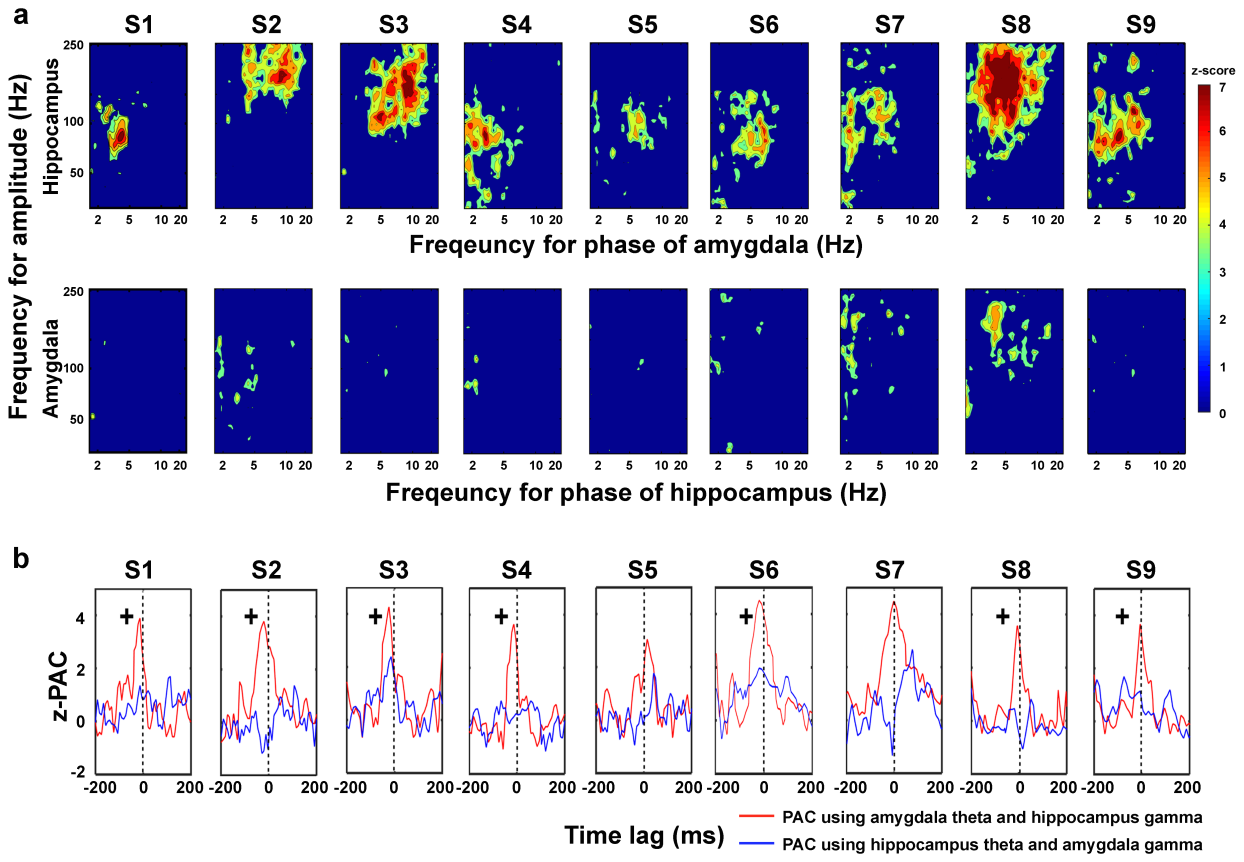

Figure 2.3. Amygdala-hippocampus directional phase amplitude coupling (PAC) and phase lag analysis. (a) PAC comodulogram for differences between the aversive and the neutral conditions is shown, with warmer colors denoting higher z-scores. The high gamma amplitude in the hippocampus was phase-locked to the phase of amygdala low frequency (theta and alpha) rhythms (all $p < 0.01$, permutation test). In contrast, the reciprocal directional PAC modulation (e.g. high gamma amplitude in the amygdala phase-locked to phase of hippocampal low frequency activity) was nearly absent. (b) Phase lag analysis. The PAC modulation index between low frequency phase and high gamma amplitude was estimated across time lags for the aversive condition. The red line represents the z-PAC between subject-specific amygdala low frequency phase and hippocampal high gamma amplitude (70-180 Hz). The blue line denotes the z-PAC between hippocampus low frequency phase and amygdala high gamma amplitude. Cross (+) denotes subjects who showed amygdala low frequency activity leading hippocampal gamma.

2.3.6 Granger Causality and Phase Slope Index

To further examine the directionality of the amygdala-hippocampal circuit, we utilized two complementary measures that rely on frequency and phase respectively: spectral Granger causality and phase slope index[136,137]. The Granger causality measure quantifies the strength of directional influences between local potentials in the frequency domain by testing whether the local potential from one structure (e.g. hippocampus) can be better predicted by incorporating information from the signal from the other structure (e.g. amygdala) and vice versa. Phase slope index quantifies phase difference as a function of frequency, with a positive phase slope indicating that the signal from the first structure is leading the signal from the second structure. In low frequency bands, we found significant Granger causal influence from the amygdala to hippocampus but not in the reciprocal direction (all $p < 0.01$, permutation test, Figure 4.4a, also Supplementary Fig. 13a, see APPENDIX A) only for the aversive condition. Significant differences between the aversive compared to the neutral condition were evident in 8 of 9 subjects (Supplementary Fig. 14, see APPENDIX A). The phase slope index analysis showed positive phase slopes from the amygdala to the hippocampus for the aversive compared to the neutral condition that remained significant between 0.58 and 1.16 seconds after stimulus onset (Figure 4.4b, also Supplementary Fig. 13b, see APPENDIX A). In the reverse direction, the phase slope index did not show a positive value and there were no differences between the two conditions. These findings provide converging evidence of the amygdala to hippocampus directionality during processing of motivationally salient information.

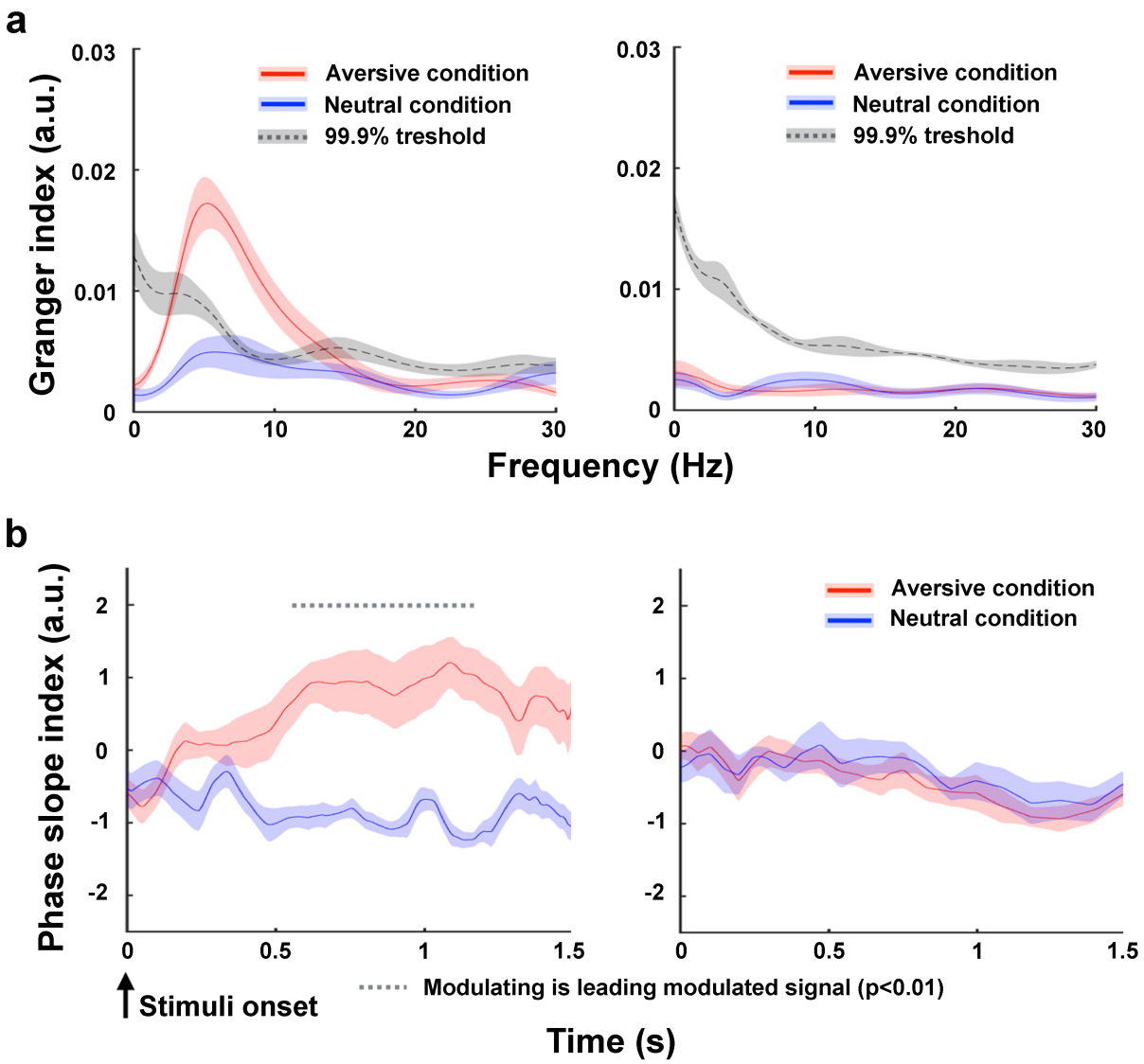

Figure 2.4. Granger causality analyses and phase slope index. (a) Granger causality analyses demonstrated consistently stronger influence for the amygdala-to-hippocampus direction (top row) than for the hippocampus-to-amygdala direction (bottom row) when contrasting the aversive to the neutral condition. The red and blue solid lines represent the real data from aversive and neutral conditions ± s.e.m., respectively. Dotted lines denote 99% confidence intervals for the null distribution. (b) Phase slope index (PSI) between the aversive and the neutral conditions calculated point-by-point across time using the low frequency signal from the modulating channel (colored in red) and high gamma signal from the modulated channel (colored in blue). Dotted lines above the graph denote significant differences between the two signals (all $p < 0.01$, permutation test), showing that low frequency activity from amygdala precedes hippocampus gamma for the majority of the stimuli duration.

2.4 Discussion

Here, we demonstrated that processing of motivationally salient stimuli depended on coordinated neural oscillations between the amygdala and hippocampus, two critical nodes in the emotion processing circuit. Prior works have suggested that the amygdala rapidly detects salient stimuli, whereas the hippocampus engages in contextual and mnemonic processing[57,148]; however, the nature of their interaction and timing remains unclear. The current findings showed that the interaction between the two structures was mediated by low frequency phase coherence and that this relationship was directional, with amygdala low frequency oscillations entraining hippocampal high gamma. Our results are robust across individual subjects and provide a mechanism by which the amygdala influences hippocampal activity during recognition and emotional memory of salient information. We were able to disentangle the temporal dynamics of the interaction between the amygdala and hippocampus during processing of aversive stimuli by demonstrating an earlier post-stimulus onset of high gamma activity in the amygdala (as early as 120 ms post-stimulus) relative to the hippocampus (around 240 ms post-stimulus). Overall, these findings showed that salient stimuli are processed with distinct temporal windows in the amygdala and hippocampus. The early amygdala activity observed in this study may reflect the fast automatic detection of motivational salience of information, while the later hippocampal onset may indicate formation or reactivation of emotional memory[57,148].

Previous research in affective processing using intracranial EEG recordings in humans has focused on either the amygdala or hippocampus, but the oscillatory mechanism mediating communication across the two structures has remained unclear. Using retrograde tracing techniques in monkeys' hippocampal formation, Amaral and Cowan demonstrated that labeled

neurons were found predominately in the anterior amygdaloid area, basolateral nucleus and periamygdaloid cortex[149]. The perirhinal and parahippocampal cortices have connections with the basolateral and accessory nuclei[150]. Although the primate tracing study could not provide anatomical specificity at the level of hippocampal subfields, rodent studies have shown that the ventral CA1 region and, to a lesser extent, CA3 receive the most robust amygdala inputs[151]. Our findings are consistent with these known anatomical connections.

We further demonstrated that amygdala-hippocampal interactions were predominantly mediated through low frequency coherence. Specifically, the phase locking value between the amygdala and hippocampus was enhanced when participants viewed fearful faces compared to landscapes. Given the long temporal window afforded by low frequency rhythms, the phase-phase coupling between different brain regions has been extensively studied in animal emotional research to understand the regulation of inter-regional communication. In rodent models, the degree of fearful memory retrieval[152,153] and its long-term consolidation[154] are directly related to the degree of theta synchrony across the amygdala and hippocampus, implicating synchronous low frequency oscillations as the neural correlate of fearful memory in the medial temporal network. Our study utilizing human intracranial EEG recording and precise medial temporal lobe subfield segmentation provides high-resolution temporo-spatial evidence for a similar oscillatory amygdala-hippocampal network in human salience processing and converges with the extant animal literature.

The directional influence of the amygdala onto hippocampus in anxiety and fearful emotional responses is increasingly recognized in animal models. Optogenetic manipulation of

this circuit has demonstrated that selective activation of BLA terminals within the ventral hippocampus increases anxiety-related behavior and reduces social interactions[10]. During contextual fear learning, enhancement of GABA neurotransmission in the BLA promotes hippocampal dendritic spine remodeling and fear retention, while blockade of GABA sites in BLA ameliorates these structural and behavioral effects[12]. In response to predatory threats, hippocampal place cells show unstable firing patterns and increased theta power, an effect that was prevented by lesioning of the amygdala[11]. Thus, the modulatory effects of the amygdala on the hippocampus for processing of fearful stimuli are supported by animal studies demonstrating downstream alterations in neurotransmission, structure, and electrophysiology. Our results provide confirmation of this directional modulation in humans and provide evidence that this modulation is controlled by neural oscillations. Specifically, amygdala low frequency activity modulates hippocampal high gamma via amygdala-hippocampal theta/alpha synchrony during detection of motivationally salient information, providing a mechanism for the computation of local and long-range communication. These findings have implications for understanding deficits in the processing of salient environmental events in neuropsychiatric disorders with altered oscillatory control[155].

There are several limitations in the current study. First, the two stimulus sets (fearful faces and landscapes) are inherently different in their properties. Thus, although we performed several analyses to show that evoked broadband activity did not influence the obtained results, potential contributions of evoked response could not be completely excluded. Second, the stimuli lacked neutral faces to contrast fearful faces and thus the differences between fearful faces and landscapes could be attributed to fearful content, emotion, facial expression, faces,

or other aversive stimuli. While our stimuli do not specifically address processing of fearful faces, contrasting fearful face movie clips with landscapes allows us to probe oscillatory mechanisms underlying processing of motivationally salient information. In accord with the recent literature highlighting a broader function of the amygdala, including processing of valence, emotion, and value, we believe that our findings would generalize to other stimuli with social or survival significance[156].

CHAPTER 3: Oscillatory Dynamics Facilitate Emotional Memory Discrimination

3.1 Introduction

Emotion is a powerful modulator of episodic memory. Emotional events are thought to generate arousal that facilitates remembering[157]. However, studies in humans have shown that the impact of emotion on memory is not always positive[15,17,158]. We often remember the emotional gist of the event but forget the details[16,21]. This asymmetric influence of emotion on gist versus detail memory can impair the discrimination of similar emotional experiences[22]. For instance, crime testimonies tend to focus on the weapon (e.g. the gun), while witnesses have impaired memory for the crime scene[17]. Although a number of theories have been proposed to explain how emotional memories are processed in the human amygdala-hippocampal circuit[148,159-161], the underlying neural mechanisms remain elusive. Prevailing models of emotional memory propose a division of labor in which the hippocampus plays a critical role in coding for overlapping events and minimizing interference[19,20], while the amygdala imparts emotional valence regardless of memory performance[162,163]. Given that these two regions are strongly connected via direct and indirect anatomical connections[44,45], it is likely that these two regions interact to modulate emotional memory. However, the mechanisms by which this interchange might occur to facilitate memory storage remain a mystery. In particular, the role of different brain oscillations in mediating this relationship is unknown.

A potential oscillatory mechanism to synergize the role of the amygdala and the hippocampus for emotional memory is frequency multiplexing of neural signals. It has been proposed that to rapidly organize information flow in real-time, computations across parallel

brain systems are carried out in distinct frequency bands to separate neural signals into different temporal channels. There is, however, little empiric evidence to support this oscillatory mechanism for emotional memory discrimination. Rodent and human electrophysiology studies have demonstrated that increased theta (4-7Hz) phase synchrony between the amygdala and hippocampus promotes cross regional communications during aversive memory retrieval and emotional processing[152,153,164]. On the other hand, scalp EEG and functional MRI studies have shown that alpha (8-12Hz) phase desynchrony and synchrony select or "gate" information in and out of the working memory system to influence behavior[165]. How theta and alpha oscillations dynamically interact within the amygdala-hippocampal circuit to determine success or failure of emotional memory remains unknown. Here, we test the hypothesis that the amygdala not only provides emotional valence but its cooperation with the hippocampus is essential for mnemonic discrimination of emotional events. As predicted by theoretical models of oscillatory multiplexing, successful mnemonic discrimination requires the synergistic engagement of theta phase synchrony and alpha phase desynchrony in the amygdala-hippocampal circuit.

To address these unanswered questions, we recorded intracranial stereo-electroencephalography (SEEG) simultaneously from the amygdala and the hippocampus while seven pre-surgical epilepsy patients performed an emotional memory recognition task[21] in which participants were asked to differentiate similar emotional scenes (Figure 3.1a). We observed that neural response in both the amygdala and the hippocampus are modulated by the emotional valence and the memory performance, which contraindicates the long-standing model that the amygdala simply transmits emotional valence to modulate hippocampal

memory. Our findings establish the oscillatory mechanisms by which the amygdala cooperates with the hippocampus to utilize two distinct frequency bands to facilitate intra- and inter-regional interactions, in which theta (3-7Hz) synchrony predict successful emotional memory discrimination and alpha (8-13Hz) synchrony predict incorrect memory. Bidirectional interactions between the amygdala and the hippocampus support emotional memory discrimination by temporally coordinating inter-regional theta phase and high gamma power. In contrast, unidirectional entrainment of alpha oscillations in the amygdala with high gamma power in the hippocampus at random phases leads to inaccurate memory recognition. Overall, these results demonstrate that discrimination of emotional memory engages reciprocal interactions within the amygdala-hippocampal circuit by sending success or failure signals via frequency specific oscillatory synchrony.

3.2 Materials and Methods

Participants. Data were obtained from 7 patients (4 Female, 3 Male, Age 21-58, Supplementary Table 1, see APPENDIX B) undergoing intracranial monitoring at the University of California, Irvine, Medical Center to localize epileptic foci for potential surgical resection. Intracranial depth electrodes (Integra or Ad-Tech, 5-mm inter-electrode spacing) were stereotactically implanted and the electrode placement was exclusively guided by clinical needs. Before testing, all subjects gave informed written consent in accordance with the Institutional Review Board of the University of California, Irvine. Patient selection was based on the following inclusion criteria: 1) having electrodes at both the amygdala and the hippocampus contralateral to the epileptogenic region; 2) having good task performance (accuracy rate above 0.7, Supplementary Table 1, see APPENDIX B).

Electrode localization. Electrodes were localized in each subject using co-registered pre-implantation and post-implantation structural T1-weighted MRI scans except S5, who has only post-implantation CT scans for electrode localization. First, we registered post-implantation scans to the pre-implantation scans using a six-parameter rigid body transformation (three rotations and three translations in x-z directions), which implanted in Advanced Normalization Tools (ANTs http:// stnava.github.io/ANTs). Then a high-resolution anatomical template (0.55mm) with labels of medial temporal lobe subfields[122] was applied to guide our localization for each electrode. The labeled template was resampled (1mm isotropic) and aligned to each subject's pre-implantation scans using ANTs Symmetric Normalization[117]. Based on the anatomical labels within each subject's space, the electrode location was determined by identifying the region of interest that encompassed the center of the electrode artifacts. The electrode localization results and also the selection of re-referencing electrodes within white matter were furthered reviewed by our neurologist (J.J.L.).

Experimental design and behavioral analysis. Participants were exposed to a series of images presented at the center of a laptop screen with the black background. The stimulus set was comprised of novel scenes freely available online. All the images were rated for emotional valence and similarity (scale from 1 to 8, with 1 indicating repetitions and 8 represents identical representations) in orthogonal experiments with separate samples. The detail information about the supplementary rating studies in the separate sample can be found in the previous paper from our group[21]. During the encoding phase, 148 images were presented in pseudorandom order and subjects were instructed to rate the emotional valence for each stimulus ('negative', 'neutral' or 'positive'). After a short delay (~1 minute), subjects were

exposed to 290 images mixed with target (repeated images, n = 54), lure (similar images, n = 97) and foil items (new images, n = 139). The lure items were roughly even distributed across emotion (NegLure = 33; NeuLure = 32; PosLure = 32) and similarity level (NegSIM = 6.29 ± 0.11; NeuSIM = 6.14 ± 0.12; PosSIM = 6.41 ± 0.08). During the test period, subjects were asked to identify whether each image has been shown in the encoding phase or not. Subjects need to make the response via key press within the 2 seconds time window and the trials where subjects failed to make a decision within the time period were excluded from the analysis. First, we evaluated subject's task performance by computing the accuracy rate, the fraction between the number of accurate trails over the total trial number within the test phase. Then we quantified their discrimination abilities by calculating the LDI, which was represented the difference of trial numbers between correct recognized lures and false rejected targets: $p('New'|Lure) - p('New'|Target)$.

Data acquisition and preprocessing. Stimuli were presented using PsychoPy2 (Version 1.82.01) software[166] on an Apple MacBook Pro, which was placed on the service tray at a comfortable distance in front of participants. An external Apple keyboard was used to capture subjects' responses. Intracranial EEG data were acquired using a Nihon Kohden recording system (256 channel amplifier, model JE120A), which are analog-filtered above 0.01Hz and digitally sampled at 5000Hz. After data acquisition, the preprocessing of raw data was conducted using customized MATLAB scripts. First, neural recordings were down sampled at 2000Hz and band-pass filtered between 1 to 250Hz using the zero phase delay finite impulse response (FIR) filter with Hamming window. Then power spectral density (PSD) was estimated using Welch's method (pwelch.m in Signal Processing Toolbox from MATLAB). Line noises

(usually 60Hz and its harmonics) inspected from PSD plots were removed via the multi-taper regression method[167]. Based on the localization results, all channels in the amygdala and the hippocampus were re-referenced to the nearest white matter electrodes on the same depth electrode probe. Then epileptiform discharges were manually inspected (visualized and marked using databrowser.m in FieldTrip[168]) under the supervision of a neurologist (J.J.L.), who was blinded to electrode locations and trial information (e.g. stimuli onsets and subject's performance). Notably, there were no seizures recorded in any subject while performing the task, and only the electrodes contralateral to the seizure onset zone were included for analyses.

Event-related potentials. We then segmented the preprocessed intracranial recordings into event-related epochs, including a 500ms pretrial baseline and a 2000ms time window after trial onset. The segmented data were zero-padded to minimize filter-induced edge effects and were low-pass filtered at 30Hz using a finite impulse response filter (eegfilt.m function in EEGLAB toolbox[128]). Task-induced ERPs were calculated within each condition (incorrect vs correct discrimination) by averaging across filtered epochs and absolute baseline correcting over the temporal mean of the pre-trial period. A two-sample t-test was performed to identify for each data point to determine the significant difference between conditions. To remove the potential contribution of signal components phase-locked to the trial onset (e.g. ERPs)[169], the cross-trial mean of raw LFPs were subtracted from each channel before further analysis[170].

Frequency decomposition and task-induced power. Time-frequency representations of power were computed for each event-related epoch, with FIR filtering between 1 to 250Hz through 28 logarithmically spaced frequencies. The adaptive bandwidths ensured precise phase

estimations within narrow bands of low frequency oscillations while a broader range of higher-frequency eliminated sideband effects and prevented spurious PAC[129]. We then applied the Hilbert transform (hilbert.m function in Signal Processing Toolbox from MATLAB) to extract analytic amplitude and phase for all filtered traces. The task-induced power was calculated by squaring the analytic amplitude envelope and was normalized to the pre-trial baseline using relative change in decibel conversion (dB). Results represented in Figure 3.2b were averaged across all the electrodes within amygdala and hippocampus individually for different conditions (correct versus incorrect discrimination; negative versus neutral valence) and normalized to the averaged baseline across all trials.

Inter-regional phase synchrony. The strength of inter-regional neural synchrony was quantified by the PLV[171], which calculates the phase θ differences between two channels (a, b) averaged across trials for a given time point t and frequency f:

$$PLV(t,f) = \frac{1}{Ntrials}\left| \sum_{n=1}^{n=Ntrials} \exp\left(i\left[\theta_{\square,a}(t,f) - \theta_{n,b}(t,f)\right]\right) \right|$$

It measures the degree of each electrode pair maintains the consistent phase relationship – independent of their absolute phases and amplitudes[170] - among repeated trials, with values approaching 1 referring to little variations across trials or strong phase synchrony between two channels. We performed the PLV analysis for each electrode pair, including one electrode from the amygdala and one from the hippocampus, within the processing period (2-second time window after stimuli onset). Then we grouped individual $PLV\ (t,f)$ spectrogram into different conditions (correct versus incorrect; negative versus neutral). To ensure that the observed inter-regional synchrony was not induced by the within region power differences, we

performed a stratification method[168,172] to trims trials with extreme power values. Thus, the PLV spectrograms were calculated using power-balanced trials across relevant conditions. To further eliminate the influence of ERPs and power differences, we tested the statistical significance for PLV using a cluster-based permutation test, in which a null distribution was created by randomly assigning trials into different conditions, computing the corresponding PLV spectrograms and repeating the same procedure for 1000 times. The results shown in Fig. 3a were depicted in P values ($P = 0.01$, observed data precedes 99% surrogate data), with warmer colors denoting stronger significance levels. For better visualization, the PLV spectrogram plots were smoothed using a cubic spline interpolation method (spline.m function in MATLAB).

Frequency-specific explained variance in PLV. We quantified task related information as the percentage variance in PLV at different frequencies bands across trials explained by each factor. Specifically, we performed an analysis of variance (ANOVA) to calculate the variances explained by the following task factors individually: subject's choice ('old' versus 'new'), task outcome ('correct' versus 'incorrect'), emotional valence ('negative' versus 'neutral'), arousal rating and similarity rating of stimuli. Since our investigated task factors were not orthogonal, for example, subject's choice and task outcomes were highly correlated ($R^2_{choice\ X\ outcomes} = 0.46, P = 10^{-12}$, Spearman rank correlation). Therefore, we computed an unbalanced ANOVA, in which PLV variance explained by each factor will be dissociable to other factors. We estimate the amount of PLV explained variance ω^2 by each factor s at specific frequency f [173]:

$$\omega^2_{(s,f)} = \frac{SS_{Between\ groups\ (s,f)} - df_{(s)} * MSE_{(s,f)}}{SS_{total\ (s,f)} + MSE_{(s,f)}}$$

$SS_{Between\ groups\ (s,f)}$ is the sum of squares between M groups, SS_{total} is the sum of squares total across N trials, $df = M - 1$ is the degree of freedom, and MSE is the mean squared error. To test the significance level of explained variance ω^2 and correct for multiple comparisons across frequencies, we used a cluster-based permutation test, which is similar as the one mentioned in the method section 'Inter-regional synchrony'. For each electrode pair, frequency and factors were randomly permuted across trials, which yield a distribution of ω^2 spectra under the null hypothesis of equal information explained by PLV. The significance threshold (gray dashed line in Figure 3.3c) was defined as the 99[th] percentile of the permuted ω^2 spectra.

Directional phase amplitude coupling. The PAC was computed for each amygdala-hippocampus electrode pair within the processing period (the 2-second time window after the stimuli onset) and was calculated as the phase coherence between the low frequency and low frequency filtered HFA[95,171]. The directionality within each electrode pair was quantified as Phase Slope Index (PSI)[136], which estimates the slope of the phase differences between the modulating (sender) and modulated (receiver) signals as a function of frequency. By applying the PSI to the phase of low frequency (f) oscillations and the amplitude envelope of high frequency (v) activities, the directional index can be defined as[137]:

$$\psi(f) = Im(\sum_{f-\frac{\beta}{2}}^{f+\frac{\beta}{2}} C^*(v,f)C(v,(f+\delta f)))$$

where $C(v,f)$ is the complex coherency as the normalized cross-spectra between two time series and Im denotes the imaginary part. Since the transmission between modulating and

modulated signal has a fixed time delay, the phase spectrum between these two signals will change systematically as a function of frequency[174,175]. In other words, when the phase differences increase with the corresponding frequencies, a positive slope of phase spectrum is expected, suggesting that low frequency phases lead the high frequency amplitude. On the other hand, a negative PSI refers to the opposite directionality. The statistical analysis of cross frequency PSI is similar as described in the method section 'Inter-regional phase synchrony', by randomly shuffling the trials for 1000 times. The PSI null distribution was calculated using shuffled low frequency phase and high frequency amplitude. The 99th percentile of the surrogate data was defined as the significant threshold. For better visualization, the PSI spectrogram plots were smoothed using a cubic spline interpolation method (spline.m function in MATLAB).

Granger Causality analysis. To further confirm the directionality between the amygdala and the hippocampus, we computed spectral Granger causality, which quantifies the prediction error of the signal in the frequency domain by introducing another time series[139,176]. Before fitting to the multivariate autoregressive model to compute the spectral Granger causality, the time series data from each amygdala-hippocampal electrode pair were low-pass filtered at 85 Hz, down-sampled to 250 Hz and normalized within each trial (e.g. subtracting the temporal mean and cross-trial mean). Then, we defined the model order using the Multivariate Granger Causality (MGVG) Toolbox based on the Akaike information criterion[140]. The model order for each subject varied from 8 to 15. The Granger Causality index was computed within the processing period (2-second time window after stimuli onset) for both directions (amygdala to hippocampus, hippocampus to amygdala). The significance analysis for Granger Causality is the

same method as described in the section 'Inter-regional phase synchrony' by randomly shuffling the trials for 1000 times. Then the Granger Causality null distribution was created and the 99th percentile of the surrogate data was defined as the significant threshold.

Pattern classification analysis. To test whether the occurring phase of HFA can decode different directional information (amygdala to hippocampus, hippocampus to amygdala), we performed a pattern classification analysis. The input of the classifier was the HFA occurring phase at the individual maximum modulating frequency (correct: theta band; incorrect: alpha band). The output of the classifier was the prediction of task outcomes for each high frequency event. Similar to the previous studies[177,178], we chose a linear classifier and convert phase values as a vector quantity in the complex plane, with cosine and sine of the phase referring to the real and imaginary part respectively. The classifier was calculated by determining the sums for correct and incorrect trials and taking the difference between them. Then, we projected the phase from new trial onto the classifier by taking the dot product in each direction:

$$q = \int_0^1 cos\,\theta(t)\left(\varphi_{real,incorrect}(t) - \varphi_{real,correct}(t)\right)dt$$

$$+ \int_0^1 sin\theta(t)\left(\varphi_{imag,incorrect}(t) - \varphi_{imag,correct}(t)\right)dt$$

We quantified the differences for the projections distributions between correct q_{CR} and incorrect q_{IC} conditions using the discriminability index d:

$$d = \frac{|\overline{q_{CR}} - \overline{q_{IC}}|}{\sqrt{\frac{1}{2}(\sigma_{CR}^2 + \sigma_{IC}^2)}}$$

A high value of d indicated greater classification ability between two conditions. We tested the significance based on the similar cluster-based permutation test and created a distribution of

pseudo discriminability indexes by randomizing the category labels (correct versus incorrect discrimination) associated with high frequency activities for 100 times. Observed discriminability index above the 95th percentile of the surrogate data was considered as significant.

3.3 Results

3.3.1 Emotion Interferes with Mnemonic Discrimination

We recorded local field potentials (LFPs) from seven pre-surgical epilepsy patients (3 males, 4 females, (see individual subject's information in supplementary table 1) with depth electrodes implanted in the amygdala (n = 15 electrodes) and the hippocampus (n = 19 electrodes). We examined neural responses while individuals performed memory recalls in which they reject similar but not identical scenes (lure items) or novel items (foils, Figure 3.1a). The localization of depth electrodes in the amygdala and hippocampus was determined based on co-registered pre- and post-implantation magnetic resonance imaging (MRI)/ computed tomography (CT), as well as registration to a high-resolution anatomical atlas, labeled with medial temporal lobe (MTL) sub-regions of interests (Figure 3.1b; Supplementary Fig. 1, see APPENDIX B).

All subjects were proficient at the task (average percent correct = 80%, range = 74% to 86%, Supplementary Table 1, see APPENDIX B). To quantify subjects' ability to discriminate similar stimuli, we calculated the lure discrimination index (LDI)[21] for each subject, operated as $p('New'|Lure) - p('New'|Target)$,), which corrected for the general tendency to reject items[179] (e.g. call an item 'New'). We found that subjects achieve a better discrimination score

for neutral stimuli compared to emotional ones (one-way ANOVA, F (2, 32) = 6.24, P = 0.0051), with diminished LDI for both negative and positive lures (post-hoc analysis: F (1, 32) = 10.45, P = 0.0028, critical Schefee = 6.32, Figure 3.1c). These results confirmed that patients' behavioral performance was similar to healthy subjects found in previous fMRI studies[22], with a comparable impairment level of mnemonic discrimination induced by emotional contents. To study the hippocampus' ability of separating overlapping events, we focused our analyses on the lure items during the retrieval phase while subjects were processing the stimuli (Figure 3.1a). Given that the behavioral effect of emotional modulation was maximally contrasted between the negative and neutral valence trials (Figure 3.1c), we compared the trials within these two types of emotional valence.

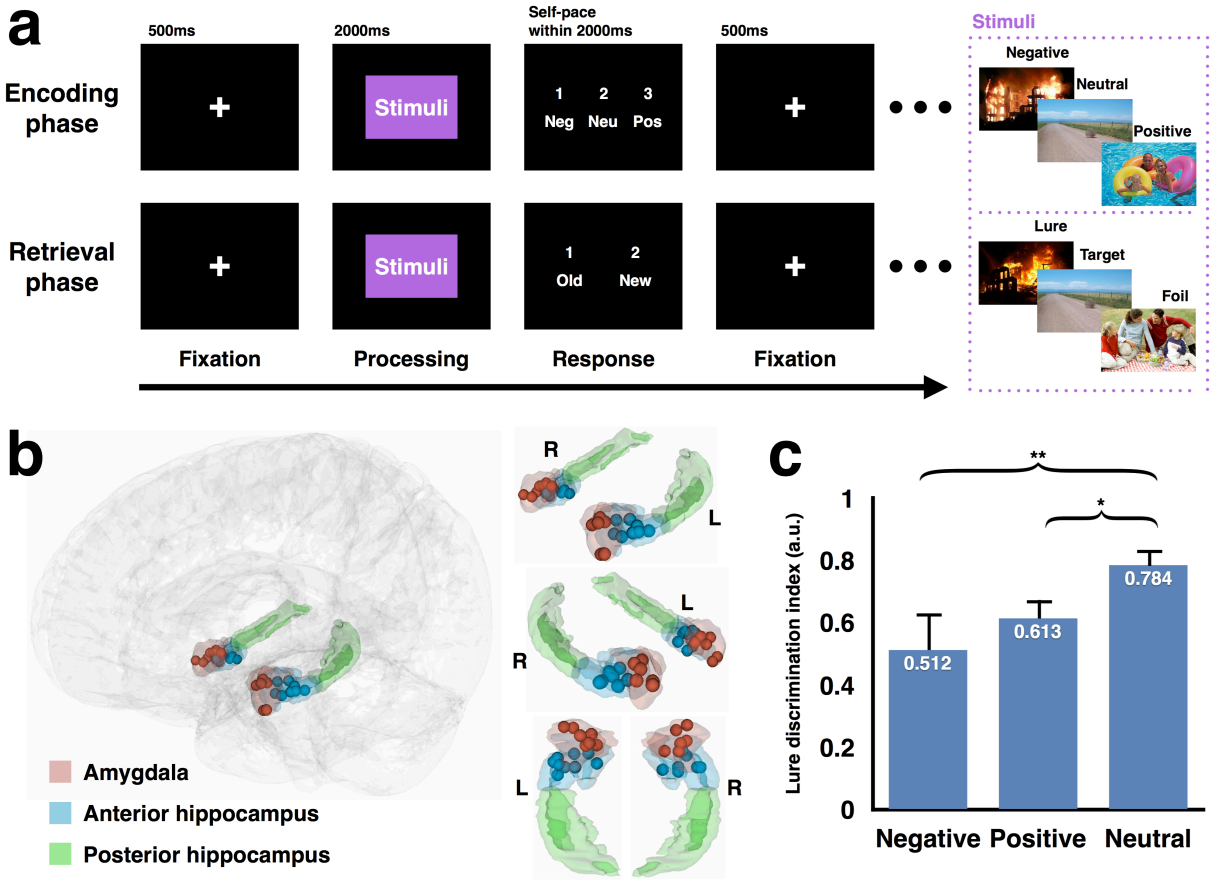

Figure 3.1 Experiment design, electrode locations and behavior results. (a) Mnemonic discrimination task with emotional stimuli. Each trial consists of three parts, including a 500-ms maintenance fixation period, followed by a 2000ms image display (processing period) and a self-paced response window up to 2000ms. During the encoding phase (upper), participants were cued to rate the emotional valence of each stimulus (Negative, Neutral, Positive). During the retrieval phase (lower), participants were cued to identify the same stimuli presented in the encoding phase as "old" or to reject similar but not identical scenes (lure items) and novel items as "new" **(b)** Electrode localization across 7 subjects, rendered onto a three-dimensional glass brain (gray) based on the high-resolution template, highlighting the amygdala (red), anterior hippocampus (blue) and posterior hippocampus (green). **(c)** Across all subjects, Lure Discrimination Index was significantly lower in negative and positive conditions compared to the neutral one. (* = *P<0.05*; ** = *P<0.01*).

3.3.2 Frequency Specific Oscillations Predict Task Performance

We compared neural responses of correct (correctly rejected lure items as 'new') and incorrect (incorrectly recognized lure items as 'old') discrimination trials. Examination of the amygdala and hippocampal raw LFP traces demonstrated slower low frequency oscillations during a correct compared to an incorrect discrimination trial (Figure 3.2a). We then examined conditional differences over the frequency and time by measuring the task-induced power changes in the amygdala and the hippocampus. Sustained low frequency oscillations and transient high gamma band activities were observed in both regions after the stimulus onset, with enhanced theta band power associated with correct trials (3-7 Hz, Figure 3.2b, top row, dashed rectangles) and increased alpha power linked to incorrect trials (8-13 Hz, Figure 3.2b, bottom row, solid rectangles). In addition, the hippocampus demonstrated a frequency-specific double dissociation, with diminished alpha and increased theta band power during correct discrimination and diminished theta and increased alpha band power during incorrect discriminations (Figure 3.2b). These frequency-specific band dissociations predicted behavior at the group level, emphasizing increased theta power and decreased alpha power in the hippocampus when comparing correct versus incorrect trials (Figure 3.2c, shaded regions, t-test, $P < 0.01$). Moreover, negative emotional valence amplified these frequency band specific power changes, augmenting theta (3-7Hz) power for correct negative valence trials and alpha (8-13Hz) power for incorrect negative valence trials. In particular, as shown in the single subject example (Figure 3.2b) and the group level analyses (Figure 3.2d), negative emotional valence enhanced power differences between correct and incorrect mnemonic discriminations. In particular, greater theta power was seen for correct trials compared to incorrect trials in the

hippocampus (Figure 3.2d, shaded region, t-test, $P < 0.01$). In contrast, stronger alpha power was noted for the incorrect trials compared to correct trials in the amygdala and hippocampus (Figure 3.2d, shaded regions, t-test, $P < 0.01$).

These frequency-specific dynamics were only evident in lure items and not in targets and foils (Supplementary Fig. 2, see APPENDIX B), suggesting that these spectral features were specific to mnemonic discrimination rather than a general error signal[180-182]. Moreover, such spectral features were only observed within anterior hippocampal electrodes; the conditional power differences between correct and incorrect discrimination and the influence of emotional valence were absent in the posterior hippocampal electrodes (Supplementary Fig. 3, see APPENDIX B). These results demonstrate that the human hippocampus is a functionally heterogeneous structure along its longitudinal axis with specialization for emotional memories in the anterior compared to the posterior hippocampus. To ensure that event-related potentials (ERPs) did not confound these spectral changes[183], we averaged LFPs for each electrode over the image-processing period within each condition and normalized to the pre-trial baseline. No significant conditional difference of ERPs has been shown in any electrode (t-test, $P > 0.05$). In sum, these results showed that the amygdala and the hippocampus both participate in mnemonic discrimination of emotional events, with theta and alpha bands served as distinct spectral fingerprints for successful versus unsuccessful memory. It also highlighted that emotional valence modulated mnemonic discrimination by enhancing power differences at these two distinct frequency bands in the amygdala and anterior hippocampus.

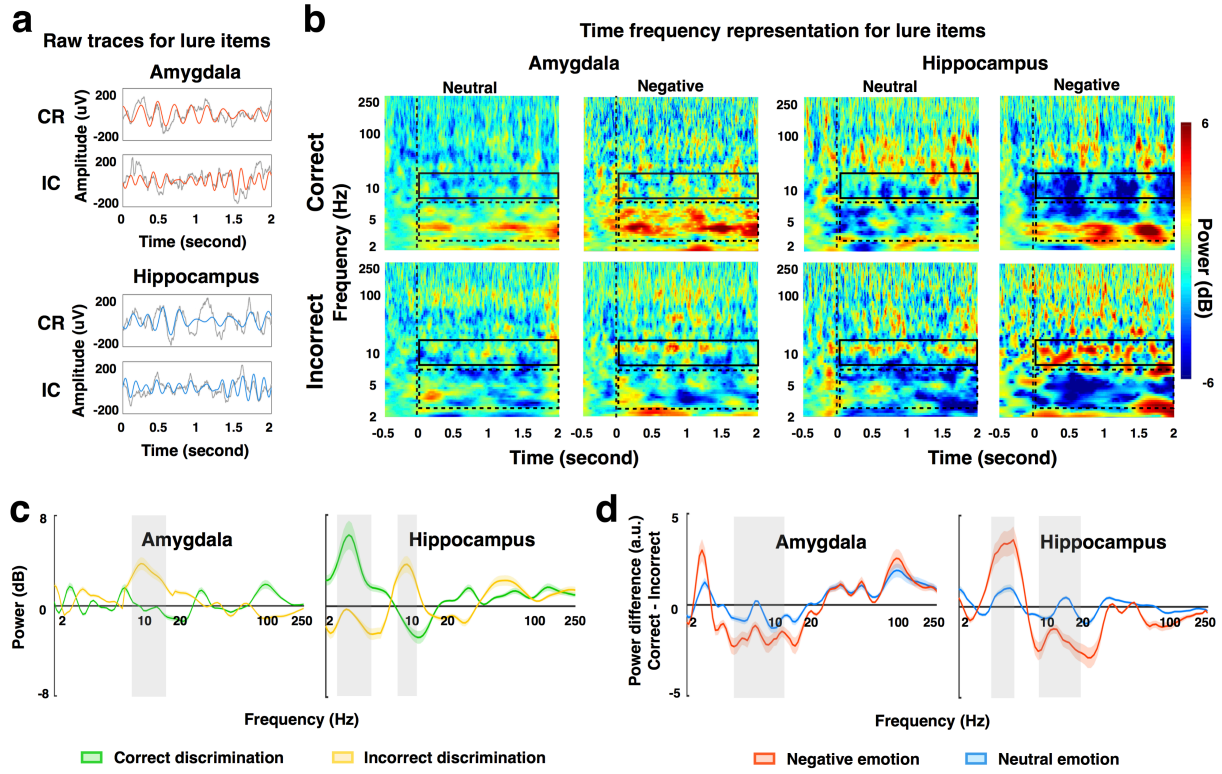

Figure 3.2. Task-evoked spectrotemporal power. (a) Example of local field potentials (LFPs) from a pair of electrodes in the amygdala (red) and the hippocampus (blue) from one subject with a correct (CR) and an incorrect (IC) trial. Gray lines represent raw LFPs and red/blue lines denote LFPs filtered within 3-12Hz. **(b)** Example of task-induced power from Subject 4 within the amygdala and the hippocampus normalized to common pre-trial baseline (500-ms fixation period) and grouped based on task outcomes (correct discrimination: upper row; incorrect discrimination: lower row) and emotional valences (neutral: left column; negative: right column). Warmer color denotes task-induced power increase from the baseline while the colder color refers to power decrease from the baseline. Dashed black lines indicate the stimuli onsets. Theta power change is highlighted using dashed rectangles while the alpha power change is emphasized using solid rectangles. **(c)** Averaged power of electrodes within amygdala and hippocampus across all subjects for correct (green) and incorrect (yellow) discrimination. Positive/negative values indicate increased/decreased power from the baseline, respectively. **(d)** Averaged conditional power difference (correct - incorrect) across all subjects within the amygdala and the hippocampus for different emotional valences (neutral: blue; negative: red). The shaded rectangles indicate the frequency bands demonstrating significant power differences between neutral and negative conditions (t-test, *P<0.01*). (shaded color area = ±s.e.m.)

3.3.3 Frequency Specific Synchrony Encodes Task Information

Given the task-related low frequency oscillations observed in the amygdala and the hippocampus and their important roles supporting inter-regional communications[114], we investigated low-frequency phase synchrony between these two brain structures. The cross-regional coordination was quantified with phase locking values (PLVs) as a metric of effective

connectivity between LFPs from each amygdala-hippocampal electrode pairs. We then averaged the PLV metrics across all the subjects and unfolded its spectral and temporal information with time-frequency plots. Since power differences can induce spurious PLV[184], all the phase synchrony analyses were performed within power-balanced trials to minimize the power effects (n = 735 trials) and survived statistical testing (permutation test, P <0.01, see method). We found that frequency-specific spectral features were observed in the amygdala-hippocampal inter-regional phase synchrony, with significant theta (~2-7 Hz) synchrony predicting correct discrimination and alpha (~8-16Hz) synchrony associated with incorrect discrimination (Figure 3.3a, permutation test, P< 0.01). In addition, within each condition, the amygdala-hippocampal theta/alpha synchrony increased with emotional valence (negative > neutral, t-test, P<0.01). Similar results remain consistent at the individual level, with 6/7 subjects demonstrating frequency switches of the peak amygdala-hippocampal synchrony from the theta toward the alpha band, paralleling the shift from correct to incorrect behavioral outcomes (Figure 3.3b, Ki-squared analysis = 18.24, P = 0.0057). Moreover, the strength of conditional PLV differences (correct discrimination – incorrect discrimination) served as a function of emotional valences, with increased PLV differences in theta and alpha bands for negative compared to neutral trials. These findings show that the frequency-specific oscillations found separately in the amygdala and the hippocampus also parsimoniously code for inter-regional interactions; enhancement of theta synchrony and the suppression of alpha synchrony in the amygdala-hippocampal circuit promote correct emotion-related mnemonic discrimination.

To confirm that different frequency bands carry distinct and dissociable task information, we quantified how synchrony between the amygdala and the hippocampus encoded different factors, including subject's choice ('old' versus 'new'), task outcome (correct versus incorrect), emotional valence ('negative' versus 'neutral'), arousal rating and similarity rating of stimuli. Information was quantified as inter-trial correlations between the amygdala-hippocampal synchrony (i.e., PLV) at different frequency bands explained by each factor[173]. All five types of information were measured independently and showed amygdala-hippocampal inter-regional synchrony carried task-related computations (Figure 3.3c). However, only task outcome, task choice and emotional valence revealed frequency-specific information with theta band carrying information for task outcome (%EV = 5.22, P = 0.00412, Rayleigh test) and task choice (%EV= 2.87, p= 0.0204), while alpha band encoded for emotional valence (%EV = 5.18, P = 0.00324, Rayleigh test). Encoding of arousal and similarity information did not show frequency band specificity. In sum, these results not only supported frequency-specific amygdala-hippocampal interactions during mnemonic discrimination, but also revealed their functional roles, with mnemonic discrimination facilitated by theta synchrony (task choice and outcome) and emotional valence communicated via alpha synchrony.

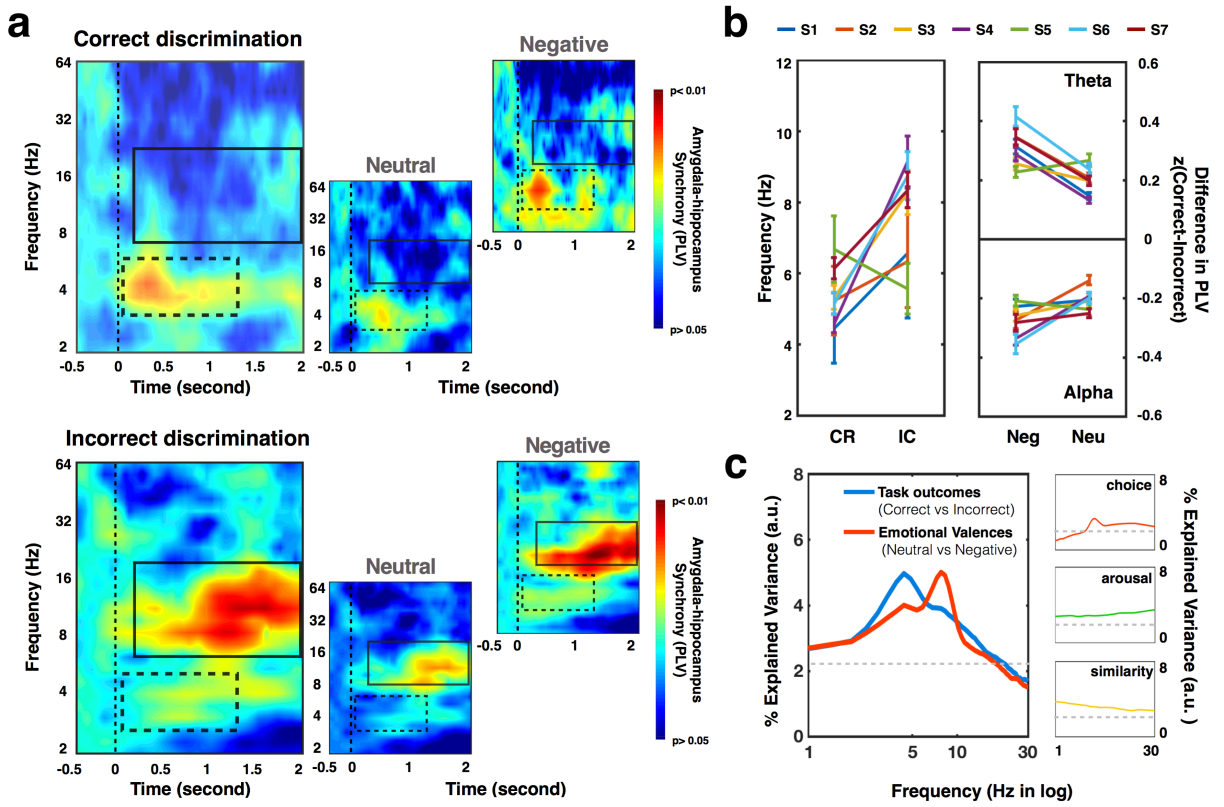

Figure 3.3 Amygdala-hippocampus theta/alpha synchrony carries the information of task outcomes and emotional valences, respectively. (a) Amygdala-hippocampus synchrony (PLV) was averaged across all subjects, with stronger theta-band synchrony (dashed rectangles) for correct (upper) discriminations and greater alpha-band synchrony (solid rectangles) for incorrect (lower) discriminations. As shown in the right column, increased theta (correct) and alpha (incorrect) synchrony has been observed in negative trials compared to the neutral ones. Black dashed lines indicate stimuli onsets; warmer colors indicate greater significance of real phase synchrony compared to the surrogate data using permutation test (see method). **(b)** Peak frequency of amygdala-hippocampus synchrony for each subject was coded in different colors, shifting from theta to alpha band when comparing between correct (CR) and incorrect (IC) discriminations (left panel). Conditional difference in amygdala-hippocampus synchrony (dPLV, correct - incorrect) was co-varied with emotional valences, with decreased theta synchrony and increased alpha synchrony for negative (Neg) trials compared to neutral (Neu) ones. **(c)** Average percentage of variance in amygdala-hippocampus synchrony accounted for different factors, including task outcomes (correct or incorrect), emotional valences of stimuli (negative or neutral), subjects' choices (yes or no), arousal and similarity ratings of stimuli. The horizontal dotted lines indicate significant thresholds ($P < 0.01$).

3.3.4 Directional Amygdala-Hippocampal Interactions and Phase-Dependent Encoding

On the basis of the strong low frequency phase synchrony in the amygdala-hippocampal network, we then examined the directional influence between these two regions. Phase amplitude coupling (PAC) has been recognized as an important mechanism to flexibly

coordinate inter-regional communications, with global phase synchrony dynamically modulating local activities simultaneously in time and space[110]. To determine the inter-regional influence between the amygdala and the hippocampus, we performed cross-region PAC in both directions (amygdala to hippocampus, hippocampus to amygdala) using the electrode pairs exhibiting the most significant low-frequency phase synchrony[164]. The inter-regional influence was quantified as the coherence between low frequency phases from one region (e.g. the modulating signal) and the amplitude of high frequency activities (HFA) from the other (e.g. the modulated signal). Frequency-specific fingerprints again emerged in inter-regional interactions between the amygdala and the hippocampus, with the bi-directional PAC modulated by theta phase for correct discrimination trials and the unidirectional influence from the amygdala to the hippocampus regulated by alpha phase for incorrect trials (Figure 3.4a). Considering the ongoing debate regarding whether the low-frequency phase drives the amplitude of the high-frequency component or vice versa[137], we quantified the phase-slope index (PSI)[136] between low frequency phases and high frequency amplitudes as an extended directionality measurement. The PSI metric tracks the circular dependencies of the phase lag between signal pair A and B across several adjacent frequency bins, with positive PSI indicating A->B, negative PSI inferring the reverse and zero PSI suggesting no lead/lag relationship. We found that theta phases from the amygdala/hippocampus drive the HFA from the hippocampus/amygdala for the correct discriminations ($PSI_{amygdala\ to\ hippocampus} = 0.385, P = 0.004$; $PSI_{\ hippocampus\ to\ amygdala} = 0.402, P = 0.004$, permutation test, see method). In contrast, for the incorrect trials, only the amygdala alpha phases lead the hippocampal HFA ($PSI_{amygdala\ to\ hippocampus} = 0.438,\ P = 0.0031; PSI_{\ hippocampus\ to\ amygdala} = -0.017, P =$

0.0621 , permutation test, see method). Due to the fact that non-sinusoidal wave morphologies (e.g. sawtooth-like waves) can result in spurious PAC and PSI[185], we further confirmed our directional findings using spectral Granger Causality (GC) analysis, which measured the degree to which the LFPs from one structure can be better predicted by incorporating information from the other in the frequency domain. Consistent with the PAC analysis, we found significant bi-directional influence for correct trials while incorrect trials demonstrated a unidirectional influence from the amygdala to the hippocampus (shown in Figure 3.4b). In addition, the significant Granger Causality ($P<0.001$, permutation test, see methods) switched from theta to alpha band when comparing between correct and incorrect trials.

To link these spatial and spectral influences to temporal neural encodings, we asked whether a specific phase of the low frequency oscillation is co-modulated with HFA in a behaviorally relevant manner, analogous to spike and phase coupling, in which local neuronal spiking is biased according to the oscillatory phase of the LPF[81]. Since the oscillatory modulation of firing rates acts as a carrier of information, the achievable signal-to-noise ratio strongly depends on the strength of modulation[177,186,187].Therefore, we band-filtered the modulating signals within the frequencies demonstrating the strongest modulation effect (extracted from Figure 3.4a; theta band for correct trials, alpha band for incorrect trials) and examined when HFA from modulated signals occurred relative to the phases of the modulating signal. We showed phase-dependent encoding mechanism in single trial examples (shown in Figure 3.4c) and further confirmed by group analysis across all subjects (shown in Figure 3.4d). Specifically, HFA from modulated signals occurred at the trough of theta oscillations in the correct trials while randomly distributed across different phases of alpha oscillations for the incorrect trials.

Notably, during correct retrieval, HFA from both the amygdala and the hippocampus occurred near the trough of theta oscillations. However the phase clusters, which encode different directional information, were significantly separated (pattern classification methods, $P < 10^{-8}$, binomial test, see method), falling at the preceding and descending side respectively. Such phase-dependent encoding provides an oscillatory mechanism to increase the coding capacity of amygdala-hippocampal circuit with different phases reflecting distinct information from bi-directional communications[177]. On the other hand, mnemonic discrimination signals might be buried by the task-irrelative information via randomly occurred HFA at non-specific phases of alpha oscillations, which eliminated efficient inter-regional interactions. In summary, the amygdala and the hippocampus used frequency- and phase-specific oscillatory multiplexing mechanism to optimize directional information transfer, highlighting that bi-directional interactions with HFA occurred at the trough phase of theta oscillations predicted successful mnemonic discrimination of emotional stimuli.

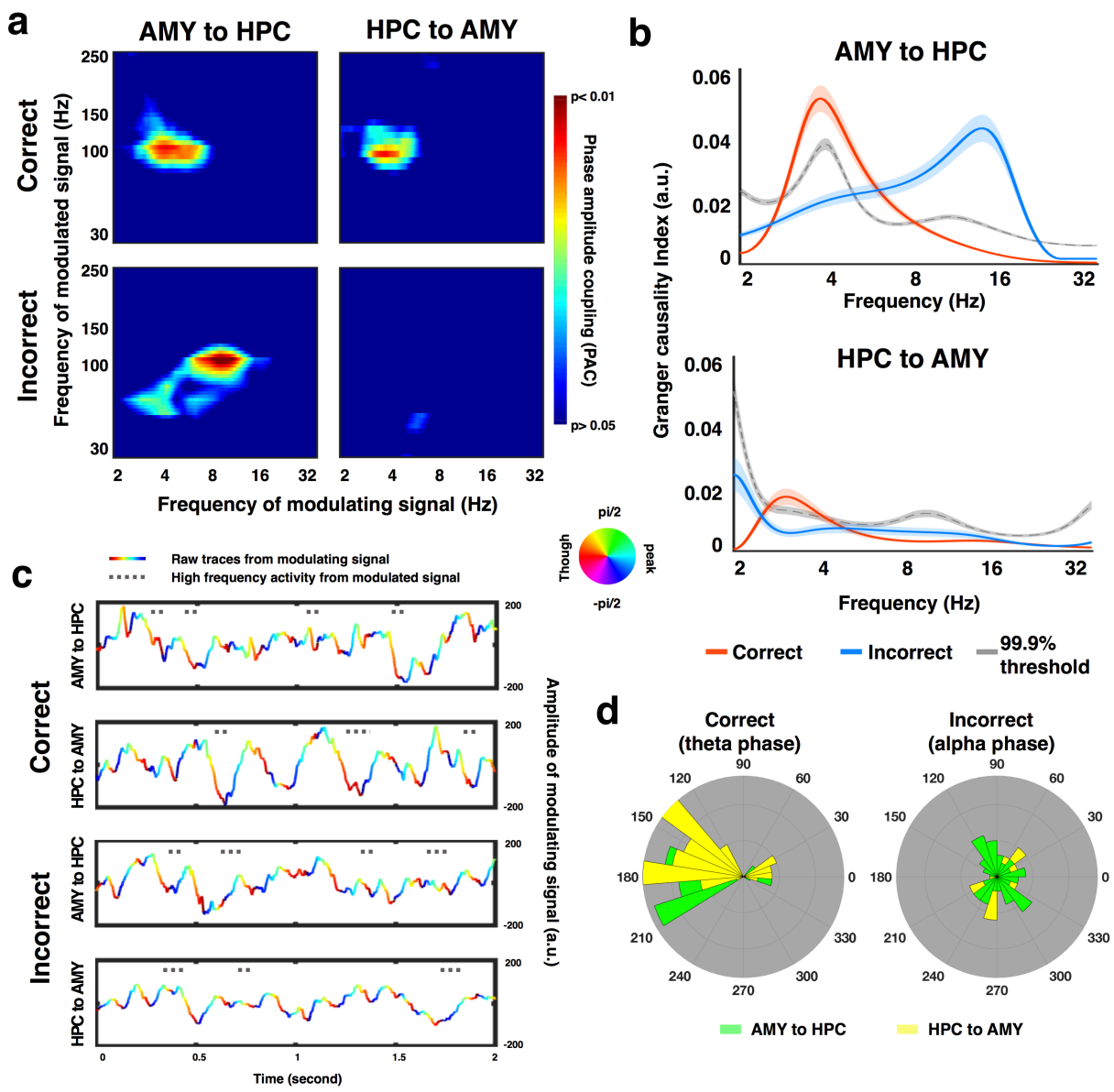

Figure 3.4. Amygdala-hippocampus directional influences and phase encodings support the mnemonic discrimination. (a) Averaged inter-regional phase amplitude coupling (PAC) across all subjects within amygdala-hippocampal network for both correct (upper row) and incorrect (lower row) discriminations. Warmer colors denote higher *P* values (permutation test, see method). **(b)** Spectral Granger Causality analysis within the amygdala-hippocampal network. The solid lines (red: correct; blue: incorrect) represent the observed Granger Causality indices while the dotted gray lines indicate 99.9% confidence intervals for the null distribution (shaded area = ±s.e.m.). **(c)** Four example trials from Subject 6 demonstrating that high gamma activities occur at different phases of low frequency oscillations for different conditions (correct: upper panel; incorrect: lower panel). The LFP traces were color-coded by the phase of peak modulating frequency from either amygdala (upper row) or hippocampus (lower row). The doted gray lines indicate the time when high frequency activities from modulated signal (upper row: hippocampus; lower row: amygdala) occurred. **(d)** Circular distributions of phases at which the high frequency activities occur across all seven subjects. For correct discriminations (left), high frequency activities occurred around the theta trough, at either preceding (hippocampus to amygdala) or descending (amygdala to hippocampus) side for different directions. For incorrect discriminations (right), the occurring phase of high frequency activities were uniformly distributed at all alpha phases. (AMY to HPC: amygdala to hippocampus; HPC to AMY: hippocampus to amygdala)

3.4 Discussion

In this study, we reconciled the seemingly disparate modulatory roles of emotion on memory by revealing distinct amygdala-hippocampal computations that occur for remembered versus forgotten events. We found that the amygdala and the hippocampus both participate in mnemonic discrimination of emotional events, utilizing oscillatory multiplexing of frequency, directionality, and phase information to partition communication channels for successful versus unsuccessful memory. In the frequency domain, enhanced theta frequency band power promotes correct discrimination in the hippocampus, whereas increased alpha frequency band power is linked to incorrect recognition in both the amygdala and the hippocampus. The theta and alpha frequency band directional interaction occurred dynamically between the amygdala and hippocampus to flexibly modulate behavior outcomes; successful mnemonic discrimination promotes bi-directional PAC, while unilateral amygdala to hippocampus interactions predicted incorrect recognition. Finally, theta phase separates neural signals by precisely biasing the timing of HFA, a correlate of neuronal population firing rate, to the trough of the theta oscillation for the correct trials. Our results emphasize that to maximize cooperation between the amygdala and the hippocampus, multiple oscillatory codes are required to index emotion and memory in this circuit.

The cooperation between the amygdala and the hippocampus is essential for mnemonic discrimination of emotional events. Conventional views of the amygdala posit that it simply signals the salience of the stimuli by prioritizing attention to influence hippocampal memory processing[6,162]. Apart from the emotional modulatory effect, we also observed a conditional difference of alpha power within the amygdala, reflecting subjects' behavior outcomes

(increased alpha power for incorrect versus correct discrimination, Figure 3.2c). These findings indicate that the human amygdala might actively discriminate overlapping mnemonic episodes while participating in emotional processing, which is in keeping with long-term potential models of emotional memory in the rodent amygdala[188]. In the hippocampus, regional-specific spectral signatures of mnemonic discrimination are only evident in the anterior, and not the posterior hippocampus (Supplementary Fig. 3, see APPENDIX B), which reinforces the functional diversification along the hippocampal longitudinal axis[41,189-193].

Theta and alpha oscillations in the MTL are thought to play critical roles to support successful memory encoding[194,195] and retrieval[152,153]. Beyond the task-induced power variations in theta and alpha bands, our results highlight a frequency-division multiplexing, in which distinct spectral bands predict task outcomes and their strength modulate emotional valence (see Figure 3.2c, 3.2d and Figure 3.3a, 3.3b). Although the functional roles of theta and alpha oscillations remain unclear, a growing number of researches have emphasized their distinct contributions to memory processing. Theta oscillatory activities[196] are thought to modulate hippocampal synaptic plasticity[197,198] and flexibly organize complex mnemonic information[199] to increase memory capacities[200,201]. In contrast, alpha oscillations have been postulated to guide inhibitory top-down control[202-206], which selectively filters task-relevant information to improve memory efficiency[207-209]. As shown in Figure 3.3c, distinct information was segregated into these two frequencies, with the mnemonic performance and emotional valences carried out by theta and alpha bands, respectively. These findings are consistent with the notion that theta oscillations route emotional memory to promote successful

discrimination and alpha oscillations are suppressed to block task-irrelative emotional information.

Oscillations also coordinate the information transfer that integrates across spatiotemporal scales. As shown in Figure 3.4a and 3.4b, bidirectional amygdala-hippocampal interactions not only align with the reciprocal anatomical connections between these two structures[41] but also suggest that an equilibrium of cooperation instead of a hierarchical system in the MTL. An infringement of this balance that favors amygdala to hippocampal directionality may lead to asymmetric information flow and impaired mnemonic discrimination. Building upon this flexible communication system that multiplexes with oscillatory frequency and directional specificity, our results also demonstrate phase-specific segregation between emotional processing and mnemonic discrimination. The PAC has been proposed to serve as an internal clock to bias HFA, an index of local neuronal spiking[210,211]. Specifically, theta-gamma PAC within the MTL has been shown to integrate complex information[90,212-216] by organizing HFA at specific theta phases[217,218]. Our results support this time-division multiplexing, with mnemonic information and emotional context encoded by HFA at distinct theta phases for accurate memory representations. In contrast, random occurrences of HFA relative to the alpha phase might induce 'neural noises' to interfere with mnemonic discrimination[219,220].

Overall, our results suggest that successful emotional memory is not a unitary process, but instead is fractionated into optimal frequency-, directionality- and phase-specific information to support amygdala-hippocampal communication. On the other hand, unidirectional influence from the amygdala to hippocampus might evoke irrelevant emotional

information, leading to memory interferences. In sum, our study provides electrophysiological mechanisms for emotional memory and learning, for which impairments form core clinical features of diverse neurological disorders such as Alzheimer's disease, autism, major depression, and epilepsy. Understanding the neural mechanisms of emotional memory in the amygdala-hippocampal system will provide a critical framework to develop circuit specific intervention in people with disordered memory[221].

CHAPTER 4: Amygdala-Hippocampus-Orbitofrontal Dynamics Support Contextual Modulation of Facial Perception

4.1 Introduction

Context influences our perception of facial expression. Although structural features of a face itself carry affective information, its emotional meaning can be further constructed from the augmented contexts. For example, a face with wide eyes and open mouth can be interpreted as 'fear' when pointed with a gun, or recognized as 'surprise' when presented with a birthday cake. This "emotional carryover" effect can be adaptive to resolve the ambiguity by integrating contextual cues with facial expressions[24,222] and enhance emotional memory[223]. On the other hand, dysfunction in contextualizing information can cause inappropriate social reactions[34,224] and lead to impaired fear extinction[26,225].

It has been proposed that subcortical-limbic structures engage in prioritizing salient information for basic face recognition[226,227] while the neocortical regions facilitate contextual processing, which involves emotional elaboration and cognitive appraisal[226,228]. Moreover, animal electrophysiology and human neuroimaging studies have shown that the amygdala-hippocampal-orbitofrontal circuit is involved in contextual modulation of facial expression perception[1,229,230] and contextual control of fear behavior[29-31,231,232]. However, the underlying mechanistic dynamics remain unknown. Specifically, how various dimensional contexts and facial expressions are encoded? How are they integrated into a single neuronal representation? And how such mixed information influence our emotional perception? These questions are of special relevance as it may reveal a currently under-appreciated mechanism (i.e. context-

dependent emotional perception) that is impaired in diverse neuropsychiatric disorders, including post traumatic stress disorders, schizophrenia, and depression[26,224,233]. Understanding the oscillatory signatures of this tripartite network would provide a circuit-level perspective for therapeutic interventions[34,234].

Here, we addressed these questions by using intracranial electroencephalography (iEEG) and directly recorded neural signals at the amygdala-hippocampal-orbitofrontal circuit at unparalleled temporal resolution[69]. Since the contextual modulation is exceedingly influential to ambiguous or expressionless faces (i.e. neutral faces)[228], we tested such affective bias by presenting neutral faces with preceding emotional scenes[24,235,236] and asking the subjects to rate the emotional valence of each face. We hypothesized that emotional contexts modulated facial perceptions in both positive and negative directions, which was facilitated by medial temporal lobe and orbitofrontal interactions. Specifically, we hypothesized that contexts were processed within the medial temporal lobe, with stronger amygdala to hippocampal directionality signaling the emotional significance[164]. We also hypothesized that active orbitofrontal-hippocampal communications maintained the contextual information during the delay period between the context and face presentation, which is predicted by the evidence of the increased prefrontal-hippocampal synchrony during the delayed contextual memory retrieval[49]. Further, based on the model of orbitofrontal to amygdala top-down regulation during the emotional evaluation[237,238], we hypothesized that orbitofrontal slow oscillations modulated the high frequency activities from the amygdala via phase amplitude coupling, which promoted synaptic plasticity[239] for context-face integration.

To test these hypotheses, we first tracked the context information represented at each region across different task stages by calculating the correlations between the valence of contexts and the cross-trial variations of high frequency activities (70-250Hz), a correlate of local neuronal spiking[210,211]. We then quantified the functional connectivity as the inter-regional low-frequency phase synchrony and assessed the directional information flow using spectral Granger causality. Further, we measured the cross–regional modulation from the global slow oscillations onto local high frequency activities using phase amplitude coupling and evaluated its trial-by-trial predictive reliability of affective perception using the Bayesian model.

4.2 Materials and Methods

Participants. Subjects were 9 patients (6 Male, 3 Female, Supplementary Table, see APPENDIX C) who had stereotactically implanted intracranial depth electrodes (Integra or Ad-Tech, 5-mm inter-electrode spacing) placed at the University of California, Irvine Medical Center. The electrode placements were exclusively guided by the clinical needs of localizing the seizure onset zone for possible surgical resection. Informed consent was obtained from each subject prior to testing and the research protocol was approved by the IRB of the University of California, Irvine. Electrode placement was exclusively guided by clinical needs. Subject selection was based on the following inclusion criteria: 1) subjects with normal IQ were included for the behavioral data analysis; 2) subjects, who have normal IQ and have electrodes implanted in either amygdala, hippocampus and orbitofrontal cortex contralateral to the epileptogenic region were included for the high gamma activity analysis; 2) subjects, who have

normal IQ and have electrodes implanted in at least two out of three regions were included for the inter-regional analysis (e.g. inter-regional phase synchrony, Granger causality).

Electrode Localization. The electrode localization was performed using pre- and post-implantation structural T1-weighted 1mm isotropic MRI scans as well as post-implantation CT scans. For each participant, the post-implantation MRI and CT scans were registered to the pre-implantation scan using a 6-parameter rigid body transformation implemented with Advanced Normalization Tools – ANTs. Electrodes were localized within MTL and orbitofrontal cortex using a high-resolution (.55 mm) in-house anatomical template with manual tracings of the amygdala and hippocampal subfields. The labeled template was aligned to each subject's pre-implantation scan using ANTs Symmetric Normalization, so that the labels could be used to guide localization. Each electrode location was determined by examining the co-registered pre- and post-implantation MRIs, and identifying the ROI label that corresponded the center of the electrode artifact in the CT.

Contextual modulation task and behavioral analysis. Neutral faces of 35 identities from NimStim Face Stimulation Set[240] were selected. Faces were displayed after the presentation of a context image from the International Affective Picture System (IAPS)[241] with 500ms delay period. Each face was paired with three context images (1 Positive, 1 Negative, 1 Neutral). In each trial, subjects were instructed to rate the emotional valence of the facial expression by marking at the appropriate position of the valence scale bar. Subjects' ratings and response time were recorded for further analyses. As the tendency of emotional perception varies from

subjects to subjects, we normalized the ratings within each subject before conducting the group analysis.

Data acquisition and preprocessing. Stimuli were presented on a laptop computer screen (15'' MacBook Pro) set using PyschoPy2 (Version 1.82.01)[166] at a comfortable distance from the patient. An external Apple keyboard was used to capture subjects' responses. Intracranial EEG data were recorded using a Nihon Khoden recording system (256 channel amplifier, model JE120A), analog-filtered above 0.01 Hz and digitally sampled at 5000 Hz. After data acquisition, neural recordings were down sampled at 2000Hz and band-pass filtered between 1 to 250Hz using the zero phase delay finite impulse response (FIR) filter with Hamming window. Power spectra were examined using Welch's method (pwelch,m in Signal Processing Toolbox from MATLAB) to identify line noise. A multi-taper regression method[167] was applied to remove the line noises inspected from the power spectra (usually 60Hz and its harmonics). All channels were re-referenced to a nearest white matter electrode[242] located on the same depth electrode probe based on the electrode localization results. A neurologist (J.L.) with subspecialty training in epilepsy visually inspected continuous recordings from each session to identify all data with interictal epileptiform discharges. Data were also inspected for excessive noise, including broadband electromagnetic noise from hospital equipment. To avoid potentially biasing the results, the neurologist was blinded to trial information (e.g. stimulus onset and behavioral performance) as well as to electrode location. The preprocessed intracranial recordings were segmented into event-related epochs, including a 500ms pretrial baseline. With the self-paced rating period, the trial length varies, with the least common length of 3500ms after stimuli

onset. Only data from recordings contralateral to the seizure source or outside of the seizure onset zone were used in subsequent analyses.

Frequency decomposition. The segmented data were zero-padded to minimize filter-induced edge effects and decomposed between 1 to 250Hz with 28 logarithmically spaced frequencies with FIR filtering. The adaptive bandwidths ensured precise phase estimations within narrow bands of low frequency oscillations while the broader range of higher-frequency eliminated sideband effects and prevented spurious PAC[129]. We then applied the Hilbert transform (hilbert.m function in Signal Processing Toolbox from MATLAB) to extract analytic amplitude and phase for all filtered traces. The task-induced power was calculated by squaring the analytic amplitude envelope and was normalized to the pre-trial baseline using relative change in decibel conversion (dB).

High Gamma Activity and Explained Variance. High gamma amplitude was extracted from frequency-decomposed data and was baseline-corrected to remove any pre-stimulus differences. We used the resulting R^2 (variance in the neural data that can be explained by the behavioral or computational regressors of interest, % explained variance, %EV) as a metric of the quality of the fit. This approach is insensitive with respect to time of task-related activation and to the direction of encoding (i.e. HFA increases or decreases). False positive rate (null), the horizontal lines indicated in the figures, was determined by estimating responses to a randomly generated regressor. We measured the time course of individual electrode encoding time courses by tracking the %EV association over time.

Low frequency Phase Synchrony. The strength of inter-regional neural synchrony was quantified by the PLV[171] with the same approach mentioned in CHAPTER 3. The statistical significance of PLV was tested using cluster-based permutation test (ft_freqstatistics.m from open source toolbox Fieldtrip[168]). The results shown in Figure 4.3b were depicted with P values ($P = 0.01$), with warmer colors denoting stronger significance levels.

Granger Causality. Before fitting to the multivariate autoregressive model to compute the spectral Granger causality, the time series data were low-pass filtered at 85 Hz, down-sampled to 250 Hz and normalized within each trial (e.g. subtracting the temporal mean and cross-trial mean). Then, we defined the model order using the Multivariate Granger Causality (MGVG) Toolbox based on the Akaike information criterion[140]. The model order for each subject varied from 6 to 12. The Granger Causality index was computed within the processing period (2-second time window after stimuli onset) for both directions (amygdala to hippocampus, hippocampus to amygdala). The significance analysis for Granger Causality is the same method as described in the section 'Inter-regional phase synchrony' by randomly shuffling the trials 1000 times. Then the Granger Causality null distribution was created and the 99th percentile of the surrogate data was defined as the significant threshold.

Bayesian Decoding. A Bayesian classifier[243] with uniform prior probability distribution was employed to estimate subjects' ratings of neutral faces. We assumed the power spectrum to be normally distributed in each of the high gamma frequency bands of the LFP. To estimate the subjects' emotional perception (positive to neutral to negative), we defined the rating scalar to denote different states. The vector $E = (E_1, \dots E_N)$ represents the neural activity of the

ensemble of all recording sites. Each E_i represents the LFP log power in one of the decomposed frequency bands. Based on the Bayes' theory, the posterior probability of time from a trial onset (time) and contextual emotion (cont) given the vector of high gamma activity vector $\boldsymbol{E}$:

$$P(time, cont|E) = \frac{P(E|time, cont) \cdot P(time, cont)}{P(E)}$$

The prior probability was estimated under the assumption of normal distribution[244].

4.3 Results

4.3.1 Emotional Context Modulates Facial Perception

We designed an emotional rating task to examine how contextual information influences individuals' facial perception (Figure 4.1a). Nine pre-surgical epilepsy patients (Supplementary Table 1, see APPENDIX C) were recruited in the task. Each trial started with a context image (1 second) from the International Affective Picture System[241]. After a delay period of 500ms, a face with a neutral expression (35 identities in total) from the NimStim Face Stimulus Set[240] was presented for one second. It was followed by a self-paced decision-making period, in which the subjects were instructed to rate the emotional valence of the face by marking at the corresponding spot on the valence scale bar. This continuous rating scale not only solved the problem of information loss compared to the category labeling, but also allowed for applying advanced statistical analyses. Each face was paired with three different context images (1 positive, 1 neutral and 1 negative). Due to the individual difference of emotional processing tendencies, we normalized the valence ratings within each subject before the group analysis. We found that the valence rating for the face was positively correlated with

the valence of its preceded context image (Figure 4.1b), suggesting an emotional 'carryover' effect from the context image onto the face. Notably, such emotional bias of facial perception was not varied with the arousal differences (Supplementary Fig. 1, see APPENDIX C). To eliminate the emotional contribution from facial expressions, for each face, we quantified the modulation strength as the rating difference between the trials with emotional (negative/positive) contexts and the ones with neutral contexts (i.e. $|R_{postivie} - R_{neutral}|$ and $|R_{negative} - R_{neutral}|$). Stronger modulation effect was observed from the negative contexts compared to the positive ones (Figure 4.1c, *t-test*, $P = 3.452e^{-4}$; Negative modulation strength: 0.281 ± 0.054, Positive modulation strength: 0.183 ± 0.042, mean ± s.t.d.). Moreover, subjects' response time was negatively correlated with the modulation strength (Figure 4.1d), with faster decisions made on the trials with strong modulation strength. Building on these behavioral observations, we next sought to investigate the neuronal features within the amygdala-hippocampal-orbitofrontal circuit to explain such emotional bias.

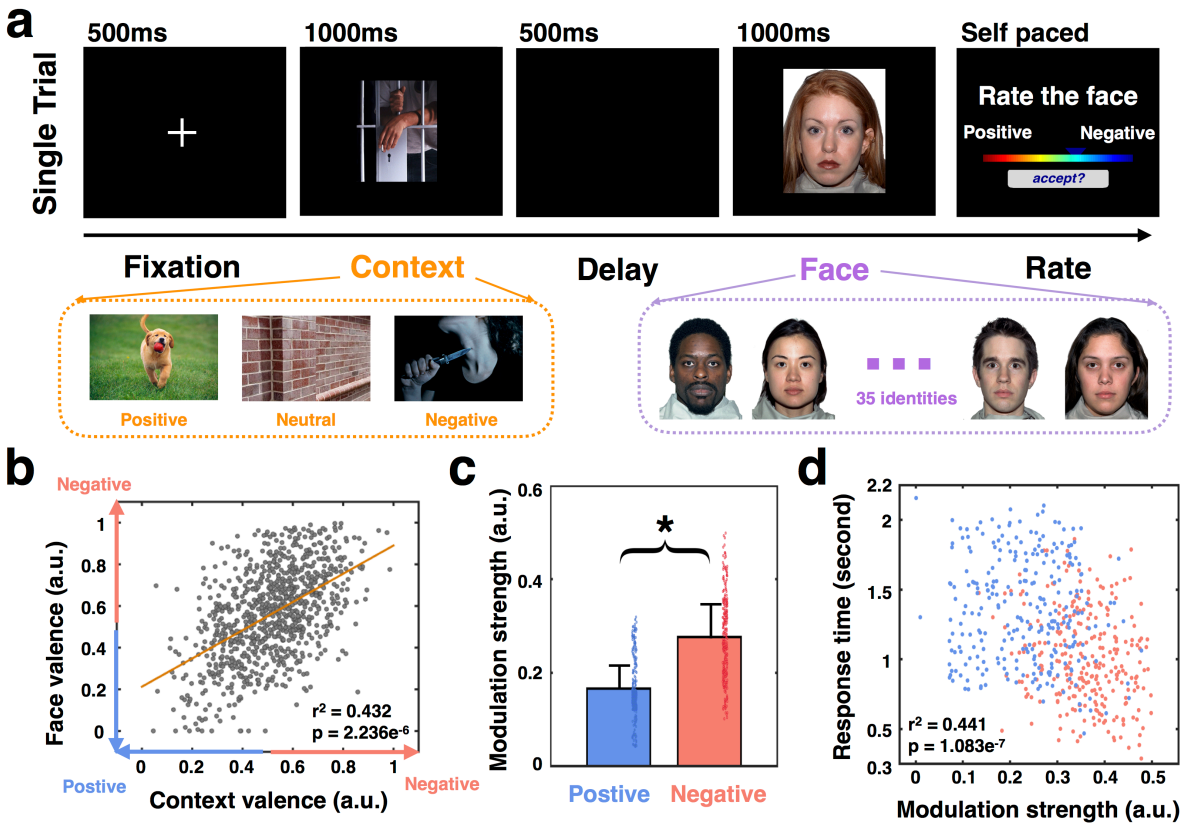

Figure 4.1 Contextual modulation task and behavior results. (a) Single trial setup. Each trial consisted of five parts: a 500-ms maintenance fixation period (Baseline), a 1000-ms context image presentation (Context), a 500ms delay with blank screen (Delay), followed by a 1000-ms face display (Face) and self-paced affective rating of the face (Rate). Each face from 35 identities was paired with three contexts of different valence (one positive, one neutral, one negative). The subjects were instructed to rate the valence of each face by moving the blue triangle to the appropriate position on the color-coded scale bar, with warm colors denoting positive valence and cold colors referring negative valence. **(b)** Subjects' valence ratings of the faces were positively correlated with the valence of the context images. **(c)** After normalizing to the neutral contexts, the modulation strength of the trials with negative contexts was significantly higher the ones with positive contexts. **(d)** Subjects' response time was negatively correlated with the modulation strength. Blue dots denote the trials with positive contexts while the red dots represent the trials with negative contexts.

4.3.2 High Gamma Activities Track Contextual Valence

Neural signals were simultaneously recorded from the amygdala (AMY), hippocampus (HPC) and orbitofrontal cortex (OFC) (Figure 4.2a, $N_{AMY} = 22$, $N_{HPC} = 20$, $N_{OFC}=21$ electrodes). We first assessed spectrotemporal features for the individual subject by plotting the time-frequency representation (TFR) at each region after baseline correction (Supplementary Fig. 2,

see APPENDIX C). Analysis of task-induced power identified widespread sustained theta/alpha (4-12Hz) oscillations and variable transient high gamma activities (HGA, 70-250Hz) in all three regions after the stimulus onset. To exam the neural representation of context at each region, we first obtained mean HGA time course for each trial by averaging high gamma powers across the whole spectrum (70-250Hz). Then the context information was quantified as the HGA variations across trials explained by context valence (i.e. the normalized emotional valence ranging from 0 to 1) using analysis of variance (ANOVA). Averaging across all the subjects revealed a significant encoding of contextual valence in all three areas (permutation test, $P < 0.05$, see Methods), but with a regional specific profile (Figure 4.2b). Information in the amygdala peaked directly after the onset of the context (312 ± 14 ms, mean ± s.e.m.) and face presentation (1966 ± 21 ms, mean ± s.e.m.), and stayed flat for the other stages. In contrast, context information in the hippocampus reached its peak slightly after the amygdala (488 ± 17ms, mean ± s.e.m.; *t-test*, $P = 0.014$) during the context representation, and sustained until the end of the delay period. The orbitofrontal cortex, instead, demonstrated a bimodal dynamic. The context information tonically elevated from the beginning of the delay period and reached its first peak right after the face presentation and earlier than the amygdala's second peak (1574 ± 11 ms, mean ± s.e.m; *t-test*, $P = 4.213e^{-3}$). Then it was followed by a dip and later rise of sustained context information at the rate period. Notably, persistent HGA from orbitofrontal cortex tracked the rate period and time locked to subjects' response onsets (Supplementary Fig. 3, see APPENDIX C). These findings not only confirmed the active engagement of these three regions but also revealed a dynamic encoding of context information at different task stages, highlighting a temporal propagation from the amygdala, hippocampus to orbitofrontal cortex.

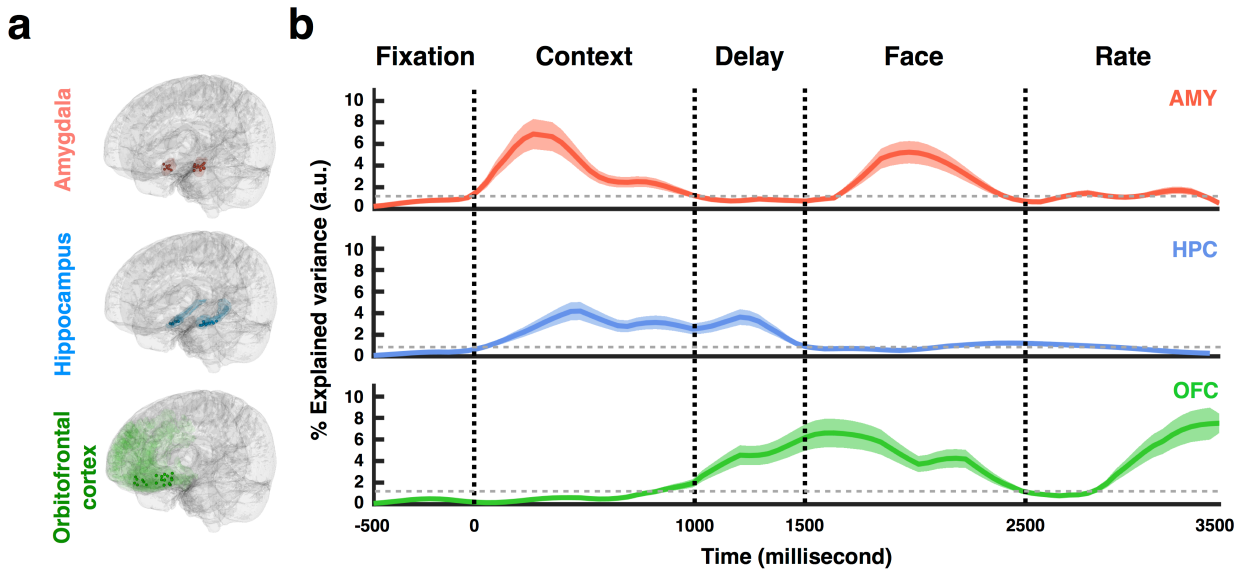

Figure 4.2 High gamma activities track context valence. (a) Electrode localizations across 9 subjects, rendered onto a three-dimensional glass brain (gray) based on the high-resolution template, with amygdala electrodes in red, hippocampal electrode in blue and orbitofrontal electrodes in green. **(b)** Averaged percentage of explained variance time courses for linear regression of high gamma activities onto contextual valence at all three sites. The color-shaded area denotes the standard error mean (s.e.m); the horizontal dotted lines (gray) indicate the significance level; the vertical dotted lines (black) indicate the onset of different stages (Context, Delay, Face, Rate).

4.3.3 Oscillatory Synchrony Mediates Cortical Limbic Interactions

Given the distinct HGA temporal profiles of the amygdala, hippocampus and orbitofrontal cortex, we then investigated whether these three regions interacted through low-frequency phase coupling. The inter-regional functional connectivity was examined with phase locking values (PLV), measuring the consistent phase difference between two channels. Then we averaged the PLV metrics across all the electrode pairs within each group ($N_{AMY\text{-}HPC}$ = 51, $N_{HPC\text{-}OFC}$ = 36, $N_{AMY\text{-}OFC}$ = 39). Sustained phase synchrony was observed among all three regions and was distributed across different stages of the trial (Figure 4.3a and Figure 4.3b; cluster-based permutation test, $P < 0.01$; see Methods). As shown in Figure 4.3c, significant amygdala-hippocampal phase synchrony rose after the stimuli onset (273ms ± 13ms, mean ± s.e.m.) and

ended at the beginning of the delay period (1139ms ± 22ms, mean ± s.e.m.). In contrast, the hippocampal-orbitofrontal phase synchrony dominated the delay period (starting at 987 ± 14ms, mean ± s.e.m.), dipped in the middle of face presentation (2100ms ± 11ms) and rose again during the decision-making period (3117 ± 22ms). The amygdala-orbitofrontal phase synchrony, instead, has a sustained pattern started around the face presentation (1512 ± 18ms, mean ± s.e.m.) and remained significant until the middle of the rate period (3196 ± 15ms, mean ± s.e.m.). Further, oscillations at different frequencies coordinated these inter-regional dialogues (Figure 4.3b and Figure 4.3d; AMY-HPC and OFC-HPC: $P < 0.01$; AMY-HPC and OFC-AMY: $P < 0.01$; OFC-HPC and OFC-AMY: $P > 0.05$), with theta synchrony (4-7Hz) for the amygdala-hippocampal communications and alpha synchrony (7-10Hz) for the cortical-limbic (i.e. hippocampal-orbitofrontal and amygdala-orbitofrontal) interactions. These findings demonstrated a close interplay among three regions during contextual emotion processing and suggested a temporal- and frequency-division oscillatory multiplexing supporting the subcortical to cortical information transfer.

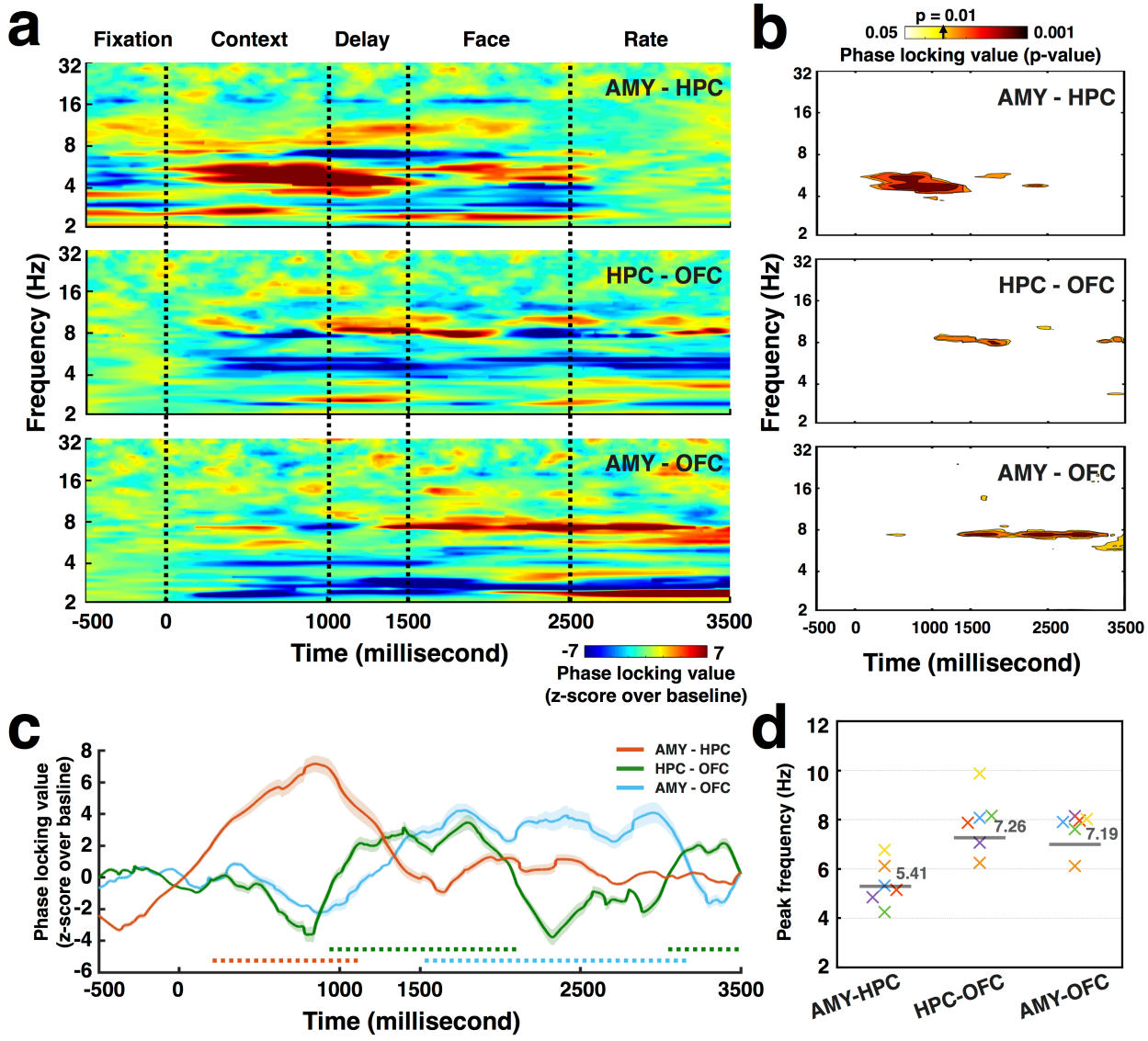

Figure 4.3 Inter-regional phase locking value (PLV). (a) Averaged PLV across all the electrode pairs for each combination (AMY-HPC, HPC-OFC, AMY-HPC). Warm/cold color denotes the increased/decreased PLV increased from the baseline. The black dashed lines represent the onset of each task stages (Context, Delay, Face, Rate). **(b)** Significant PLV cluster (P<0.01) survived after non-parametric permutation test (see Material and Method). Warmer colors represent smaller p values. **(c)** PLV time courses averaged within the significant frequency cluster detected in (b). The dashed color lines denote the significant increase from the baseline. (Orange: AMY-HPC; Green: HPC-OFC; Blue: AMY-OFC) **(d)** Peak frequency of PLV for each subject was coded in different colors and grouped into three combinations (AMY-HPC, HPC-OFC, AMY-HPC). The horizontal gray lines denote the averaged frequency across all the subjects.

4.3.4 Directional Influence Promotes Contextual Modulation

Based on the strong low frequency synchrony in the amygdala-hippocampal-orbitofrontal circuit, we then examined how the direction of putative causal influence varied among different regions across time. We conducted spectral Granger causality indices for each electrode pair up to 30Hz at five different task stages (baseline, context, delay, face and rate). The directional influence ($P < 0.01$) was considered significant when the Granger causality index exceeding the 99^{th} percentile of the null distribution, which was generated for each electrode pair by shuffling trial for 100 times. We then projected the significant maximum Granger indices for each electrode pair into a three-dimensional space and accessed the cross-subjects' directional pattern. As shown in Figure 4.4a, each node represented one electrode and was color-coded for three different regions (Red: amygdala; Blue: hippocampus; Green: orbitofrontal cortex). The arrows connected the electrode pairs with significant causal relationships, with the line thickness representing the strength of Granger causality index and the line color denoting the origin of the influence (e.g., a red line between the amygdala and hippocampus node refers to a directional influence from the amygdala to the hippocampus). The node size increased with the number of causal links it connected with and the large node was considered as the information hub or a higher-level region of the hierarchical network. We observed a dynamic directional pattern evolving across time (Figure 4.4a). The trial started with bi-directional interactions between the amygdala and hippocampus during the context presentation and then shifted to a unidirectional influence from HPC to OFC at the delay period. When the face was presented, bidirectional communications occurred between the AMY-OFC nodes and was followed by an OFC dominated unidirectional influence on medial temporal lobe (i.e., including both the amygdala and hippocampus) at the valence-rating period. These results

highlighted an information flow flexibly traveling between the medial temporal lobe and orbitofrontal cortex, and suggested distinct functional roles for each region at different task stages.

We then investigated how such cross-regional directional influence shaped local neuronal representations. Phase amplitude coupling (PAC), has been proposed to serve as a rhythmic clocking mechanisms, in which high gamma activities are nested at specific phases of low frequency oscillations[210,211]. For the electrode pairs (e.g. A-B) demonstrating the significant Granger indices, we calculated the inter-regional PAC for both directions (A-> B: low frequency phase from A modulated high gamma activities from B; B->A: vise versa) and applied a sliding window to unfold its temporal dynamics[245]. The strength of coupling was quantified as the Euclidean norm of the complex signal, consisting of the low frequency phase from one region and the high gamma amplitude from the other (see Methods). We then averaged each PAC time course across trials and across subjects. Consistent with the results from Granger causality analysis, similar patterns of directional influence was observed and was further extended with exceptional temporal dynamics (Figure 4.4b). Unidirectional influence from the amygdala to hippocampus ($T_{AMYtoHPC}$ = 247 ± 12 ms) led the context processing and was followed by the coupling of reciprocal direction ($T_{HPCtoAMY}$ = 695 ± 11 ms). Moving to the delay period, all the cross-regional modulation went flat except for a unidirectional influence from the hippocampus to the orbitofrontal cortex ($T_{HPCtoOFC}$ = 1059 ± 17 ms). This HPC -> OFC PAC sustained until the face presented and was taken over by bidirectional couplings between the amygdala and orbitofrontal cortex ($T_{AMYtoOFC}$ = 1603 ± 8 ms; $T_{OFCoAMY}$ = 1722 ± 13 ms). During the rate period,

both amygdala and hippocampal HGA were entrained by orbitofrontal low frequency oscillations.

Further, to exam potential behavioral influence induced by these inter-regional couplings, we investigated the correlations between the inter-regional PACs and contextual modulation strength. We stacked all the PAC time courses for six directional combinations (AMY to HPC, HPC to AMY, HPC to OFC, OFC to HPC, AMY to OFC and OFC to AMY) and sorted the trials with increased modulation strength. As shown in Figure 4.4c, $PAC_{HPCtoOFC}$ during the delay period and $PAC_{OFCtoAMY}$ at the face display were positive correlated with the modulation strength, with enhanced cross-regional phase amplitude coupling for strong contextual modulated trials (Supplementary Fig. 4, see APPENDIX C). Notably, $PAC_{AMYtoHPC}$ and $PAC_{HPCtoAMY}$ during the context presentation were positively correlated with the contextual valence instead of the modulation strength. These findings revealed a sequential engagement among three regions, with contextual valence first extracted through bidirectional amygdala-hippocampal interactions and later processed via $PAC_{HPCtoOFC}$ and $PAC_{OFCtoAMY}$ to influence subjects' facial perception.

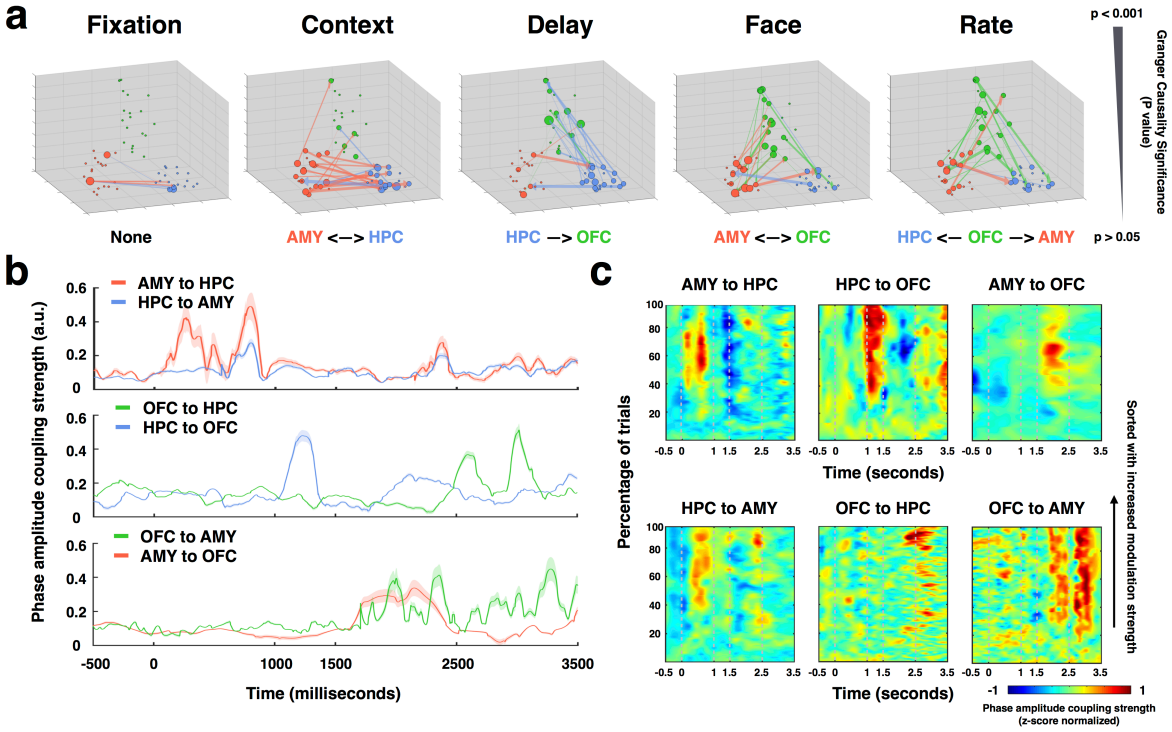

Figure 4.4 Cross-region directional communications. (a) Significant directional influence from all the electrode pairs projected onto a three dimensional space at different task stages. The dot represented each electrode and was color-coded for different brain regions (Red: amygdala; Blue: hippocampus; Green: orbitofrontal cortex). The connected line between each electrode pair denotes the directional interaction, with the thickness of the line represents the significance (i.e. p-value) and the color indicates the origin site of the directional flow. The size of the dot increased with the number of connected lines. **(b)** Averaged time-resolved phase amplitude coupling (tPAC) across all the trials. The color indicates the modulating sites and the shaded area denotes standard error mean (s.e.m.). **(c)** Single trial of tPAC stacked and sorted with the increasing modulation strength. Warmer colors denote stronger phase amplitude coupling. The vertical dashed lines represent the onset of each task stage (Context, Delay, Face, Rate).

4.3.5 Selective Phase Predicts Contextual Modulation Strength

To further investigate the functional roles of $PAC_{HPCtoOFC}$ and $PAC_{OFCtoAMY}$, and how they modulated subjects' behavioral outcome, we investigated the occurring phase sequence of HGA in the trials using a Bayesian decoding technique[244,246,247]. The probability densities of time information were reconstructed from the HGA time traces from the orbitofrontal cortex and amygdala using a 5-ms time step in each trial. As shown in Figure 4.5a, the OFC HGA at the delay period decoded the future state of face presentation while the AMY HGA at the face

presentation predicted the rating. Moreover, the switch between the current and future states was roughly fitted to theta/alpha cycles. Therefore, we aligned the reconstructed time information with concurrent phases from the modulating signal (HPC theta for OFC HGA; OFC theta for AMY HGA). The probability densities of the reconstructed time at each theta phase (Figure 4.5b and Figure 4.5c) demonstrated a phase specific information decoding mechanism. On descending phases of HPC/OFC theta (0-180^{o}), the decoded probability densities of time reflected the current period while the future state was decoded at the ascending phases of HPC theta (180^{o} ~ 360^{o}). Further, we examined whether the observed phase division included information reflecting the received context valence and the planned face rating. We equally divided all the trials into two groups based on their modulation strengths (strong modulation trials vs. weak modulation trials). The probability densities of time and valence (including the valence of context and face), i.e., P (time, valence|HGA), were estimated from OFC HGA at the delay period and the AMY HGA during the face presentation for both groups. Context valence was represented by the OFC HGA on the ascending phase of HPC theta during the delay period and was transferred to the AMY HGA during the face presentation, with descending phase of OFC theta reflecting the context valence while the ascending phase predicting the future rating of the face. On the other hand, the decoded and predicted information were absent for the weak modulation trails, implying that the contextual valence was either unsuccessfully transferred or inappropriately integrated with the face. These results indicated that $PAC_{HPCtoOFC}$ and $PAC_{OFCtoAMY}$ carried the context information at the delay and face presentation period, with current state information and the planned future actions compressed within theta cycles at specific phases.

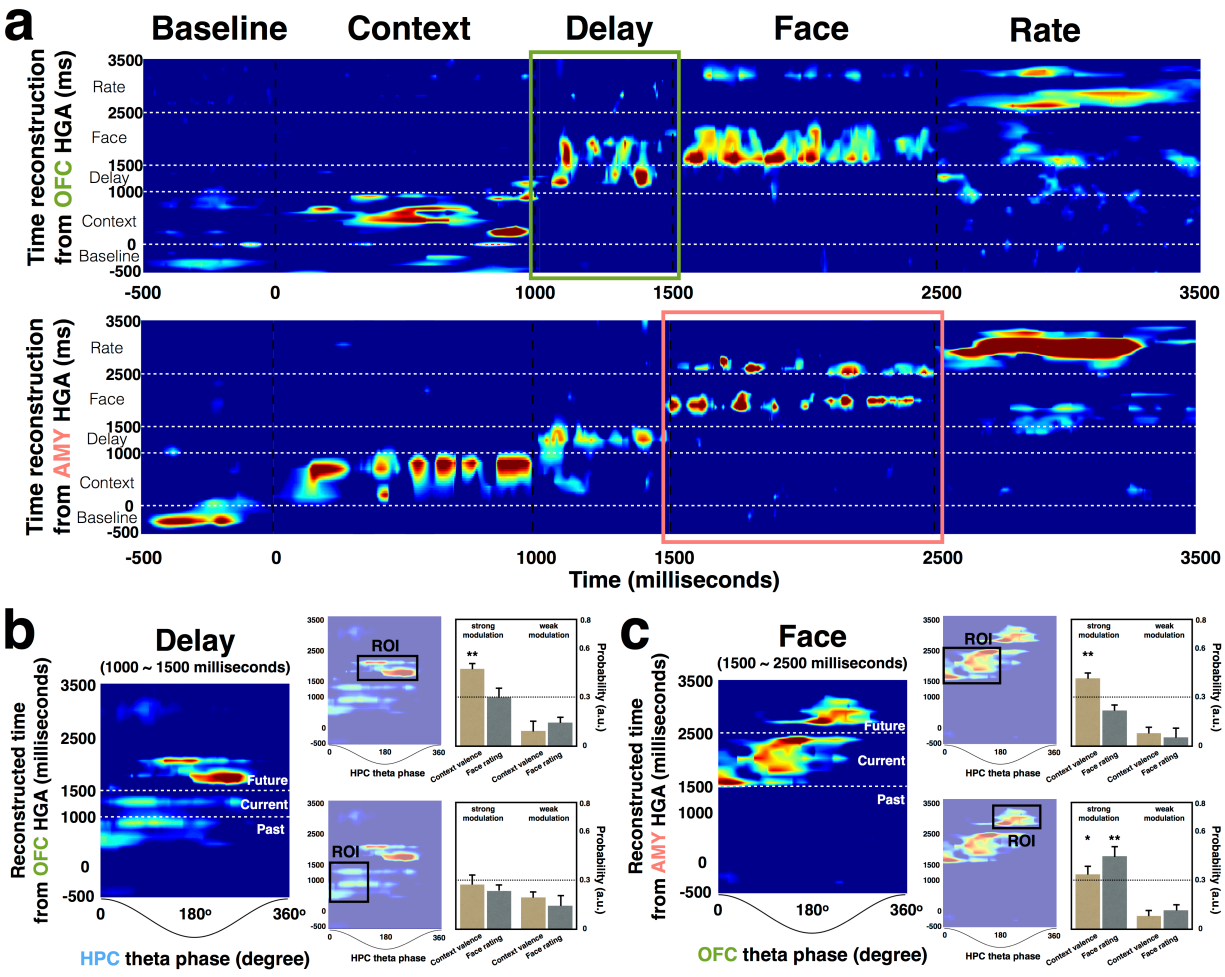

Figure 4.5 Bayesian decoding. (a) Probability density of time information computed from simultaneously recorded OFC HGA (top) and AMY HGA (bottom). Bayesian decoding was performed at every 5-ms time step with a 20-ms time window. Warmer colors denote higher probability. Dashed black lines indicate the onsets of different task stages in the real time scale. Dashed white lines represent the onsets of different task stages in the reconstructed time scale. The green and red square boxes indicate the time frame with future prediction. **(b)** Left panel: probability density of time information as a function of HPC theta phase, estimated in the delay period (1000~1500ms). Right panel: decoded probabilities of context valence (brown) and face rating (gray) in strong and weak modulated trials with ascending phase (upper) and descending phase (lower) of HPC theta. **(c)** Left panel: probability density of time information as a function of OFC theta phase, estimated during the face presentation (1500~2500ms). Right panel: decoded probabilities of context valence (brown) and face rating (gray) in strong and weak modulated trials with descending phase (upper) and ascending phase (lower) of OFC theta.

4.4 Discussion

It is widely acknowledged that contextual information can modulate how we perceive facial expressions. Although prior work has demonstrated robust behavioral outcomes[24,228,248] and their associated brain regions[226,228], less is known about how these regions coordinate to induce affective biases. Here, to further exam the neural signatures underlying contextual modulation on facial perception, we recorded direct neural signals from the OFC-AMY-HPC circuit, a well-established contextual processing network, while subjects performed valence ratings of neutral faces with preceding emotional contexts. In sum, our results provide the first demonstration of spatial and temporal neural dynamics of how context influences the judgment of facial expressions. Specifically, we have revealed a sequential processing system, in which 1) the context image was first processed within the medial temporal lobe, leading with the earlier engagement of AMY and stronger influence from AMY to HPC to signal the affective significance; 2) then the contextual valence was carried over from the medial temporal lobe to OFC during the delay period, with enhanced unidirectional information flow from HPC to OFC; 3) Finally, the contextual valence was integrated with the face via precisely coordinated timing between the OFC theta oscillations and AMY HGA, which predicted successful context-induced emotional bias on the face. Together, instead of a segregated circuit, our findings emphasized a cascade of amygdala-hippocampal-orbitofrontal interplay, which fostered the interactions between affective context and facial expressions, leading to a further constructed percept.

In the presented work, we observed affective modulation from preceding images with both the negative and positive valence. However, negative contexts induced a greater emotional bias of facial expressions (Figure 4.1c, *t-test*, $P = 3.452e^{-4}$), which is consistent with the asymmetric emotional influence observed in previous studies, including the memory

consolidation[15], decision making[249] and social discrimination[250]. Moreover, stronger contextual modulation effect was correlated with faster rating (Figure 4.1d), exhibiting a shorter averaged response time for negative contexts compared to the positive ones ($RT_{negative}$ = 921 ± 21 ms , $RT_{positive}$ =1.436 ± 18, *t-test*, *P* = 0.0174). A similar trend has been observed in the learning behavior, with the punishment avoidance more effective in enhancing learning speed than rewards. These findings might be supported by an evolutionary account, in which negative emotions carry more direct and immediate adaptive benefits for survival[251] and self-development[252].

The medial prefrontal cortex (mPFC) and hippocampus (HPC) are strongly connected by direct and indirect pathways[49]. Among these, the monosynaptic projection from the ventral HPC to the mPFC, including OFC[51,253,254] provides the most immediate access to the global context information rather than detailed memories[255-258]. Strong HPC-mPFC coherence was observed in the context-guided reward tasks[259-262] and exhibited an enhanced pattern during the memory-demanding delay[259]. Moreover, it has been proposed that bidirectional communication between the HPC and mPFC carries different functional roles. In the working memory tasks, directional influence from HPC to mPFC was involved during the memory delay or when cued by a context[259,263], whereas retrieving the previous memory or planning the choice response engaged mPFC-to-HPC communication[210,264]. Our results are consistent with these findings. In the present study, we observed increased HPC-OFC theta/alpha synchrony covering the delay period and towards the end of decision-making (Figure 4.3a and 4.3c). Moreover, these two stages exhibited opposite directional interactions, with HPC->OFC for the delay period and OFC-> HPC for the face rating. Notably, during the delay period, HPC

modulated OFC activities through theta-gamma phase amplitude coupling, with the context valence encoded by OFC HGA on the ascending phase of HPC theta (Figure 4.5b). These results indicated a shift of information carrier[265], in which OFC took over the processed information from the medial temporal lobe to "offloaded" encoding spaces for upcoming events[49]and maintained the context information for further analysis (i.e. integration with the face). On the other hand, the reciprocal influence from OFC to HPC during the rating period supported retrospective information retrieval and prospective decision-making[266].

Then the question is how processed contextual information integrates with face and therefore influences subsequence emotional ratings. Subcortical amygdala pathways have been proposed to enable rapid face processing[267] and were regulated by a top-down control from the orbitofrontal cortex during emotional evaluation[237]. Our results are consistent with the current model, with directional influence from OFC to AMY sustained over the face presentation and rating period (Figure 4.4b). Moreover, precise temporal modulations from the orbitofrontal theta to amygdala high gamma activities have been observed during the face presentation, with processed context valence and future facial ratings represented at the descending and ascending phase of OFC theta (Figure 4.5c). Such phase specific encoding mechanism suggested an automatic emotional face-context integration[268] supported by OFC->AMY phase amplitude coupling, which predicted subsequence emotional ratings of the faces. Notably, a reciprocal interaction from AMY to OFC has also presented during the face presentation. This might be served as a feedback system[269-271], with integrated information conveyed to OFC for cognitive reappraisal[272] and the control of future action[273,274].

Overall, our results suggest that the interpretation of facial expressions does not solely rely on the structural features of the face. Instead, we observed dynamic cooperation among the AMY-HPC-OFC network to support contextual modulation on facial expression perception. Specifically, contextual information was processed within the medial temporal lobe, projected to the orbitofrontal cortex via HPC to OFC route and was further integrated with the face through AMY-OFC feedforward and feedback interactions. These electrophysiological signatures extend our understanding of context on emotional processing, which is often impaired in patients with neuropsychiatric disorders[26,233,275]. The future work can be focused on translating this mechanistic framework to circuit specific intervention approaches.

CHAPTER 5: Conclusion and Future Directions

5.1 Overview of Findings

Our findings suggest that emotional processing is not limited to a single region but instead relies on close interactions among the amygdala-hippocampus-orbitofrontal circuit. Specifically, a unifying model for emotional processing is implied, in which the amygdala gates contextual information based on salience priority and binds emotional factors with hippocampal cognitive map to form an integrated representation (i.e. a emotion-weighted portrayal of external and internal states); such abstract contextual cues are conveyed from the medial temporal lobe to the orbitofrontal cortex, mainly through hippocampal-orbitofrontal pathway; the orbitofrontal cortex exerts top-down control over the amygdala and hippocampus for flexible goal-directed decision making.

In the daily life, swift response to the contextual environment is required, indicating a network coordinated parallel processing instead of the serial processing from a single region. Then how do multiple streams of emotional information (e.g. context, face, and memory) share the same neural circuitry? In our study, we found that oscillatory multiplexing (i.e. distinct bands carrying different information in parallel) might serve as a potential mechanism to link the amygdala, the hippocampus and the orbitofrontal cortex together in emotional processing. It rapidly organizes information flow in real-time, computations across parallel brain systems and separates neural signals into different communication channels through distinct frequency, directionality, and phase information[186]. **Oscillatory Multiplexing of Frequency:** We examined the oscillatory activities within each region and quantify the inter-regional communications as phase locking values, the measurement of the consistency of the phase relationship between

two signals [89,276]. We found that oscillatory synchrony among three regions uses different frequency bands to index distinct computations. Such dissociation of frequency bands has also been found in other human intracranial studies, in which increased prefrontal-parahippocampal network connectivity in delta/theta band (1-4 Hz) predicted successful spatial context retrieval and enhanced theta/alpha coherence (7-10 Hz) predicted correct temporal context retrieval[277]. **Oscillatory Multiplexing of Phase:** These distinct spectral fingerprints do not occur in isolation but are functionally coupled through phase amplitude coupling (PAC) and support neural tuning of high gamma activity linked to different cognitive function[278,279]. We found that PAC serves as a rhythmic clocking mechanism to bias high gamma activity. Specifically, theta/alpha-high gamma PAC integrates task complex information by organizing HGA at specific theta/alpha phases. This is consistent with previous findings in both rodents and human electrophysiological studies, in which low-frequency oscillations modulate the probability of single unit and high gamma activities, with the occurrence phase [217,218] indexing distinct information[90,212-216]. **Oscillatory Multiplexing of Directionality**: We have employed a number of directional connectivity metrics to examine dynamics of brain oscillations including inter-regional PAC, phase slope index (PSI) and spectral Granger causality. We observed bidirectional communications among these three brain regions, which are supported by reciprocal anatomical connections. Moreover, the directionality of information flow changes at behavioral timescales, facilitating a flexible network reconfiguration along with different task states. In sum, oscillatory multiplexing of frequency, phase and directionality supports amygdala-hippocampus-orbitofrontal circuit to rapidly and flexibly facilitate emotional processing in humans.

5.2 Future Directions

5.2.1 Extended Network for Emotional Regulation

Other brain regions have also been proposed to facilitate salience processing and emotional regulation, such as **anterior insula**, **dorsal anterior cingulate cortex (dACC)** and **dorsolateral prefrontal cortex (dlPFC)**. Specifically, **anterior insula** is involved in salient detections via direct sensory inputs from auditory/visual systems[280-284] and emotional saliency from subcortical nodes, including the amygdala, the ventral striatum and the ventral tegmental nuclei[285]. Moreover, it is also sensitive to internal autonomic processes, such as heart rate, skin conductance and respiration[286,287], which are linked to interceptive awareness of salient events. **dACC** and the associated dorsomedial prefrontal cortex receive very little sensory inputs[288,289]. Instead, dACC and dorsomedial prefrontal cortex can send strong motor output via direct connections to the spinal cord and subcortical oculomotor areas[290], which plays a prominent role in response selection to salient stimuli[291,292]. **dlPFC** has strong connections with orbitofrontal cortex and hippocampus and has been considered as a critical brain structure involved in working memory[69] and cognitive flexibility[293]. Neuroimaging studies[294] have shown that exposure to severe stress reduces working memory related activities in the dlPFC and leads to impaired memory performance. Moreover, damage or lesion to the dlPFC increases the likelihood of depressive symptoms[295], which indicates the contribution of positive affect from dlPFC for a balanced emotional regulation system[296]. Applying similar analysis onto these regions could bring us extended knowledge of salient information processing and provide more intact understandings for emotional regulation.

5.2.2 Microcircuit Configuration and Single Unit Recording

Based on the knowledge of the group-level oscillatory dynamics, the next-level question is: what are the functional/anatomical configurations of neural microcircuit underlying the current emotional? Specifically, how do different classes of cells interact to produce various spatial, temporal and spectral oscillatory features linked with diverse emotional processes? Single-unit recordings provide a method of measuring the electrophysiological responses of single neurons. Simultaneous recording of a large number of single neurons and local field potentials in multiple brain regions will allow us to map activities from the emotional network, bringing more robust characterization of the interested effects and the diversity of encoding across neural populations.

5.2.3 Stimulation and Computational Psychiatry

Emotional processing imbues appropriate salience to our experiences and facilitates flexible behavioral adaptation. Dysfunction in contextualizing information increases the risk of inappropriate responses to environmental conditions and has been implicated in a broad range of psychopathologies, including post-traumatic stress disorder, schizophrenia, and substance abuse disorders[224]. The public health and economic burden of mental illness exceed that of cancer, diabetes, and respiratory ailments put together (World Health Organization, 2011), accounting for over 30% morbidities across all medical conditions. Neuropsychiatric disorders are primarily treated with pharmacological means, targeting large swaths of brain tissue. To capture the underlying mechanistic process, a circuit-level perspective might provide a deeper understanding of neuropsychiatric disorders and improved interventions with greater efficacy

and fewer side effects. A potential clinical application of our study is the modulation of oscillatory interactions within the amygdala-hippocampus-orbitofrontal circuit. Phase alignment or coupling between these three regions provides a temporal window for coordinated inter-regional information transfer and communication. Information transfer errors may occur due to over-coupling or under-coupling between brain structures, including failures in terminating irrelevant communication or extracting meaningful signals. These alterations in communication dynamics have been proposed to underlie neuropsychiatric disorders[155]. To 'break' such pathological couplings, inter-regional interactions could be altered with stimulation-based therapy to induce temporal phase synchronization (e.g., enhanced phase alignment with phase resetting) or desynchronization (e.g., reduced phase alignment with neural noises) between two brain structures. This provides a theoretical framework for circuit-specific and stimulation-based intervention approaches, such as deep brain stimulation, transcranial alternating current stimulation (tACS), and transcranial magnetic stimulation. Furthermore, greater specificity can also be achieved by taking individual oscillatory variation into account. For example, using tACS parameters specific to individuals' dominant theta frequency improves short-term memory capacity[297]. Our study also demonstrated that instead of conforming to the conventional definition of theta (4–7 Hz)/alpha (8–12 Hz) frequency rhythms, amygdala–hippocampus-orbitofrontal dynamics are contingent upon subject-specific low frequency oscillations. Identifying such individualized electrophysiological features in patients with psychiatric disorders could enable stimulation parameters to be tailored for subject-preferred neuronal firing frequencies, leading to personalized therapeutic interventions.

5.3 Concluding Remarks

The series of studies described in this dissertation extend the current knowledge of emotional processing in humans with direct electrophysiological dynamics. It emphasizes that single region analysis is not sufficient to understand the complex nature of the emotional processing. Instead, dynamic interactions among amygdala, hippocampus, and orbitofrontal cortex are crucial to emotion-related cognitive functions. Given the essential role of emotional processing in adaptive behavior and its derangement in neuropsychiatric disorders, our findings propose a core emotional network and dictate its underlying oscillatory mechanisms, which is critical to complete the translation from ‘circuit neuroscience’ to ‘circuit neurotherapy’.

REFERENCES

1 Adolphs, R. Recognizing emotion from facial expressions: psychological and neurological mechanisms. *Behav Cogn Neurosci Rev* **1**, 21-62, doi:10.1177/1534582302001001003 (2002).

2 Dailey, M. N., Cottrell, G. W., Padgett, C. & Adolphs, R. EMPATH: a neural network that categorizes facial expressions. *J Cogn Neurosci* **14**, 1158-1173, doi:10.1162/089892902760807177 (2002).

3 Calder, A. J., Young, A. W., Keane, J. & Dean, M. Configural information in facial expression perception. *J Exp Psychol Hum Percept Perform* **26**, 527-551 (2000).

4 Adolphs, R. Fear, faces, and the human amygdala. *Curr Opin Neurobiol* **18**, 166-172, doi:10.1016/j.conb.2008.06.006 (2008).

5 Adolphs, R., Tranel, D., Damasio, H. & Damasio, A. Impaired recognition of emotion in facial expressions following bilateral damage to the human amygdala. *Nature* **372**, 669-672, doi:10.1038/372669a0 (1994).

6 Phelps, E. A. & LeDoux, J. E. Contributions of the amygdala to emotion processing: from animal models to human behavior. *Neuron* **48**, 175-187, doi:10.1016/j.neuron.2005.09.025 (2005).

7 Vuilleumier, P., Armony, J. L., Driver, J. & Dolan, R. J. Effects of attention and emotion on face processing in the human brain: an event-related fMRI study. *Neuron* **30**, 829-841 (2001).

8 Anderson, A. K., Christoff, K., Panitz, D., De Rosa, E. & Gabrieli, J. D. Neural correlates of the automatic processing of threat facial signals. *J Neurosci* **23**, 5627-5633 (2003).

9 Williams, M. A., Morris, A. P., McGlone, F., Abbott, D. F. & Mattingley, J. B. Amygdala responses to fearful and happy facial expressions under conditions of binocular suppression. *J Neurosci* **24**, 2898-2904, doi:10.1523/JNEUROSCI.4977-03.2004 (2004).

10 Allsop, S. A., Vander Weele, C. M., Wichmann, R. & Tye, K. M. Optogenetic insights on the relationship between anxiety-related behaviors and social deficits. *Front Behav Neurosci* **8**, 241, doi:10.3389/fnbeh.2014.00241 (2014).

11 Kim, E. J. *et al.* Alterations of hippocampal place cells in foraging rats facing a "predatory" threat. *Curr Biol* **25**, 1362-1367, doi:10.1016/j.cub.2015.03.048 (2015).

12 Giachero, M., Calfa, G. D. & Molina, V. A. Hippocampal dendritic spines remodeling and fear memory are modulated by GABAergic signaling within the basolateral amygdala complex. *Hippocampus* **25**, 545-555, doi:10.1002/hipo.22409 (2015).

13 Bradley, M. M., Greenwald, M. K., Petry, M. C. & Lang, P. J. Remembering pictures: pleasure and arousal in memory. *J Exp Psychol Learn Mem Cogn* **18**, 379-390 (1992).

14 Kensinger, E. A. & Schacter, D. L. Remembering the specific visual details of presented objects: neuroimaging evidence for effects of emotion. *Neuropsychologia* **45**, 2951-2962, doi:10.1016/j.neuropsychologia.2007.05.024 (2007).

15 Kensinger, E. A. Remembering the Details: Effects of Emotion. *Emot Rev* **1**, 99-113, doi:10.1177/1754073908100432 (2009).

16 Mather, M. & Sutherland, M. R. Arousal-Biased Competition in Perception and Memory. *Perspect Psychol Sci* **6**, 114-133, doi:10.1177/1745691611400234 (2011).

17 Loftus, E. F., Loftus, G. R. & Messo, J. Some Facts About Weapon Focus. *Law Human Behav* **11**, 55-62, doi:Doi 10.1007/Bf01044839 (1987).

18 Segal, S. K., Stark, S. M., Kattan, D., Stark, C. E. & Yassa, M. A. Norepinephrine-mediated emotional arousal facilitates subsequent pattern separation. *Neurobiol Learn Mem* **97**, 465-469, doi:10.1016/j.nlm.2012.03.010 (2012).

19 GoodSmith, D. *et al.* Spatial Representations of Granule Cells and Mossy Cells of the Dentate Gyrus. *Neuron* **93**, 677-690 e675, doi:10.1016/j.neuron.2016.12.026 (2017).

20 Leutgeb, J. K., Leutgeb, S., Moser, M. B. & Moser, E. I. Pattern separation in the dentate gyrus and CA3 of the hippocampus. *Science* **315**, 961-966, doi:10.1126/science.1135801 (2007).

21 Leal, S. L., Tighe, S. K. & Yassa, M. A. Asymmetric effects of emotion on mnemonic interference. *Neurobiol Learn Mem* **111**, 41-48, doi:10.1016/j.nlm.2014.02.013 (2014).

22 Leal, S. L., Tighe, S. K., Jones, C. K. & Yassa, M. A. Pattern separation of emotional information in hippocampal dentate and CA3. *Hippocampus* **24**, 1146-1155, doi:10.1002/hipo.22298 (2014).

23 Stoltzfus, B. How Movies Work - Kawin,B. *Am Book Rev* **15**, 6-6 (1993).

24 Mobbs, D. *et al.* The Kuleshov Effect: the influence of contextual framing on emotional attributions. *Soc Cogn Affect Neurosci* **1**, 95-106, doi:10.1093/scan/nsl014 (2006).

25 Sahakyan, L. & Kelley, C. M. A contextual change account of the directed forgetting effect. *J Exp Psychol Learn Mem Cogn* **28**, 1064-1072 (2002).

26 Liberzon, I. & Abelson, J. L. Context Processing and the Neurobiology of Post-Traumatic Stress Disorder. *Neuron* **92**, 14-30, doi:10.1016/j.neuron.2016.09.039 (2016).

27 den Stock, J. & de Gelder, B. Emotional information in body and background hampers recognition memory for faces. *Neurobiology of learning and memory* **97**, 321-325, doi:10.1016/j.nlm.2012.01.007 (2012).

28 Girardeau, G., Inema, I. & Buzsáki, G. Reactivations of emotional memory in the hippocampus-amygdala system during sleep. *Nature neuroscience*, doi:10.1038/nn.4637 (2017).

29 Likhtik, E., Stujenske, J. M., Topiwala, M. A., Harris, A. Z. & Gordon, J. A. Prefrontal entrainment of amygdala activity signals safety in learned fear and innate anxiety. *Nat Neurosci* **17**, 106-113, doi:10.1038/nn.3582 (2014).

30 Padilla-Coreano, N. *et al.* Direct Ventral Hippocampal-Prefrontal Input Is Required for Anxiety-Related Neural Activity and Behavior. *Neuron* **89**, 857-866, doi:10.1016/j.neuron.2016.01.011 (2016).

31 Phelps, E. A., Delgado, M. R., Nearing, K. I. & LeDoux, J. E. Extinction learning in humans: role of the amygdala and vmPFC. *Neuron* **43**, 897-905, doi:10.1016/j.neuron.2004.08.042 (2004).

32 Onat, S. & Büchel, C. The neuronal basis of fear generalization in humans. *Nature neuroscience* **18**, 1811-1818, doi:10.1038/nn.4166 (2015).

33 Maren, S., Phan, L. K. & Liberzon, I. The contextual brain: implications for fear conditioning, extinction and psychopathology. *Nature Reviews Neuroscience* **14**, 417-428, doi:10.1038/nrn3492 (2013).

34 Zheng, J. & Lin, J. J. Modulating Amygdala-Hippocampal Network Communication: A Potential Therapy for Neuropsychiatric Disorders. *Neuropsychopharmacology* **43**, 218-219, doi:10.1038/npp.2017.201 (2018).

35 Swanson, L. W. & Petrovich, G. D. What is the amygdala? *Trends Neurosci* **21**, 323-331 (1998).

36 Sah, P., Faber, E. S., Lopez De Armentia, M. & Power, J. The amygdaloid complex: anatomy and physiology. *Physiol Rev* **83**, 803-834, doi:10.1152/physrev.00002.2003 (2003).

37 Andersen, P. *The hippocampus book*. (Oxford University Press, 2007).

38 Amaral, D. G. Emerging principles of intrinsic hippocampal organization. *Curr Opin Neurobiol* **3**, 225-229 (1993).

39 Foster, D. J. & Wilson, M. A. Reverse replay of behavioural sequences in hippocampal place cells during the awake state. *Nature* **440**, 680-683, doi:10.1038/nature04587 (2006).

40 Strange, B. A., Witter, M. P., Lein, E. S. & Moser, E. I. Functional organization of the hippocampal longitudinal axis. *Nat Rev Neurosci* **15**, 655-669, doi:10.1038/nrn3785 (2014).

41 Fanselow, M. S. & Dong, H. W. Are the dorsal and ventral hippocampus functionally distinct structures? *Neuron* **65**, 7-19, doi:10.1016/j.neuron.2009.11.031 (2010).

42 Kringelbach, M. L. The human orbitofrontal cortex: linking reward to hedonic experience. *Nat Rev Neurosci* **6**, 691-702, doi:10.1038/nrn1747 (2005).

43 Boller, F. *et al. Handbook of neuropsychology*. 2nd edn, (Elsevier, 2000).

44 Pitkanen, A., Pikkarainen, M., Nurminen, N. & Ylinen, A. Reciprocal connections between the amygdala and the hippocampal formation, perirhinal cortex, and postrhinal cortex in rat. A review. *Ann N Y Acad Sci* **911**, 369-391 (2000).

45 Petrovich, G. D., Canteras, N. S. & Swanson, L. W. Combinatorial amygdalar inputs to hippocampal domains and hypothalamic behavior systems. *Brain Res Brain Res Rev* **38**, 247-289 (2001).

46 Amaral, D. G. & Price, J. L. Amygdalo-cortical projections in the monkey (Macaca fascicularis). *J Comp Neurol* **230**, 465-496, doi:10.1002/cne.902300402 (1984).

47 Carmichael, S. T. & Price, J. L. Limbic connections of the orbital and medial prefrontal cortex in macaque monkeys. *J Comp Neurol* **363**, 615-641, doi:10.1002/cne.903630408 (1995).

48 Eblen, F. & Graybiel, A. M. Highly restricted origin of prefrontal cortical inputs to striosomes in the macaque monkey. *J Neurosci* **15**, 5999-6013 (1995).

49 Eichenbaum, H. Prefrontal-hippocampal interactions in episodic memory. *Nat Rev Neurosci* **18**, 547-558, doi:10.1038/nrn.2017.74 (2017).

50 Elliott, R., Dolan, R. J. & Frith, C. D. Dissociable functions in the medial and lateral orbitofrontal cortex: evidence from human neuroimaging studies. *Cereb Cortex* **10**, 308-317 (2000).

51 Jay, T. M. & Witter, M. P. Distribution of hippocampal CA1 and subicular efferents in the prefrontal cortex of the rat studied by means of anterograde transport of Phaseolus vulgaris-leucoagglutinin. *J Comp Neurol* **313**, 574-586, doi:10.1002/cne.903130404 (1991).

52 McEwen, B. S., Nasca, C. & Gray, J. D. Stress Effects on Neuronal Structure: Hippocampus, Amygdala, and Prefrontal Cortex. *Neuropsychopharmacology* **41**, 3-23, doi:10.1038/npp.2015.171 (2016).

53 Janak, P. H. & Tye, K. M. From circuits to behaviour in the amygdala. *Nature* **517**, 284-292, doi:10.1038/nature14188 (2015).

54 Jin, J., Zelano, C., Gottfried, J. A. & Mohanty, A. Human Amygdala Represents the Complete Spectrum of Subjective Valence. *J Neurosci* **35**, 15145-15156, doi:10.1523/JNEUROSCI.2450-15.2015 (2015).

55 Jennings, J. H. *et al.* Distinct extended amygdala circuits for divergent motivational states. *Nature* **496**, 224-228, doi:10.1038/nature12041 (2013).

56 Ji, J. & Maren, S. Hippocampal involvement in contextual modulation of fear extinction. *Hippocampus* **17**, 749-758, doi:10.1002/hipo.20331 (2007).

57 Holland, A. C. & Kensinger, E. A. Emotion and autobiographical memory. *Phys Life Rev* **7**, 88-131, doi:10.1016/j.plrev.2010.01.006 (2010).

58 Izquierdo, A., Suda, R. K. & Murray, E. A. Comparison of the effects of bilateral orbital prefrontal cortex lesions and amygdala lesions on emotional responses in rhesus monkeys. *J Neurosci* **25**, 8534-8542, doi:10.1523/JNEUROSCI.1232-05.2005 (2005).

59 Stalnaker, T. A. *et al.* Orbitofrontal neurons infer the value and identity of predicted outcomes. *Nature communications* **5**, 3926, doi:10.1038/ncomms4926 (2014).

60 Clarke, H. F., Horst, N. K. & Roberts, A. C. Regional inactivations of primate ventral prefrontal cortex reveal two distinct mechanisms underlying negative bias in decision making. *Proc Natl Acad Sci U S A* **112**, 4176-4181, doi:10.1073/pnas.1422440112 (2015).

61 Agustin-Pavon, C. *et al.* Lesions of ventrolateral prefrontal or anterior orbitofrontal cortex in primates heighten negative emotion. *Biological psychiatry* **72**, 266-272, doi:10.1016/j.biopsych.2012.03.007 (2012).

62 Wikenheiser, A. M. & Schoenbaum, G. Over the river, through the woods: cognitive maps in the hippocampus and orbitofrontal cortex. *Nature reviews. Neuroscience* **17**, 513-523, doi:10.1038/nrn.2016.56 (2016).

63 Stachenfeld, K. L., Botvinick, M. M. & Gershman, S. J. The hippocampus as a predictive map. *Nature neuroscience* **20**, 1643-1653, doi:10.1038/nn.4650 (2017).

64 O'Doherty, J., Kringelbach, M. L., Rolls, E. T., Hornak, J. & Andrews, C. Abstract reward and punishment representations in the human orbitofrontal cortex. *Nature neuroscience* **4**, 95-102, doi:10.1038/82959 (2001).

65 Zangemeister, L., Grabenhorst, F. & Schultz, W. Neural Basis for Economic Saving Strategies in Human Amygdala-Prefrontal Reward Circuits. *Current biology : CB* **26**, 3004-3013, doi:10.1016/j.cub.2016.09.016 (2016).

66 Morrison, S. E. & Salzman, D. C. Re-valuing the amygdala. *Current opinion in neurobiology* **20**, 221-230, doi:10.1016/j.conb.2010.02.007 (2010).

67 Palmini, A. The concept of the epileptogenic zone: a modern look at Penfield and Jasper's views on the role of interictal spikes. *Epileptic Disord* **8 Suppl 2**, S10-15 (2006).

68 Cohen, M. X. Where Does EEG Come From and What Does It Mean? *Trends Neurosci* **40**, 208-218, doi:10.1016/j.tins.2017.02.004 (2017).

69 Johnson, E. L. & Knight, R. T. Intracranial recordings and human memory. *Curr Opin Neurobiol* **31**, 18-25, doi:10.1016/j.conb.2014.07.021 (2015).

70 Buzsaki, G. & Draguhn, A. Neuronal oscillations in cortical networks. *Science* **304**, 1926-1929, doi:10.1126/science.1099745 (2004).

71 Wang, X. J. Neurophysiological and computational principles of cortical rhythms in cognition. *Physiol Rev* **90**, 1195-1268, doi:10.1152/physrev.00035.2008 (2010).

72 Salinas, E. & Sejnowski, T. J. Correlated neuronal activity and the flow of neural information. *Nat Rev Neurosci* **2**, 539-550, doi:10.1038/35086012 (2001).

73 Singer, W. Neuronal synchrony: a versatile code for the definition of relations? *Neuron* **24**, 49-65, 111-125 (1999).

74 Siegel, M., Donner, T. H. & Engel, A. K. Spectral fingerprints of large-scale neuronal interactions. *Nat Rev Neurosci* **13**, 121-134, doi:10.1038/nrn3137 (2012).

75 Knyazev, G. G. Motivation, emotion, and their inhibitory control mirrored in brain oscillations. *Neurosci Biobehav R* **31**, 377-395, doi:10.1016/j.neubiorev.2006.10.004 (2007).

76 Braitenberg, V., Schüz, A. & Braitenberg, V. *Cortex : statistics and geometry of neuronal connectivity*. 2nd thoroughly rev. edn.

77 Nunez, P. L. & Cutillo, B. A. *Neocortical dynamics and human EEG rhythms*. (Oxford University Press, 1995).

78 Steriade, M., Timofeev, I. & Grenier, F. Natural waking and sleep states: a view from inside neocortical neurons. *J Neurophysiol* **85**, 1969-1985, doi:10.1152/jn.2001.85.5.1969 (2001).

79 Csicsvari, J., Jamieson, B., Wise, K. D. & Buzsaki, G. Mechanisms of gamma oscillations in the hippocampus of the behaving rat. *Neuron* **37**, 311-322 (2003).

80 Buzsaki, G., Geisler, C., Henze, D. A. & Wang, X. J. Interneuron Diversity series: Circuit complexity and axon wiring economy of cortical interneurons. *Trends Neurosci* **27**, 186-193, doi:10.1016/j.tins.2004.02.007 (2004).

81 Buzsaki, G., Anastassiou, C. A. & Koch, C. The origin of extracellular fields and currents--EEG, ECoG, LFP and spikes. *Nat Rev Neurosci* **13**, 407-420, doi:10.1038/nrn3241 (2012).

82 Rasch, M. J., Gretton, A., Murayama, Y., Maass, W. & Logothetis, N. K. Inferring spike trains from local field potentials. *J Neurophysiol* **99**, 1461-1476, doi:10.1152/jn.00919.2007 (2008).

83 Fries, P. Neuronal gamma-band synchronization as a fundamental process in cortical computation. *Annu Rev Neurosci* **32**, 209-224, doi:10.1146/annurev.neuro.051508.135603 (2009).

84 Bragin, A. *et al.* Gamma (40-100 Hz) oscillation in the hippocampus of the behaving rat. *J Neurosci* **15**, 47-60 (1995).

85 Ray, S., Crone, N. E., Niebur, E., Franaszczuk, P. J. & Hsiao, S. S. Neural correlates of high-gamma oscillations (60-200 Hz) in macaque local field potentials and their potential implications in electrocorticography. *J Neurosci* **28**, 11526-11536, doi:10.1523/JNEUROSCI.2848-08.2008 (2008).

86 Klimesch, W. alpha-band oscillations, attention, and controlled access to stored information. *Trends Cogn Sci* **16**, 606-617, doi:10.1016/j.tics.2012.10.007 (2012).

87 Mirollo, R. E. & Strogatz, S. H. Synchronization of Pulse-Coupled Biological Oscillators. *Siam J Appl Math* **50**, 1645-1662, doi:Doi 10.1137/0150098 (1990).

88 Winfree, A. T. *The geometry of biological time*. (Springer Verlag, 1980).

89 Fries, P. A mechanism for cognitive dynamics: neuronal communication through neuronal coherence. *Trends Cogn Sci* **9**, 474-480, doi:10.1016/j.tics.2005.08.011 (2005).

90 Lisman, J. E. & Jensen, O. The theta-gamma neural code. *Neuron* **77**, 1002-1016, doi:10.1016/j.neuron.2013.03.007 (2013).

91 Buzsaki, G. Neural syntax: cell assemblies, synapsembles, and readers. *Neuron* **68**, 362-385, doi:10.1016/j.neuron.2010.09.023 (2010).

92 Varela, F., Lachaux, J. P., Rodriguez, E. & Martinerie, J. The brainweb: phase synchronization and large-scale integration. *Nat Rev Neurosci* **2**, 229-239, doi:10.1038/35067550 (2001).

93 Engel, A. K., Fries, P. & Singer, W. Dynamic predictions: oscillations and synchrony in top-down processing. *Nat Rev Neurosci* **2**, 704-716, doi:10.1038/35094565 (2001).

94 Crone, N. E., Sinai, A. & Korzeniewska, A. High-frequency gamma oscillations and human brain mapping with electrocorticography. *Prog Brain Res* **159**, 275-295, doi:10.1016/S0079-6123(06)59019-3 (2006).

95 Colgin, L. L. *et al.* Frequency of gamma oscillations routes flow of information in the hippocampus. *Nature* **462**, 353-357, doi:10.1038/nature08573 (2009).

96 Gaona, C. M. *et al.* Nonuniform high-gamma (60-500 Hz) power changes dissociate cognitive task and anatomy in human cortex. *J Neurosci* **31**, 2091-2100, doi:10.1523/JNEUROSCI.4722-10.2011 (2011).

97 Menon, V. *et al.* Spatio-temporal correlations in human gamma band electrocorticograms. *Electroencephalogr Clin Neurophysiol* **98**, 89-102 (1996).

98 Meador, K. J. Cognitive outcomes and predictive factors in epilepsy. *Neurology* **58**, S21-26 (2002).

99 Foster, B. L., Rangarajan, V., Shirer, W. R. & Parvizi, J. Intrinsic and task-dependent coupling of neuronal population activity in human parietal cortex. *Neuron* **86**, 578-590, doi:10.1016/j.neuron.2015.03.018 (2015).

100 Schomburg, E. W. *et al.* Theta phase segregation of input-specific gamma patterns in entorhinal-hippocampal networks. *Neuron* **84**, 470-485, doi:10.1016/j.neuron.2014.08.051 (2014).

101 Zemankovics, R., Veres, J. M., Oren, I. & Hajos, N. Feedforward inhibition underlies the propagation of cholinergically induced gamma oscillations from hippocampal CA3 to CA1. *J Neurosci* **33**, 12337-12351, doi:10.1523/JNEUROSCI.3680-12.2013 (2013).

102 Brunet, N. M. *et al.* Stimulus repetition modulates gamma-band synchronization in primate visual cortex. *Proc Natl Acad Sci U S A* **111**, 3626-3631, doi:10.1073/pnas.1309714111 (2014).

103 Buzsaki, G. & Schomburg, E. W. What does gamma coherence tell us about inter-regional neural communication? *Nat Neurosci* **18**, 484-489, doi:10.1038/nn.3952 (2015).

104 Freeman, W. J., Rogers, L. J., Holmes, M. D. & Silbergeld, D. L. Spatial spectral analysis of human electrocorticograms including the alpha and gamma bands. *J Neurosci Methods* **95**, 111-121 (2000).

105 Bak, P., Tang, C. & Wiesenfeld, K. Self-organized criticality: An explanation of the 1/f noise. *Phys Rev Lett* **59**, 381-384, doi:10.1103/PhysRevLett.59.381 (1987).

106 Steriade, M. Impact of network activities on neuronal properties in corticothalamic systems. *J Neurophysiol* **86**, 1-39, doi:10.1152/jn.2001.86.1.1 (2001).

107 Sirota, A., Csicsvari, J., Buhl, D. & Buzsaki, G. Communication between neocortex and hippocampus during sleep in rodents. *Proc Natl Acad Sci U S A* **100**, 2065-2069, doi:10.1073/pnas.0437938100 (2003).

108 Canolty, R. T. & Knight, R. T. The functional role of cross-frequency coupling. *Trends Cogn Sci* **14**, 506-515, doi:10.1016/j.tics.2010.09.001 (2010).

109 Demiralp, T. *et al.* Gamma amplitudes are coupled to theta phase in human EEG during visual perception. *Int J Psychophysiol* **64**, 24-30, doi:10.1016/j.ijpsycho.2006.07.005 (2007).

110 Helfrich, R. F. & Knight, R. T. Oscillatory Dynamics of Prefrontal Cognitive Control. *Trends Cogn Sci* **20**, 916-930, doi:10.1016/j.tics.2016.09.007 (2016).

111 Adolphs, R. Cognitive neuroscience of human social behaviour. *Nat Rev Neurosci* **4**, 165-178, doi:10.1038/nrn1056 (2003).

112 Wang, S. *et al.* Neurons in the human amygdala selective for perceived emotion. *Proc Natl Acad Sci U S A* **111**, E3110-3119, doi:10.1073/pnas.1323342111 (2014).

113 Buzsaki, G. & Moser, E. I. Memory, navigation and theta rhythm in the hippocampal-entorhinal system. *Nat Neurosci* **16**, 130-138, doi:10.1038/nn.3304 (2013).

114 Pape, H. C. & Driesang, R. B. Ionic mechanisms of intrinsic oscillations in neurons of the basolateral amygdaloid complex. *J Neurophysiol* **79**, 217-226 (1998).

115 LeDoux, J. E. *The emotional brain : the mysterious underpinnings of emotional life*. (Simon & Schuster, 1996).

116 LaBar, K. S., Crupain, M. J., Voyvodic, J. T. & McCarthy, G. Dynamic perception of facial affect and identity in the human brain. *Cereb Cortex* **13**, 1023-1033 (2003).

117 Avants, B. B. *et al.* A reproducible evaluation of ANTs similarity metric performance in brain image registration. *Neuroimage* **54**, 2033-2044, doi:10.1016/j.neuroimage.2010.09.025 (2011).

118 Reagh, Z. M., Watabe, J., Ly, M., Murray, E. & Yassa, M. A. Dissociated signals in human dentate gyrus and CA3 predict different facets of recognition memory. *J Neurosci* **34**, 13301-13313, doi:10.1523/JNEUROSCI.2779-14.2014 (2014).

119 Reagh, Z. M. & Yassa, M. A. Object and spatial mnemonic interference differentially engage lateral and medial entorhinal cortex in humans. *Proc Natl Acad Sci U S A* **111**, E4264-4273, doi:10.1073/pnas.1411250111 (2014).

120 Duvernoy, H. M. & SpringerLink (Online service). xxiv, 630 p. (Springer-Verlag Berlin Heidelberg, Berlin, Heidelberg, 2005).

121 Entis, J. J., Doerga, P., Barrett, L. F. & Dickerson, B. C. A reliable protocol for the manual segmentation of the human amygdala and its subregions using ultra-high resolution MRI. *Neuroimage* **60**, 1226-1235, doi:10.1016/j.neuroimage.2011.12.073 (2012).

122 Yassa, M. A. & Stark, C. E. A quantitative evaluation of cross-participant registration techniques for MRI studies of the medial temporal lobe. *Neuroimage* **44**, 319-327, doi:10.1016/j.neuroimage.2008.09.016 (2009).

123 Entis, J. J., Doerga, P., Barrett, L. F. & Dickerson, B. C. A reliable protocol for the manual segmentation of the human amygdala and its subregions using ultra-high resolution MRI. *Neuroimage* **60**, 1226-1235, doi:10.1016/j.neuroimage.2011.12.073 (2012).

124 Avants, B. B. *et al.* A reproducible evaluation of ANTs similarity metric performance in brain image registration. *Neuroimage* **54**, 2033-2044, doi:10.1016/j.neuroimage.2010.09.025 (2011).

125 Mitra, P. & Bokil, H. *Observed brain dynamics*. (Oxford University Press, 2008).

126 Bell, A. J. & Sejnowski, T. J. An information-maximization approach to blind separation and blind deconvolution. *Neural Comput* **7**, 1129-1159 (1995).

127 Miller, K. J., Sorensen, L. B., Ojemann, J. G. & den Nijs, M. Power-law scaling in the brain surface electric potential. *PLoS Comput Biol* **5**, e1000609, doi:10.1371/journal.pcbi.1000609 (2009).

128 Delorme, A. & Makeig, S. EEGLAB: an open source toolbox for analysis of single-trial EEG dynamics including independent component analysis. *J Neurosci Methods* **134**, 9-21, doi:10.1016/j.jneumeth.2003.10.009 (2004).

129 Aru, J. *et al.* Untangling cross-frequency coupling in neuroscience. *Curr Opin Neurobiol* **31**, 51-61, doi:10.1016/j.conb.2014.08.002 (2015).

130 Grandchamp, R. & Delorme, A. Single-trial normalization for event-related spectral decomposition reduces sensitivity to noisy trials. *Front Psychol* **2**, 236, doi:10.3389/fpsyg.2011.00236 (2011).

131 Maris, E. & Oostenveld, R. Nonparametric statistical testing of EEG- and MEG-data. *J Neurosci Methods* **164**, 177-190, doi:10.1016/j.jneumeth.2007.03.024 (2007).

132 Krzywinski, M., Birol, I., Jones, S. J. & Marra, M. A. Hive plots--rational approach to visualizing networks. *Brief Bioinform* **13**, 627-644, doi:10.1093/bib/bbr069 (2012).

133 Berens, P. CircStat: A MATLAB Toolbox for Circular Statistics. *J Stat Softw* **31**, 1-21 (2009).

134 Voytek, B. *et al.* Shifts in gamma phase-amplitude coupling frequency from theta to alpha over posterior cortex during visual tasks. *Frontiers in human neuroscience* **4**, 191, doi:10.3389/fnhum.2010.00191 (2010).

135 Cohen, M. X. Assessing transient cross-frequency coupling in EEG data. *J Neurosci Methods* **168**, 494-499, doi:10.1016/j.jneumeth.2007.10.012 (2008).

136 Nolte, G. *et al.* Robustly estimating the flow direction of information in complex physical systems. *Phys Rev Lett* **100**, 234101, doi:10.1103/PhysRevLett.100.234101 (2008).

137 Jiang, H., Bahramisharif, A., van Gerven, M. A. & Jensen, O. Measuring directionality between neuronal oscillations of different frequencies. *Neuroimage* **118**, 359-367, doi:10.1016/j.neuroimage.2015.05.044 (2015).

138 Barnett, L. & Seth, A. K. The MVGC multivariate Granger causality toolbox: a new approach to Granger-causal inference. *J Neurosci Methods* **223**, 50-68, doi:10.1016/j.jneumeth.2013.10.018 (2014).

139 Ding, M., Bressler, S. L., Yang, W. & Liang, H. Short-window spectral analysis of cortical event-related potentials by adaptive multivariate autoregressive modeling: data preprocessing, model validation, and variability assessment. *Biol Cybern* **83**, 35-45, doi:10.1007/s004229900137 (2000).

140 Akaike, H. Citation Classic - a New Look at the Statistical-Model Identification. *Cc/Eng Tech Appl Sci*, 22-22 (1981).

141 LaBar, K. S., Crupain, M. J., Voyvodic, J. T. & McCarthy, G. Dynamic perception of facial affect and identity in the human brain. *Cerebral Cortex* **13**, 1023-1033, doi:DOI 10.1093/cercor/13.10.1023 (2003).

142 Bastos, A. M., Vezoli, J. & Fries, P. Communication through coherence with inter-areal delays. *Current Opinion in Neurobiology* **31**, 173-180, doi:10.1016/j.conb.2014.11.001 (2015).

143 Liu, J. & Newsome, W. T. Local field potential in cortical area MT: stimulus tuning and behavioral correlations. *J Neurosci* **26**, 7779-7790, doi:10.1523/JNEUROSCI.5052-05.2006 (2006).

144 Mussel, P., Ulrich, N., Allen, J. J., Osinsky, R. & Hewig, J. Patterns of theta oscillation reflect the neural basis of individual differences in epistemic motivation. *Sci Rep* **6**, 29245, doi:10.1038/srep29245 (2016).

145 von Nicolai, C. *et al.* Corticostriatal Coordination through Coherent Phase-Amplitude Coupling. *J Neurosci* **34**, 5938-5948, doi:10.1523/Jneurosci.5007-13.2014 (2014).

146 Sweeney-Reed, C. M. *et al.* Thalamic theta phase alignment predicts human memory formation and anterior thalamic cross-frequency coupling. *Elife* **4**, doi:ARTN e07578 10.7554/eLife.07578 (2015).

147 Aru, J. *et al.* Untangling cross-frequency coupling in neuroscience. *Current Opinion in Neurobiology* **31**, 51-61, doi:10.1016/j.conb.2014.08.002 (2015).

148 Phelps, E. A. Human emotion and memory: interactions of the amygdala and hippocampal complex. *Curr Opin Neurobiol* **14**, 198-202, doi:10.1016/j.conb.2004.03.015 (2004).

149 Amaral, D. G. & Cowan, W. M. Subcortical afferents to the hippocampal formation in the monkey. *J Comp Neurol* **189**, 573-591, doi:10.1002/cne.901890402 (1980).

150 Stefanacci, L., Suzuki, W. A. & Amaral, D. G. Organization of connections between the amygdaloid complex and the perirhinal and parahippocampal cortices in macaque monkeys. *J Comp Neurol* **375**, 552-582, doi:10.1002/(SICI)1096-9861(19961125)375:4<552::AID-CNE2>3.0.CO;2-0 (1996).

151 McDonald, A. J. & Mott, D. D. Functional neuroanatomy of amygdalohippocampal interconnections and their role in learning and memory. *J Neurosci Res* **95**, 797-820, doi:10.1002/jnr.23709 (2017).

152 Seidenbecher, T., Laxmi, T. R., Stork, O. & Pape, H. C. Amygdalar and hippocampal theta rhythm synchronization during fear memory retrieval. *Science* **301**, 846-850, doi:10.1126/science.1085818 (2003).

153 Popa, D., Duvarci, S., Popescu, A. T., Lena, C. & Pare, D. Coherent amygdalocortical theta promotes fear memory consolidation during paradoxical sleep. *Proc Natl Acad Sci U S A* **107**, 6516-6519, doi:10.1073/pnas.0913016107 (2010).

154 Pape, H. C., Narayanan, R. T., Smid, J., Stork, O. & Seidenbecher, T. Theta activity in neurons and networks of the amygdala related to long-term fear memory. *Hippocampus* **15**, 874-880, doi:10.1002/hipo.20120 (2005).

155 Voytek, B. & Knight, R. T. Dynamic network communication as a unifying neural basis for cognition, development, aging, and disease. *Biol Psychiatry* **77**, 1089-1097, doi:10.1016/j.biopsych.2015.04.016 (2015).

156 Morrison, S. E., Saez, A., Lau, B. & Salzman, C. D. Different time courses for learning-related changes in amygdala and orbitofrontal cortex. *Neuron* **71**, 1127-1140, doi:10.1016/j.neuron.2011.07.016 (2011).

157 McGaugh, J. L. Making lasting memories: remembering the significant. *Proc Natl Acad Sci U S A* **110 Suppl 2**, 10402-10407, doi:10.1073/pnas.1301209110 (2013).

158 Kensinger, E. A. What factors need to be considered to understand emotional memories? *Emot Rev* **1**, 120-121, doi:10.1177/1754073908100436 (2009).

159 Richter-Levin, G. & Akirav, I. Amygdala-hippocampus dynamic interaction in relation to memory. *Mol Neurobiol* **22**, 11-20, doi:10.1385/MN:22:1-3:011 (2000).

160 Richter-Levin, G. The amygdala, the hippocampus, and emotional modulation of memory. *Neuroscientist* **10**, 31-39, doi:10.1177/1073858403259955 (2004).

161 McGaugh, J. L., Cahill, L. & Roozendaal, B. Involvement of the amygdala in memory storage: interaction with other brain systems. *Proc Natl Acad Sci U S A* **93**, 13508-13514 (1996).

162 McGaugh, J. L. The amygdala modulates the consolidation of memories of emotionally arousing experiences. *Annu Rev Neurosci* **27**, 1-28, doi:10.1146/annurev.neuro.27.070203.144157 (2004).

163 LeDoux, J. The amygdala. *Curr Biol* **17**, R868-874, doi:10.1016/j.cub.2007.08.005 (2007).

164 Zheng, J. *et al.* Amygdala-hippocampal dynamics during salient information processing. *Nat Commun* **8**, 14413, doi:10.1038/ncomms14413 (2017).

165 Sadaghiani, S. *et al.* Alpha-Band Phase Synchrony Is Related to Activity in the Fronto-Parietal Adaptive Control Network. *J Neurosci* **32**, 14305-14310, doi:10.1523/Jneurosci.1358-12.2012 (2012).

166 Peirce, J. W. Generating Stimuli for Neuroscience Using PsychoPy. *Front Neuroinform* **2**, 10, doi:10.3389/neuro.11.010.2008 (2008).

167 Bokil, H., Purpura, K., Schoffelen, J. M., Thomson, D. & Mitra, P. Comparing spectra and coherences for groups of unequal size. *J Neurosci Methods* **159**, 337-345, doi:10.1016/j.jneumeth.2006.07.011 (2007).

168 Oostenveld, R., Fries, P., Maris, E. & Schoffelen, J. M. FieldTrip: Open source software for advanced analysis of MEG, EEG, and invasive electrophysiological data. *Comput Intell Neurosci* **2011**, 156869, doi:10.1155/2011/156869 (2011).

169 Tass, P. *et al.* Detection of n : m phase locking from noisy data: Application to magnetoencephalography. *Physical Review Letters* **81**, 3291-3294, doi:DOI 10.1103/PhysRevLett.81.3291 (1998).

170 Kalcher, J. & Pfurtscheller, G. Discrimination between phase-locked and non-phase-locked event-related EEG activity. *Electroencephalogr Clin Neurophysiol* **94**, 381-384 (1995).

171 Lachaux, J. P., Rodriguez, E., Martinerie, J. & Varela, F. J. Measuring phase synchrony in brain signals. *Hum Brain Mapp* **8**, 194-208 (1999).

172 Schoffelen, J. M., Oostenveld, R. & Fries, P. Neuronal coherence as a mechanism of effective corticospinal interaction. *Science* **308**, 111-113, doi:10.1126/science.1107027 (2005).

173 Siegel, M., Buschman, T. J. & Miller, E. K. Cortical information flow during flexible sensorimotor decisions. *Science* **348**, 1352-1355, doi:10.1126/science.aab0551 (2015).

174 Levenson, R. W. & Gottman, J. M. Marital interaction: physiological linkage and affective exchange. *J Pers Soc Psychol* **45**, 587-597 (1983).

175 Mima, T., Matsuoka, T. & Hallett, M. Functional coupling of human right and left cortical motor areas demonstrated with partial coherence analysis. *Neurosci Lett* **287**, 93-96 (2000).

176 Schelter, B., Timmer, J., Winterhalder, M. & ebrary Inc. *Handbook of time series analysis : recent theoretical developments and applications*. (Wiley-VCH, 2006).

177 Watrous, A. J., Deuker, L., Fell, J. & Axmacher, N. Phase-amplitude coupling supports phase coding in human ECoG. *Elife* **4**, doi:10.7554/eLife.07886 (2015).

178 Lopour, B. A., Tavassoli, A., Fried, I. & Ringach, D. L. Coding of information in the phase of local field potentials within human medial temporal lobe. *Neuron* **79**, 594-606, doi:10.1016/j.neuron.2013.06.001 (2013).

179 Yassa, M. A. & Stark, C. E. Pattern separation in the hippocampus. *Trends Neurosci* **34**, 515-525, doi:10.1016/j.tins.2011.06.006 (2011).

180 Ullsperger, M., Danielmeier, C. & Jocham, G. Neurophysiology of performance monitoring and adaptive behavior. *Physiol Rev* **94**, 35-79, doi:10.1152/physrev.00041.2012 (2014).

181 Ullsperger, M., Fischer, A. G., Nigbur, R. & Endrass, T. Neural mechanisms and temporal dynamics of performance monitoring. *Trends Cogn Sci* **18**, 259-267, doi:10.1016/j.tics.2014.02.009 (2014).

182 Wessel, J. R. Error awareness and the error-related negativity: evaluating the first decade of evidence. *Front Hum Neurosci* **6**, 88, doi:10.3389/fnhum.2012.00088 (2012).

183 Roach, B. J. & Mathalon, D. H. Event-related EEG time-frequency analysis: an overview of measures and an analysis of early gamma band phase locking in schizophrenia. *Schizophr Bull* **34**, 907-926, doi:10.1093/schbul/sbn093 (2008).

184 Kovach, C. K. A Biased Look at Phase Locking: Brief Critical Review and Proposed Remedy. *Ieee T Signal Proces* **65**, 4468-4480, doi:10.1109/Tsp.2017.2711517 (2017).

185 Lozano-Soldevilla, D., Ter Huurne, N. & Oostenveld, R. Neuronal Oscillations with Non-sinusoidal Morphology Produce Spurious Phase-to-Amplitude Coupling and Directionality. *Front Comput Neurosci* **10**, 87, doi:10.3389/fncom.2016.00087 (2016).

186 Akam, T. & Kullmann, D. M. Oscillatory multiplexing of population codes for selective communication in the mammalian brain. *Nat Rev Neurosci* **15**, 111-122, doi:10.1038/nrn3668 (2014).

187 Siegel, M., Warden, M. R. & Miller, E. K. Phase-dependent neuronal coding of objects in short-term memory. *Proc Natl Acad Sci U S A* **106**, 21341-21346, doi:10.1073/pnas.0908193106 (2009).

188 Maren, S. Long-term potentiation in the amygdala: a mechanism for emotional learning and memory. *Trends Neurosci* **22**, 561-567 (1999).

189 Bannerman, D. M. *et al.* Regional dissociations within the hippocampus--memory and anxiety. *Neurosci Biobehav Rev* **28**, 273-283, doi:10.1016/j.neubiorev.2004.03.004 (2004).

190 Moser, E., Moser, M. B. & Andersen, P. Spatial learning impairment parallels the magnitude of dorsal hippocampal lesions, but is hardly present following ventral lesions. *J Neurosci* **13**, 3916-3925 (1993).

191 Henke, P. G. Limbic system modulation of stress ulcer development. *Ann N Y Acad Sci* **597**, 201-206 (1990).

192 Maggio, N. & Segal, M. Differential corticosteroid modulation of inhibitory synaptic currents in the dorsal and ventral hippocampus. *J Neurosci* **29**, 2857-2866, doi:10.1523/JNEUROSCI.4399-08.2009 (2009).

193 Matus-Amat, P., Higgins, E. A., Barrientos, R. M. & Rudy, J. W. The role of the dorsal hippocampus in the acquisition and retrieval of context memory representations. *J Neurosci* **24**, 2431-2439, doi:10.1523/JNEUROSCI.1598-03.2004 (2004).

194 Stipacek, A., Grabner, R. H., Neuper, C., Fink, A. & Neubauer, A. C. Sensitivity of human EEG alpha band desynchronization to different working memory components and increasing levels of memory load. *Neurosci Lett* **353**, 193-196 (2003).

195 Fell, J. *et al.* Medial temporal theta/alpha power enhancement precedes successful memory encoding: evidence based on intracranial EEG. *J Neurosci* **31**, 5392-5397, doi:10.1523/JNEUROSCI.3668-10.2011 (2011).

196 Jacobs, J. Hippocampal theta oscillations are slower in humans than in rodents: implications for models of spatial navigation and memory. *Philos T R Soc B* **369**, doi:ARTN 20130304

10.1098/rstb.2013.0304 (2014).

197 Huerta, P. T. & Lisman, J. E. Bidirectional synaptic plasticity induced by a single burst during cholinergic theta oscillation in CA1 in vitro. *Neuron* **15**, 1053-1063 (1995).

198 Orr, G., Rao, G., Houston, F. P., McNaughton, B. L. & Barnes, C. A. Hippocampal synaptic plasticity is modulated by theta rhythm in the fascia dentata of adult and aged freely behaving rats. *Hippocampus* **11**, 647-654, doi:10.1002/hipo.1079 (2001).

199 Roux, F. & Uhlhaas, P. J. Working memory and neural oscillations: alpha-gamma versus theta-gamma codes for distinct WM information? *Trends Cogn Sci* **18**, 16-25, doi:10.1016/j.tics.2013.10.010 (2014).

200 Seager, M. A., Johnson, L. D., Chabot, E. S., Asaka, Y. & Berry, S. D. Oscillatory brain states and learning: Impact of hippocampal theta-contingent training. *Proc Natl Acad Sci U S A* **99**, 1616-1620, doi:10.1073/pnas.032662099 (2002).

201 Jacobs, J. & Kahana, M. J. Direct brain recordings fuel advances in cognitive electrophysiology. *Trends Cogn Sci* **14**, 162-171, doi:10.1016/j.tics.2010.01.005 (2010).

202 Pfurtscheller, G. Functional brain imaging based on ERD/ERS. *Vision Res* **41**, 1257-1260 (2001).

203 Hanslmayr, S. *et al.* Prestimulus oscillations predict visual perception performance between and within subjects. *Neuroimage* **37**, 1465-1473, doi:10.1016/j.neuroimage.2007.07.011 (2007).

204 Klimesch, W., Sauseng, P. & Hanslmayr, S. EEG alpha oscillations: the inhibition-timing hypothesis. *Brain Res Rev* **53**, 63-88, doi:10.1016/j.brainresrev.2006.06.003 (2007).

205 Cooper, N. R., Croft, R. J., Dominey, S. J., Burgess, A. P. & Gruzelier, J. H. Paradox lost? Exploring the role of alpha oscillations during externally vs. internally directed attention

and the implications for idling and inhibition hypotheses. *Int J Psychophysiol* **47**, 65-74 (2003).

206 Min, B. K. & Herrmann, C. S. Prestimulus EEG alpha activity reflects prestimulus top-down processing. *Neurosci Lett* **422**, 131-135, doi:10.1016/j.neulet.2007.06.013 (2007).

207 Jokisch, D. & Jensen, O. Modulation of gamma and alpha activity during a working memory task engaging the dorsal or ventral stream. *J Neurosci* **27**, 3244-3251, doi:10.1523/JNEUROSCI.5399-06.2007 (2007).

208 Nerad, L. & Bilkey, D. K. Ten- to 12-Hz EEG oscillation in the rat hippocampus and rhinal cortex that is modulated by environmental familiarity. *Journal of Neurophysiology* **93**, 1246-1254, doi:10.1152/jn.00199.2004 (2005).

209 Sauseng, P., Klimesch, W., Schabus, M. & Doppelmayr, M. Fronto-parietal EEG coherence in theta and upper alpha reflect central executive functions of working memory. *Int J Psychophysiol* **57**, 97-103, doi:10.1016/j.ijpsycho.2005.03.018 (2005).

210 Cardin, J. A. *et al.* Driving fast-spiking cells induces gamma rhythm and controls sensory responses. *Nature* **459**, 663-667, doi:10.1038/nature08002 (2009).

211 Jacobs, J., Kahana, M. J., Ekstrom, A. D. & Fried, I. Brain oscillations control timing of single-neuron activity in humans. *J Neurosci* **27**, 3839-3844, doi:10.1523/JNEUROSCI.4636-06.2007 (2007).

212 Buzsaki, G. Theta rhythm of navigation: link between path integration and landmark navigation, episodic and semantic memory. *Hippocampus* **15**, 827-840, doi:10.1002/hipo.20113 (2005).

213 O'Keefe, J. & Recce, M. L. Phase relationship between hippocampal place units and the EEG theta rhythm. *Hippocampus* **3**, 317-330, doi:10.1002/hipo.450030307 (1993).

214 Jensen, O. & Lisman, J. E. Hippocampal sequence-encoding driven by a cortical multi-item working memory buffer. *Trends Neurosci* **28**, 67-72, doi:10.1016/j.tins.2004.12.001 (2005).

215 Axmacher, N. *et al.* Cross-frequency coupling supports multi-item working memory in the human hippocampus. *Proc Natl Acad Sci U S A* **107**, 3228-3233, doi:10.1073/pnas.0911531107 (2010).

216 Staudigl, T. & Hanslmayr, S. Theta Oscillations at Encoding Mediate the Context-Dependent Nature of Human Episodic Memory. *Current Biology* **23**, 1101-1106, doi:10.1016/j.cub.2013.04.074 (2013).

217 Heusser, A. C., Poeppel, D., Ezzyat, Y. & Davachi, L. Episodic sequence memory is supported by a theta-gamma phase code. *Nat Neurosci* **19**, 1374-1380, doi:10.1038/nn.4374 (2016).

218 Axmacher, N. A useful code for sequences. *Nature Neuroscience* **19**, 1276-1277, doi:10.1038/nn.4391 (2016).

219 Hasselmo, M. E., Bodelon, C. & Wyble, B. P. A proposed function for hippocampal theta rhythm: Separate phases of encoding and retrieval enhance reversal of prior learning. *Neural Comput* **14**, 793-817, doi:Doi 10.1162/089976602317318965 (2002).

220 Akam, T. & Kullmann, D. M. Oscillatory multiplexing of population codes for selective communication in the mammalian brain. *Nature Reviews Neuroscience* **15**, 111-122, doi:10.1038/nrn3668 (2014).

221 Gordon, J. A. On being a circuit psychiatrist. *Nature Neuroscience* **19**, 1385-1386 (2016).

222 Vogel, B. O., Shen, C. & Neuhaus, A. H. Emotional context facilitates cortical prediction error responses. *Hum Brain Mapp* **36**, 3641-3652, doi:10.1002/hbm.22868 (2015).

223 Tambini, A., Rimmele, U., Phelps, E. A. & Davachi, L. Emotional brain states carry over and enhance future memory formation. *Nat Neurosci* **20**, 271-278, doi:10.1038/nn.4468 (2017).

224 Maren, S., Phan, K. L. & Liberzon, I. The contextual brain: implications for fear conditioning, extinction and psychopathology. *Nat Rev Neurosci* **14**, 417-428, doi:10.1038/nrn3492 (2013).

225 Van den Stock, J. & de Gelder, B. Emotional information in body and background hampers recognition memory for faces. *Neurobiol Learn Mem* **97**, 321-325, doi:10.1016/j.nlm.2012.01.007 (2012).

226 Lee, K. H. & Siegle, G. J. Different brain activity in response to emotional faces alone and augmented by contextual information. *Psychophysiology* **51**, 1147-1157, doi:10.1111/psyp.12254 (2014).

227 Dalgleish, T. & Power, M. J. *Handbook of cognition and emotion*. (Wiley, 1999).

228 Wieser, M. J. & Brosch, T. Faces in context: a review and systematization of contextual influences on affective face processing. *Front Psychol* **3**, 471, doi:10.3389/fpsyg.2012.00471 (2012).

229 Northoff, G. *et al.* Self-referential processing in our brain--a meta-analysis of imaging studies on the self. *Neuroimage* **31**, 440-457, doi:10.1016/j.neuroimage.2005.12.002 (2006).

230 Gruber, A. J. & McDonald, R. J. Context, emotion, and the strategic pursuit of goals: interactions among multiple brain systems controlling motivated behavior. *Front Behav Neurosci* **6**, 50, doi:10.3389/fnbeh.2012.00050 (2012).

231 Girardeau, G., Inema, I. & Buzsaki, G. Reactivations of emotional memory in the hippocampus-amygdala system during sleep. *Nat Neurosci* **20**, 1634-1642, doi:10.1038/nn.4637 (2017).

232 Onat, S. & Buchel, C. The neuronal basis of fear generalization in humans. *Nat Neurosci* **18**, 1811-1818, doi:10.1038/nn.4166 (2015).

233 Kring, A. M. & Elis, O. Emotion deficits in people with schizophrenia. *Annu Rev Clin Psychol* **9**, 409-433, doi:10.1146/annurev-clinpsy-050212-185538 (2013).

234 Gordon, J. A. On being a circuit psychiatrist. *Nat Neurosci* **19**, 1385-1386, doi:10.1038/nn.4419 (2016).

235 Kim, H. *et al.* Contextual modulation of amygdala responsivity to surprised faces. *J Cogn Neurosci* **16**, 1730-1745, doi:10.1162/0898929042947865 (2004).

236 Schwarz, K. A., Wieser, M. J., Gerdes, A. B., Muhlberger, A. & Pauli, P. Why are you looking like that? How the context influences evaluation and processing of human faces. *Soc Cogn Affect Neurosci* **8**, 438-445, doi:10.1093/scan/nss013 (2013).

237 Wright, P. *et al.* Dissociated responses in the amygdala and orbitofrontal cortex to bottom-up and top-down components of emotional evaluation. *Neuroimage* **39**, 894-902, doi:10.1016/j.neuroimage.2007.09.014 (2008).

238 Zald, D. H. & Rauch, S. L. *The orbitofrontal cortex*. (Oxford University Press, 2006).

239 Bergmann, T. O. & Born, J. Phase-Amplitude Coupling: A General Mechanism for Memory Processing and Synaptic Plasticity? *Neuron* **97**, 10-13, doi:10.1016/j.neuron.2017.12.023 (2018).

240 Tottenham, N. *et al.* The NimStim set of facial expressions: judgments from untrained research participants. *Psychiatry Res* **168**, 242-249, doi:10.1016/j.psychres.2008.05.006 (2009).

241 Mikels, J. A. *et al.* Emotional category data on images from the International Affective Picture System. *Behav Res Methods* **37**, 626-630 (2005).

242 Arnulfo, G., Hirvonen, J., Nobili, L., Palva, S. & Palva, J. M. Phase and amplitude correlations in resting-state activity in human stereotactical EEG recordings. *Neuroimage* **112**, 114-127, doi:10.1016/j.neuroimage.2015.02.031 (2015).

243 Terada, S., Sakurai, Y., Nakahara, H. & Fujisawa, S. Temporal and Rate Coding for Discrete Event Sequences in the Hippocampus. *Neuron* **94**, 1248-1262 e1244, doi:10.1016/j.neuron.2017.05.024 (2017).

244 Scherberger, H., Jarvis, M. R. & Andersen, R. A. Cortical local field potential encodes movement intentions in the posterior parietal cortex. *Neuron* **46**, 347-354, doi:10.1016/j.neuron.2005.03.004 (2005).

245 Samiee, S. & Baillet, S. Time-resolved phase-amplitude coupling in neural oscillations. *Neuroimage* **159**, 270-279, doi:10.1016/j.neuroimage.2017.07.051 (2017).

246 Zhang, G. Q., Patuwo, B. E. & Hu, M. Y. Forecasting with artificial neural networks: The state of the art. *Int J Forecasting* **14**, 35-62, doi:Doi 10.1016/S0169-2070(97)00044-7 (1998).

247 Terada, N. *et al.* Exploring the optimal sequence of abiraterone and enzalutamide in patients with chemotherapy-naive castration-resistant prostate cancer: The Kyoto-Baltimore collaboration. *Int J Urol* **24**, 441-448, doi:10.1111/iju.13346 (2017).

248 Barrett, L. F. & Kensinger, E. A. Context is routinely encoded during emotion perception. *Psychol Sci* **21**, 595-599, doi:10.1177/0956797610363547 (2010).

249 Cahir, C. & Thomas, K. Asymmetric effects of positive and negative affect on decision making. *Psychol Rep* **106**, 193-204, doi:10.2466/PR0.106.1.193-204 (2010).

250 Mummendey, A., Otten, S., Berger, U. & Kessler, T. Positive-negative asymmetry in social discrimination: Valence of evaluation and salience of categorization. *Pers Soc Psychol B* **26**, 1258-1270, doi:Doi 10.1177/0146167200262007 (2000).

251 Holmes, G. Bad is stronger than good. *Psychologist* **23**, 866-867 (2010).

252 Vaish, A., Grossmann, T. & Woodward, A. Not all emotions are created equal: the negativity bias in social-emotional development. *Psychol Bull* **134**, 383-403, doi:10.1037/0033-2909.134.3.383 (2008).

253 Jay, T. M., Glowinski, J. & Thierry, A. M. Selectivity of the hippocampal projection to the prelimbic area of the prefrontal cortex in the rat. *Brain Res* **505**, 337-340 (1989).

254 Hoover, W. B. & Vertes, R. P. Anatomical analysis of afferent projections to the medial prefrontal cortex in the rat. *Brain Struct Funct* **212**, 149-179, doi:10.1007/s00429-007-0150-4 (2007).

255 Kjelstrup, K. B. *et al.* Finite scale of spatial representation in the hippocampus. *Science* **321**, 140-143, doi:10.1126/science.1157086 (2008).

256 Royer, S., Sirota, A., Patel, J. & Buzsaki, G. Distinct representations and theta dynamics in dorsal and ventral hippocampus. *J Neurosci* **30**, 1777-1787, doi:10.1523/JNEUROSCI.4681-09.2010 (2010).

257 Komorowski, R. W. *et al.* Ventral hippocampal neurons are shaped by experience to represent behaviorally relevant contexts. *J Neurosci* **33**, 8079-8087, doi:10.1523/JNEUROSCI.5458-12.2013 (2013).

258 Jadhav, S. P., Rothschild, G., Roumis, D. K. & Frank, L. M. Coordinated Excitation and Inhibition of Prefrontal Ensembles during Awake Hippocampal Sharp-Wave Ripple Events. *Neuron* **90**, 113-127, doi:10.1016/j.neuron.2016.02.010 (2016).

259 Place, R., Farovik, A., Brockmann, M. & Eichenbaum, H. Bidirectional prefrontal-hippocampal interactions support context-guided memory. *Nat Neurosci* **19**, 992-994, doi:10.1038/nn.4327 (2016).

260 O'Neill, P. K., Gordon, J. A. & Sigurdsson, T. Theta oscillations in the medial prefrontal cortex are modulated by spatial working memory and synchronize with the hippocampus through its ventral subregion. *J Neurosci* **33**, 14211-14224, doi:10.1523/JNEUROSCI.2378-13.2013 (2013).

261 Jones, M. W. & Wilson, M. A. Theta rhythms coordinate hippocampal-prefrontal interactions in a spatial memory task. *PLoS Biol* **3**, e402, doi:10.1371/journal.pbio.0030402 (2005).

262 Sigurdsson, T., Stark, K. L., Karayiorgou, M., Gogos, J. A. & Gordon, J. A. Impaired hippocampal-prefrontal synchrony in a genetic mouse model of schizophrenia. *Nature* **464**, 763-767, doi:10.1038/nature08855 (2010).

263 Siapas, A. G., Lubenov, E. V. & Wilson, M. A. Prefrontal phase locking to hippocampal theta oscillations. *Neuron* **46**, 141-151, doi:10.1016/j.neuron.2005.02.028 (2005).

264 Hallock, H. L., Wang, A. & Griffin, A. L. Ventral Midline Thalamus Is Critical for Hippocampal-Prefrontal Synchrony and Spatial Working Memory. *J Neurosci* **36**, 8372-8389, doi:10.1523/JNEUROSCI.0991-16.2016 (2016).

265 Sobotka, S., Diltz, M. D. & Ringo, J. L. Can delay-period activity explain working memory? *J Neurophysiol* **93**, 128-136, doi:10.1152/jn.01002.2003 (2005).

266 Myroshnychenko, M., Seamans, J. K., Phillips, A. G. & Lapish, C. C. Temporal Dynamics of Hippocampal and Medial Prefrontal Cortex Interactions During the Delay Period of a Working Memory-Guided Foraging Task. *Cereb Cortex* **27**, 5331-5342, doi:10.1093/cercor/bhx184 (2017).

267 Garvert, M. M., Friston, K. J., Dolan, R. J. & Garrido, M. I. Subcortical amygdala pathways enable rapid face processing. *Neuroimage* **102 Pt 2**, 309-316, doi:10.1016/j.neuroimage.2014.07.047 (2014).

268 Aviezer, H., Bentin, S., Dudarev, V. & Hassin, R. R. The automaticity of emotional face-context integration. *Emotion* **11**, 1406-1414, doi:10.1037/a0023578 (2011).

269 Schoenbaum, G. & Roesch, M. Orbitofrontal cortex, associative learning, and expectancies. *Neuron* **47**, 633-636, doi:10.1016/j.neuron.2005.07.018 (2005).

270 Lucantonio, F. *et al.* Neural Estimates of Imagined Outcomes in Basolateral Amygdala Depend on Orbitofrontal Cortex. *J Neurosci* **35**, 16521-16530, doi:10.1523/JNEUROSCI.3126-15.2015 (2015).

271 Sharpe, M. J. & Schoenbaum, G. Back to basics: Making predictions in the orbitofrontal-amygdala circuit. *Neurobiol Learn Mem* **131**, 201-206, doi:10.1016/j.nlm.2016.04.009 (2016).

272 Saez, R. A., Saez, A., Paton, J. J., Lau, B. & Salzman, C. D. Distinct Roles for the Amygdala and Orbitofrontal Cortex in Representing the Relative Amount of Expected Reward. *Neuron* **95**, 70-77 e73, doi:10.1016/j.neuron.2017.06.012 (2017).

273 Schoenbaum, G., Chiba, A. A. & Gallagher, M. Neural encoding in orbitofrontal cortex and basolateral amygdala during olfactory discrimination learning. *J Neurosci* **19**, 1876-1884 (1999).

274 Baxter, M. G., Parker, A., Lindner, C. C., Izquierdo, A. D. & Murray, E. A. Control of response selection by reinforcer value requires interaction of amygdala and orbital prefrontal cortex. *J Neurosci* **20**, 4311-4319 (2000).

275 El Zein, M., Wyart, V. & Grezes, J. Anxiety dissociates the adaptive functions of sensory and motor response enhancements to social threats. *Elife* **4**, doi:10.7554/eLife.10274 (2015).

276 Harris, A. Z. & Gordon, J. A. Long-range neural synchrony in behavior. *Annual review of neuroscience* **38**, 171-194, doi:10.1146/annurev-neuro-071714-034111 (2015).

277 Watrous, A. J., Tandon, N., Conner, C. R., Pieters, T. & Ekstrom, A. D. Frequency-specific network connectivity increases underlie accurate spatiotemporal memory retrieval. *Nature neuroscience* **16**, 349-356, doi:10.1038/nn.3315 (2013).

278 Canolty, R. T. & Knight, R. T. The functional role of cross-frequency coupling. *Trends in cognitive sciences* **14**, doi:10.1016/j.tics.2010.09.001 (2010).

279 Canolty, R. T. *et al.* High gamma power is phase-locked to theta oscillations in human neocortex. *Science* **313**, 1626-1628, doi:10.1126/science.1128115 (2006).

280 Augustine, J. R. Circuitry and functional aspects of the insular lobe in primates including humans. *Brain Res Brain Res Rev* **22**, 229-244 (1996).

281 Bamiou, D. E., Musiek, F. E. & Luxon, L. M. The insula (Island of Reil) and its role in auditory processing. Literature review. *Brain Res Brain Res Rev* **42**, 143-154 (2003).

282 Butti, C. & Hof, P. R. The insular cortex: a comparative perspective. *Brain Struct Funct* **214**, 477-493, doi:10.1007/s00429-010-0264-y (2010).

283 Mesulam, M. M. & Mufson, E. J. Insula of the old world monkey. III: Efferent cortical output and comments on function. *J Comp Neurol* **212**, 38-52, doi:10.1002/cne.902120104 (1982).

284 Nieuwenhuys, R. The insular cortex: a review. *Prog Brain Res* **195**, 123-163, doi:10.1016/B978-0-444-53860-4.00007-6 (2012).

285 Toga, A. W. *Brain mapping : an encyclopedic reference*.

286 Critchley, H. D., Eccles, J. & Garfinkel, S. N. Interaction between cognition, emotion, and the autonomic nervous system. *Handb Clin Neurol* **117**, 59-77, doi:10.1016/B978-0-444-53491-0.00006-7 (2013).

287 Singer, T., Critchley, H. D. & Preuschoff, K. A common role of insula in feelings, empathy and uncertainty. *Trends Cogn Sci* **13**, 334-340, doi:10.1016/j.tics.2009.05.001 (2009).

288 Averbeck, B. B. & Seo, M. The statistical neuroanatomy of frontal networks in the macaque. *PLoS Comput Biol* **4**, e1000050, doi:10.1371/journal.pcbi.1000050 (2008).

289 Vogt, B. A. & Pandya, D. N. Cingulate cortex of the rhesus monkey: II. Cortical afferents. *J Comp Neurol* **262**, 271-289, doi:10.1002/cne.902620208 (1987).

290 Fries, W. Cortical projections to the superior colliculus in the macaque monkey: a retrograde study using horseradish peroxidase. *J Comp Neurol* **230**, 55-76, doi:10.1002/cne.902300106 (1984).

291 Ide, J. S., Shenoy, P., Yu, A. J. & Li, C. S. Bayesian prediction and evaluation in the anterior cingulate cortex. *J Neurosci* **33**, 2039-2047, doi:10.1523/JNEUROSCI.2201-12.2013 (2013).

292 Rushworth, M. F. & Behrens, T. E. Choice, uncertainty and value in prefrontal and cingulate cortex. *Nat Neurosci* **11**, 389-397, doi:10.1038/nn2066 (2008).

293 Kaplan, J. T., Gimbel, S. I. & Harris, S. Neural correlates of maintaining one's political beliefs in the face of counterevidence. *Sci Rep* **6**, 39589, doi:10.1038/srep39589 (2016).

294 Qin, S., Hermans, E. J., van Marle, H. J., Luo, J. & Fernandez, G. Acute psychological stress reduces working memory-related activity in the dorsolateral prefrontal cortex. *Biol Psychiatry* **66**, 25-32, doi:10.1016/j.biopsych.2009.03.006 (2009).

295 Gainotti, G. Emotional behavior and hemispheric side of the lesion. *Cortex* **8**, 41-55 (1972).

296 Herrington, J. D. *et al.* Emotion-modulated performance and activity in left dorsolateral prefrontal cortex. *Emotion* **5**, 200-207, doi:10.1037/1528-3542.5.2.200 (2005).

297 Vosskuhl, J., Huster, R. J. & Herrmann, C. S. Increase in short-term memory capacity induced by down-regulating individual theta frequency via transcranial alternating current stimulation. *Front Hum Neurosci* **9**, 257, doi:10.3389/fnhum.2015.00257 (2015).

APPENDIX A: Supplementary Materials for Chapter 2

Supplementary Table 1: Patient information

Subject	Implanted Side	Age	Gender	MRI	Surgery	Side Analyzed
1	Right	24	Male	Right MTS	Right ATL with AH	Right
2	Left	25	Male	Normal	Left ATL with AH	Left
3	Bilateral	51	Male	Normal	Right ATL with AH	Right
4	Left	49	Female	Normal	Left ATL with AH	Left
5	Bilateral	33	Female	Right MTS	Right ATL with AH	Left*
6	Bilateral	32	Female	Right periventricular heterotopia	Right ATL with AH	Left*
7	Right	25	Male	Normal	Right ATL without removing Amygdala and Hippocampus	Right*
8	Bilateral	34	Male	Normal	Right ATL with AH	Left*
9	Bilateral	48	Female	Normal	Left ATL with AH	Right*

ATL anterior temporal lobectomy; AH = amygdalohippocampectomy

MTS = mesial temporal sclerosis

*= Contralateral or outside of the seizure onset zone

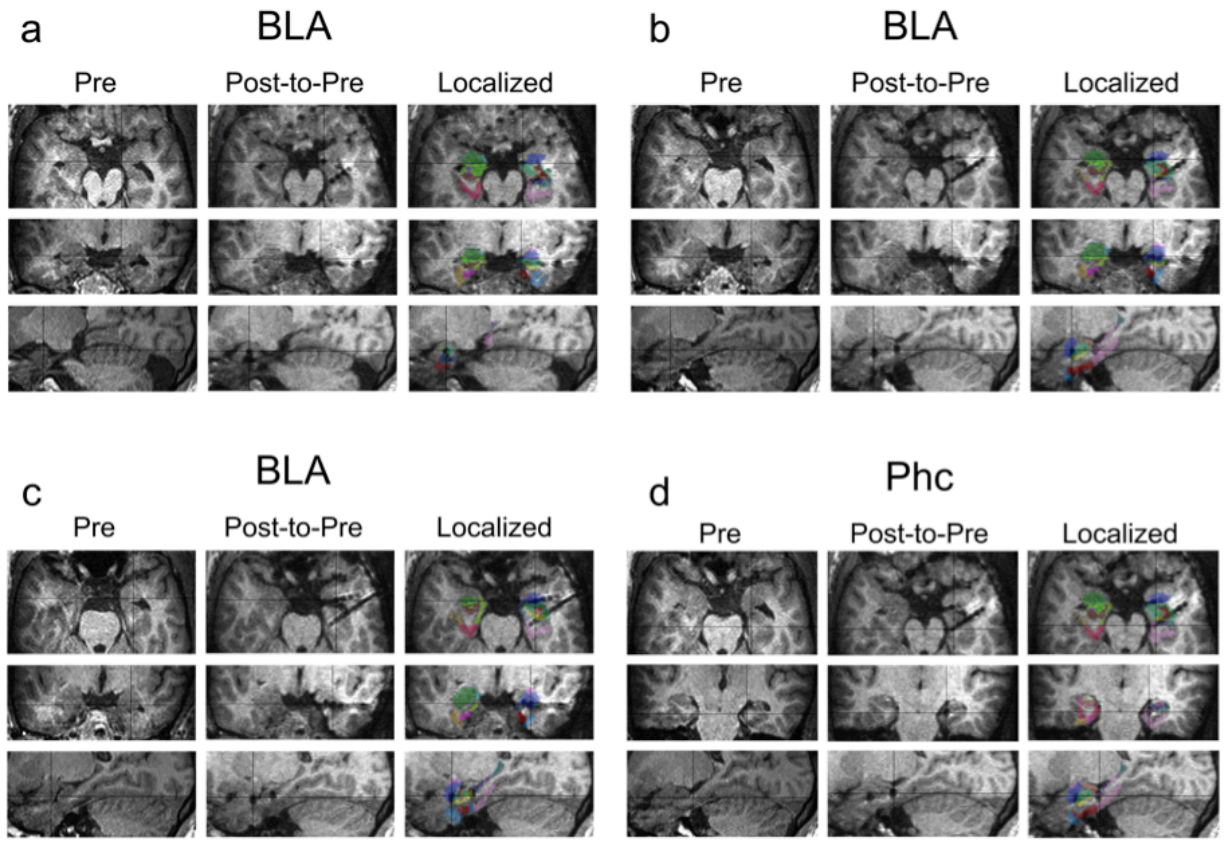
a
BLA
Pre
Post-to-Pre
Localized
b
BLA
Pre
Post-to-Pre
Localized
c
BLA
Pre
Post-to-Pre
Localized
d
Phc
Pre
Post-to-Pre
Localized

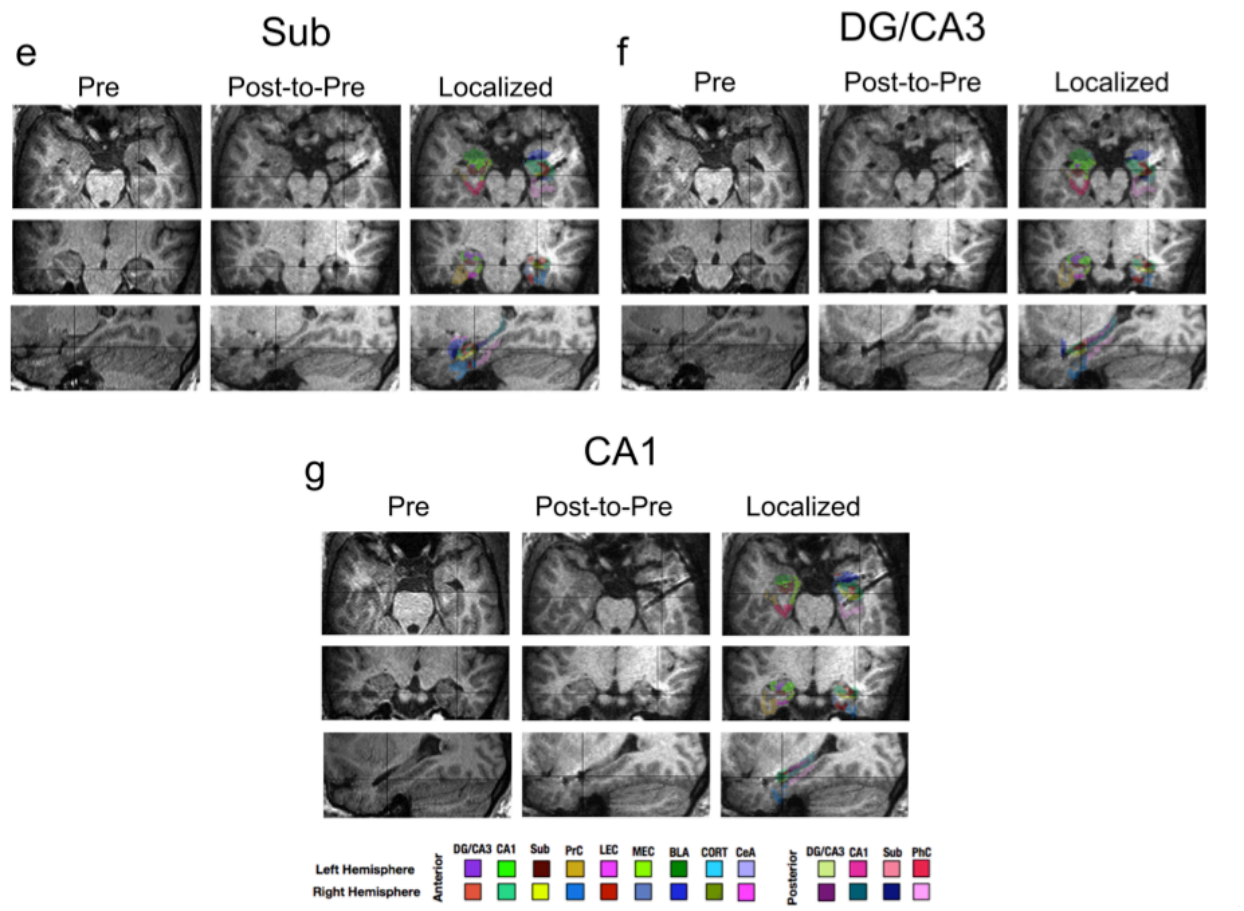

Supplementary Figure 1. Localization of depth electrodes. Pre-implantation MRI (1 mm isotropic) in a representative subject (left panel), post-implantation MRI aligned using rigid body alignment to the pre-implantation MRI (middle panel), and the translucent overlay of registered regions of interests (ROIs) overlaid on the post-to-pre aligned MRI (right panel) for the basolateral amygdala (BLA; a-c), parahippocampal cortex (Phc; d), subiculum (Sub; e), dentate gyrus/CA3 (DG/CA3; f), and CA1 (g). Cross hairs are centered on the electrode in each region.

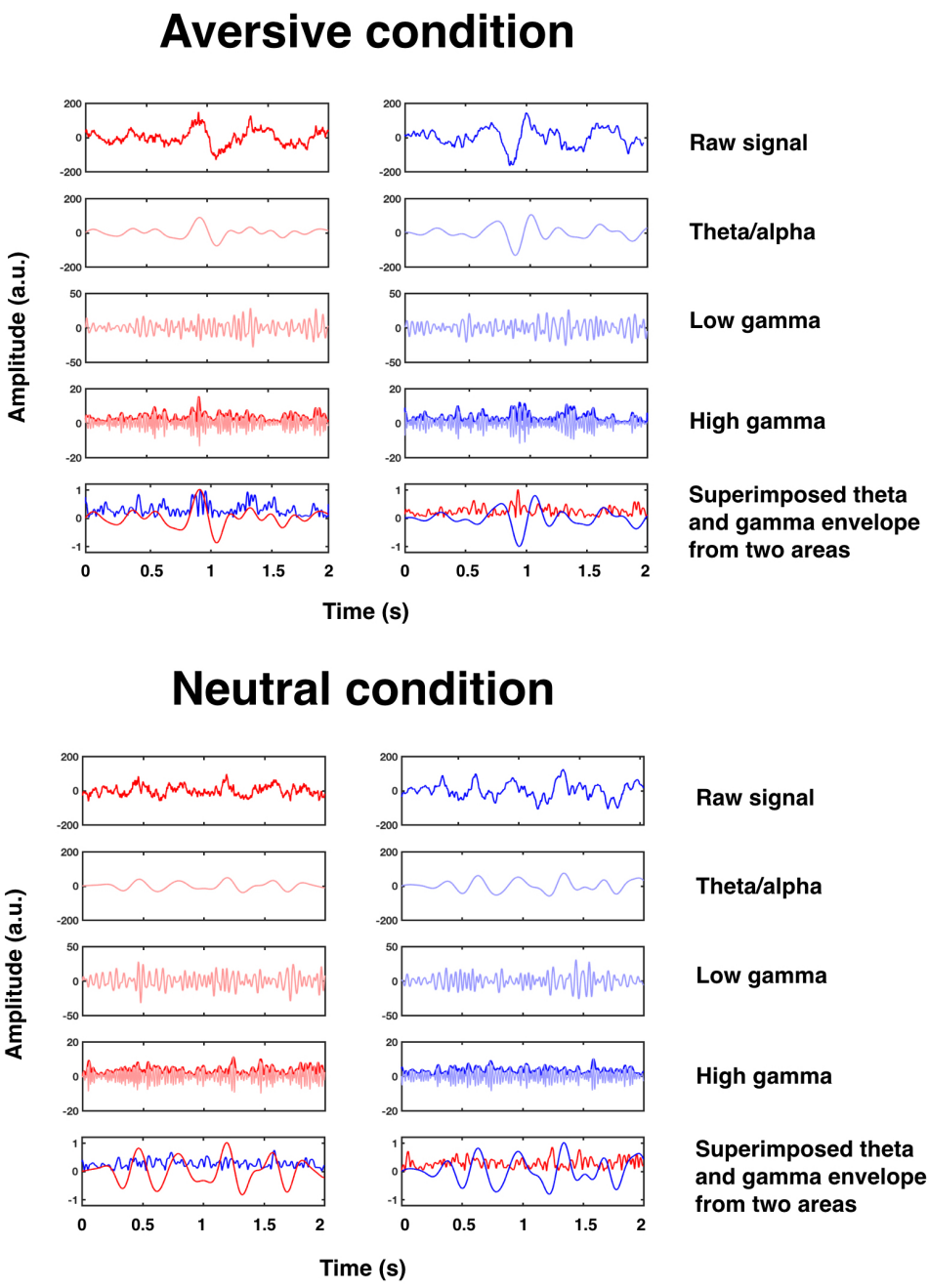

Supplementary Figure 2. Raw traces of a single trial for the aversive and the neutral conditions in the amygdala and the hippocampus. Traces from top to bottom show unfiltered raw, filtered theta/alpha (5-9 Hz), filtered low gamma (30-70 Hz), and filtered high gamma (70-180 Hz) signals, with the analytic amplitude envelope traced in bold. The lowest row in each panel shows the high gamma banded amplitude envelope from one region that is superimposed with the low frequency banded signal from the other region. A stronger

synchronization between amygdala theta and hippocampus gamma is evident in the aversive condition compared to the neutral condition. Red = signals from the amygdala; blue = signals from the hippocampus.

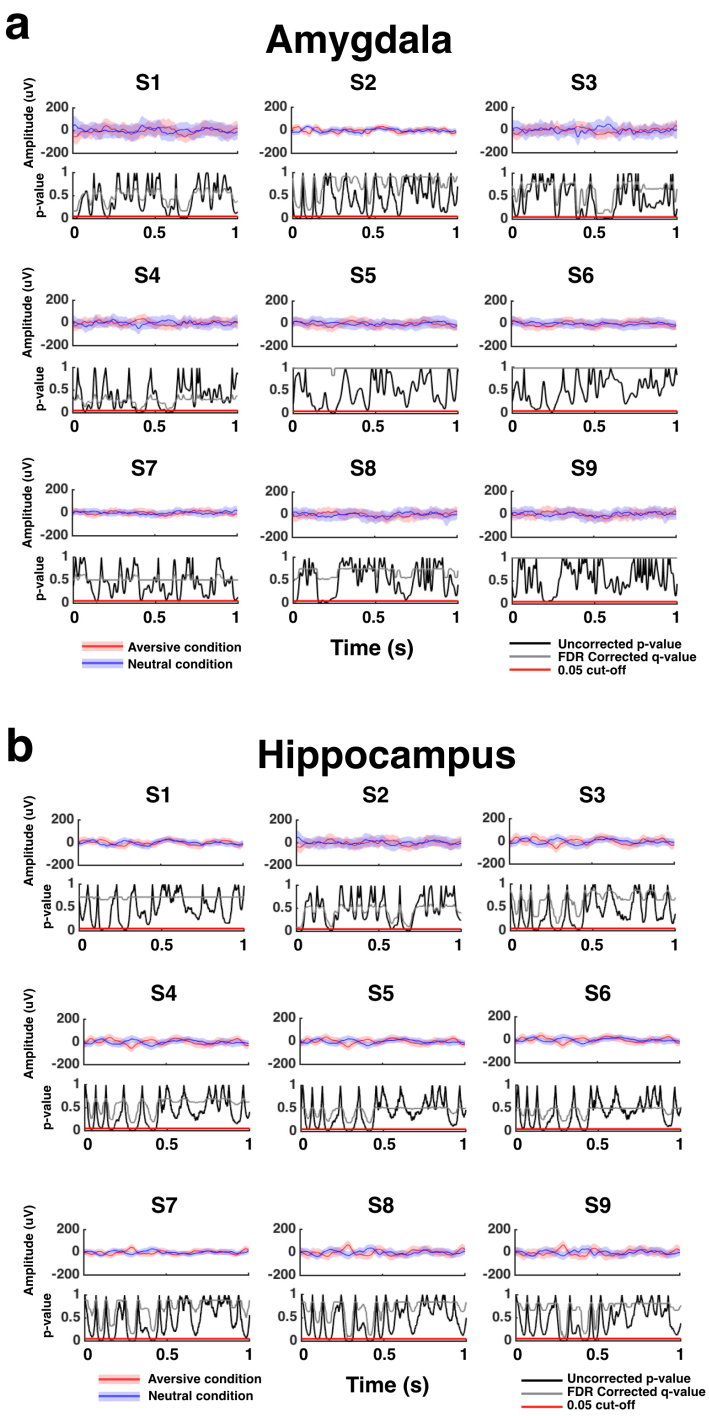

Supplementary Figure 3. Movie clip-based event related potentials (ERPs) in each subject for (a) the amygdala and (b) the hippocampus. Comparisons of ERPs between the aversive (red traces) and neutral (blue traces) condition (top colored traces) and point by point *t*-tests (bottom traces). Significant group differences in ERP amplitudes with uncorrected $p < 0.05$

threshold were found for a small number of time points (amygdala = 6.5% and hippocampus = 8.3%). No data points survived correction for multiple comparisons. Shaded regions denote s.e.m. across trials.

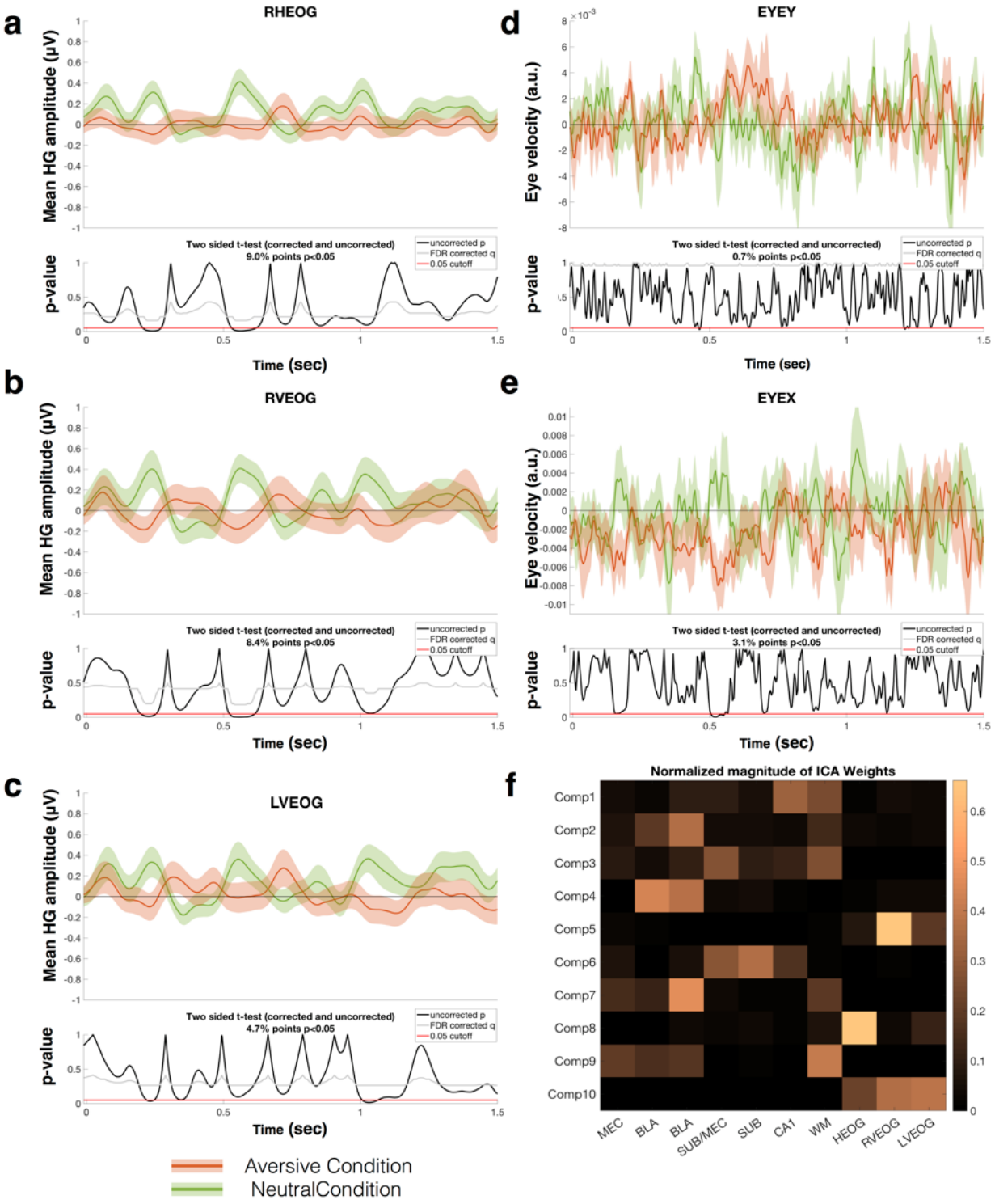
a
RHEOG
Mean HG amplitude (μV)
Two sided t-test (corrected and uncorrected)
9.0% points p<0.05
uncorrected p
FDR corrected q
0.05 cutoff
p-value
Time (sec)
b
RVEOG
Mean HG amplitude (μV)
Two sided t-test (corrected and uncorrected)
8.4% points p<0.05
uncorrected p
FDR corrected q
0.05 cutoff
p-value
Time (sec)
c
LVEOG
Mean HG amplitude (μV)
Two sided t-test (corrected and uncorrected)
4.7% points p<0.05
uncorrected p
FDR corrected q
0.05 cutoff
p-value
Time (sec)
Aversive Condition
NeutralCondition
d
EYEY
Eye velocity (a.u.)
Two sided t-test (corrected and uncorrected)
0.7% points p<0.05
uncorrected p
FDR corrected q
0.05 cutoff
p-value
Time (sec)
e
EYEX
Eye velocity (a.u.)
Two sided t-test (corrected and uncorrected)
3.1% points p<0.05
uncorrected p
FDR corrected q
0.05 cutoff
p-value
Time (sec)
f
Normalized magnitude of ICA Weights
Comp1
Comp2
Comp3
Comp4
Comp5
Comp6
Comp7
Comp8
Comp9
Comp10
MEC
BLA
BLA
SUB/MEC
SUB
CA1
WM
HEOG
RVEOG
LVEOG

Supplementary Figure 4. Eye movement related responses and independent component analysis for Subject 9. Comparisons of estimated high gamma time courses from the electrooculogram (EOG) activity between the aversive (fearful face) and neutral (landscape) condition (top colored traces) and point-by-point t-tests (bottom traces) for (a) the right horizontal EOG (RHEOG), (b) right vertical EOG (RVEOG) and (c) left horizontal EOG (LVEOG). A small number of data points were found to be significant at the uncorrected $p < 0.05$ threshold (RHEOG = 9.0%, RVEOG = 8.4%, LVEOG = 4.7%), and multiple comparison correction eliminated any significant differences. Ocular velocity in (d) the X dimension and (e) the Y dimension recorded from the eye tracker averaged across clips and compared between the two conditions (top colored traces) and the point-by-point *t*-tests (bottom traces). A small number of data points were found to be significant at the uncorrected $p < 0.05$ threshold (X= 0.7% and Y = 3.1%), and no significant differences were present after multiple comparison correction. (f) Independent component analysis (ICA) of EOG combined with white matter referenced amygdala and hippocampal activity. ICA weights were normalized by taking the magnitude (absolute value) of all weights and then dividing all weights across each row (component) by the sum of all weight magnitudes in each row. This effectively shows the relative contributions of channels to each component. EOG signals contributed to components 5, 8, and 10, which had relatively small contributions from amygdala and hippocampal electrodes. The sub-regions used for the eye movement analyses were the same as in Fig 2, subject 9. HG = high gamma; a.u.=arbitrary units

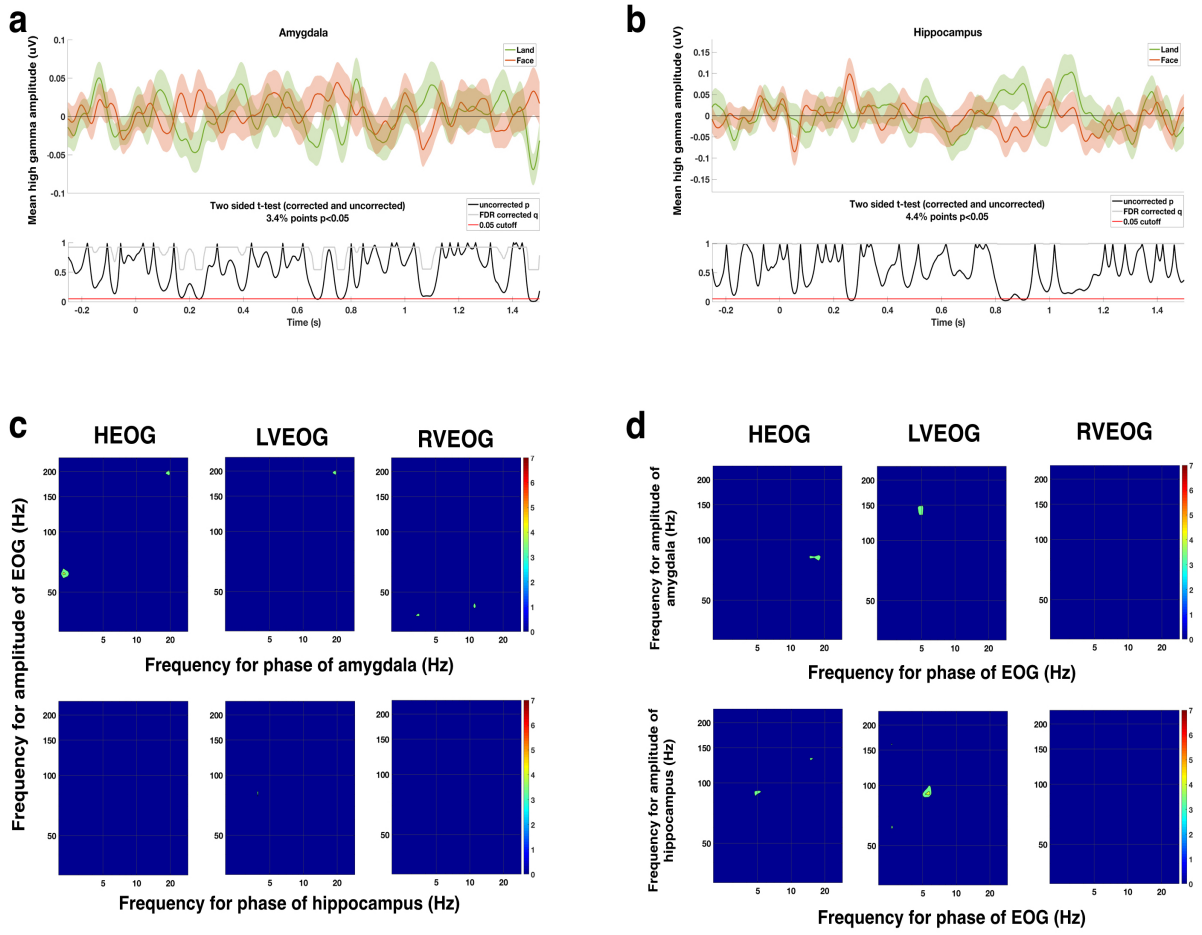

Supplementary Figure 5. Perisaccadic high gamma activity and electrooculogram (EOG) derived phase amplitude coupling for subject 9. Comparisons of estimated high gamma time courses from (a) the amygdala and (b) the hippocampus between the aversive (fearful face) and neutral (landscape) condition. A small number of data points were found to be significant at the uncorrected $p < 0.05$ threshold (amygdala = 3.4%, hippocampus = 4.4%), and multiple comparison correction eliminated any significant differences. No significant phase amplitude coupling pattern was observed between the EOG activity and signals from the amygdala and hippocampus (c, d).

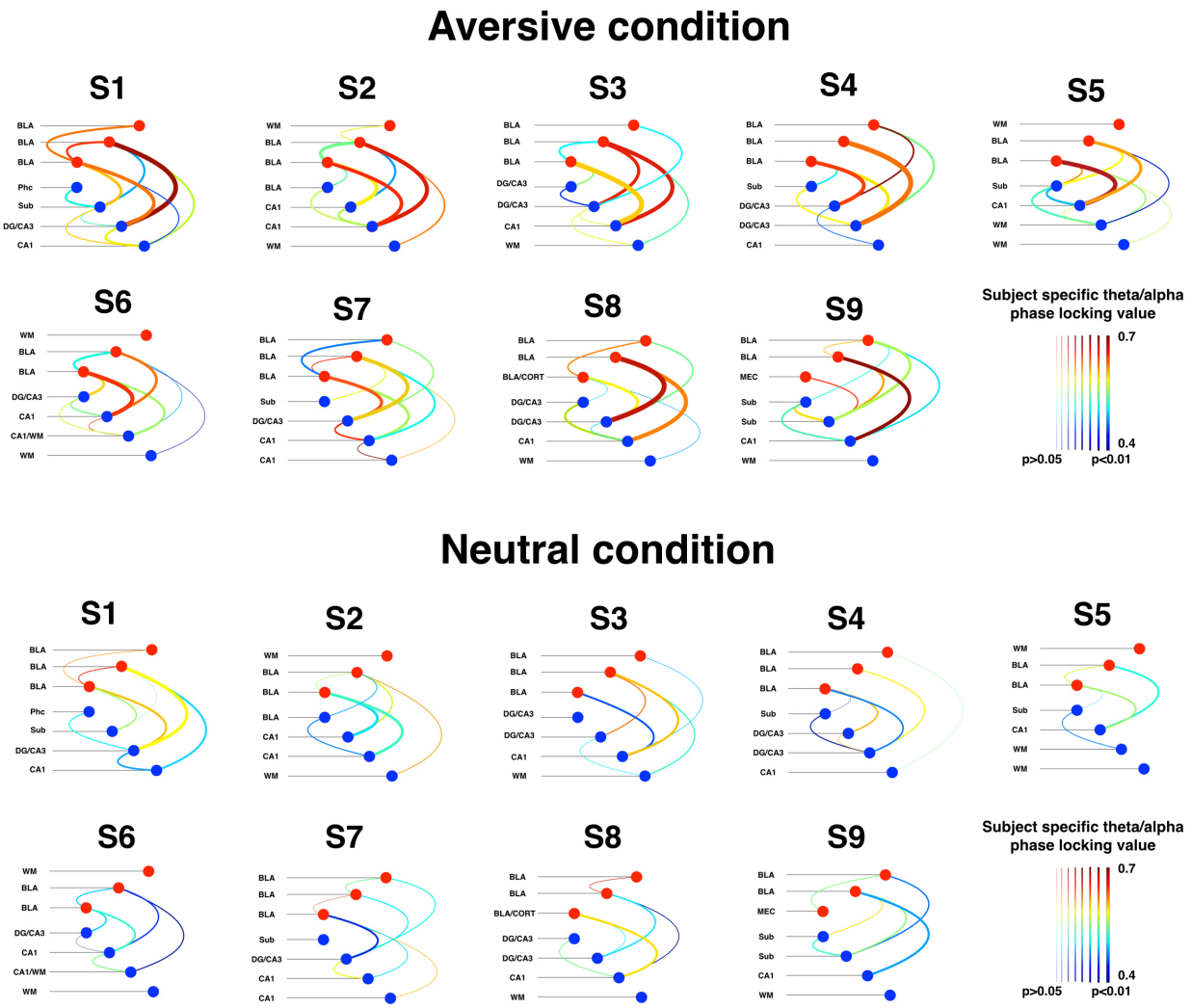

Supplementary Figure 6. Amygdala-hippocampal theta phase coherence for each condition. Theta phase coherence between pairs of electrodes targeting the amygdala (red dots) and hippocampal subfields (blue dots), depicted with hive plots for the aversive (a) and neutral (b) conditions. The magnitude of the phase locking value (PLV) between electrode pairs is presented in color, with warmer colors indicating a greater magnitude. Significance levels derived from permutation testing are indicated by the thickness of lines connecting each electrode pair.

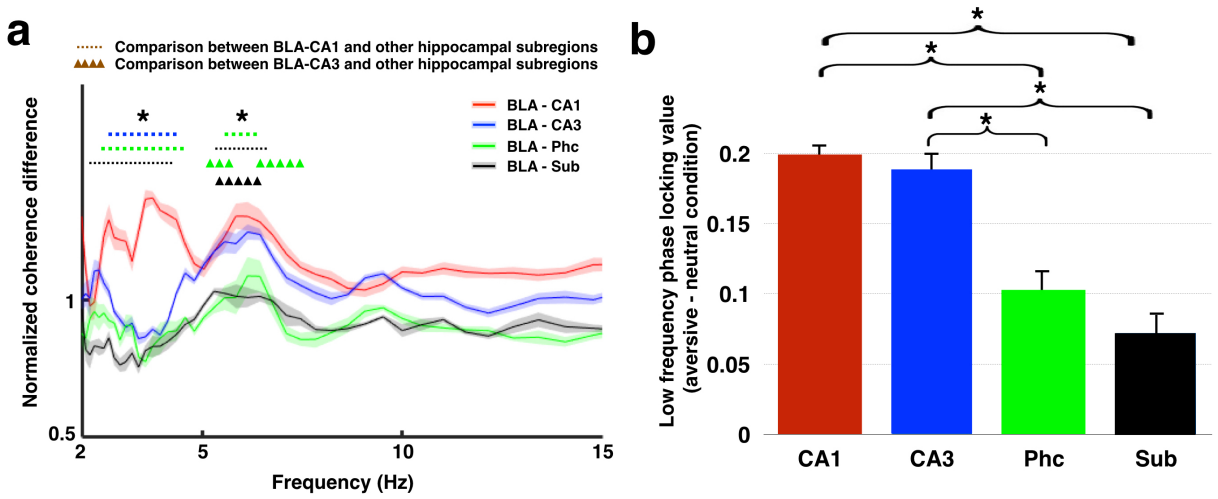

Supplementary Figure 7. Phase locking values (PLV) between basolateral amygdala (BLA) and hippocampal sub-regions. (a) Normalized coherence spectra averaged over all electrodes pairs between the BLA and the hippocampal subregions (CA1, CA3, Phc, and Sub). Increased theta PLV was observed in BLA-CA1 (red line) in contrast to BLA-CA3 (blue line), BLA-Phc (green line), and BLA-Sub (black line) electrode pairs when viewing aversive compared to neutral stimuli. The dots on top represent frequency ranges showing significant differences between BLA-CA1 and other electrode pairs ($p < 0.01$); triangles on the top denote significant differences between BLA-CA3 and other electrode pairs ($p < 0.01$). (b) PLV enhancement between BLA and hippocampal sub-regions when viewing the aversive vs. neutral stimuli among all 9 subjects. Error bars indicate ± s.e.m. across participants, and asterisk denotes significant differences at $p < 0.05$ with a post-hoc pairwise t-test (main effect for hippocampal sub-regions: $p = 0.004$). Phc = parahippocampal gyrus; Sub = subiculum.

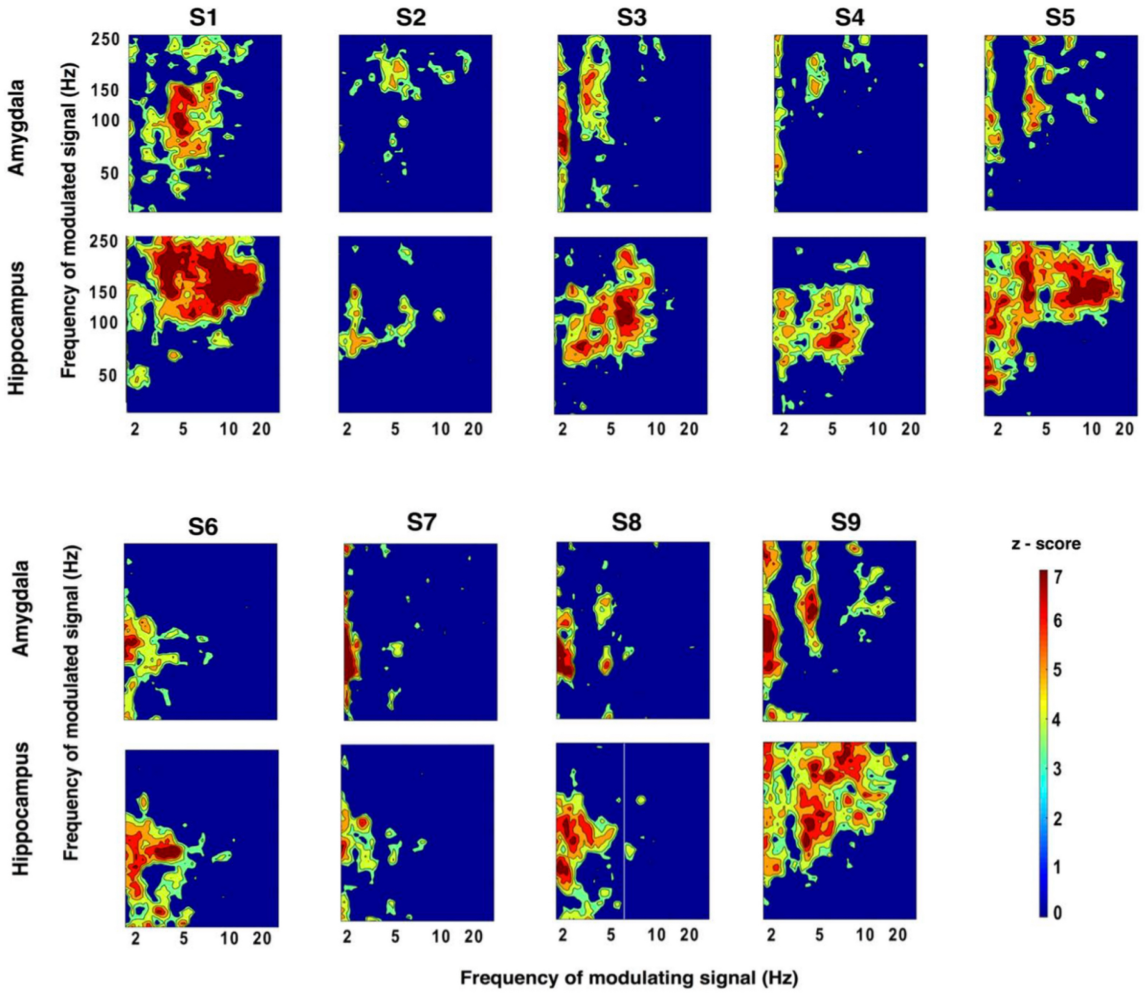

Supplementary Figure 8. Amygdala and hippocampus within electrode phase amplitude coupling (PAC). PAC comodulogram for differences between the aversive and the neutral condition is shown separately for the amygdala and hippocampus, with warmer colors denoting higher z-scores. Within each structure, increased PAC was observed when viewing the aversive compared to the neutral condition, with high gamma amplitude phase locked to phase of theta/alpha rhythms.

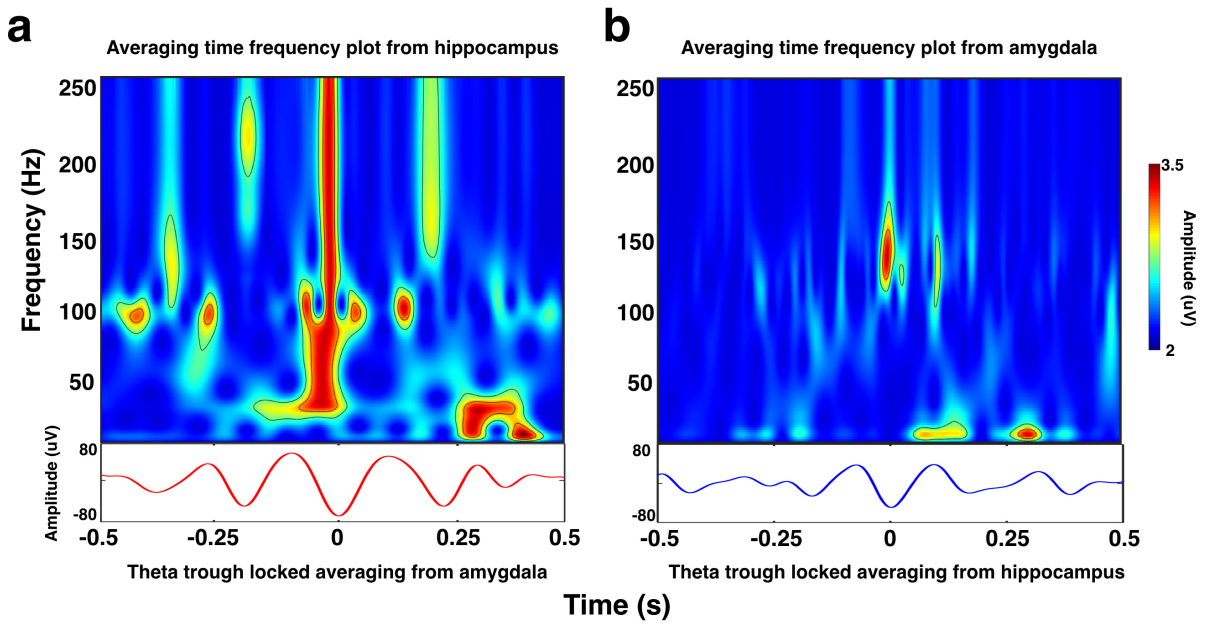

Supplementary Figure 9. Example of theta trough locked time frequency averaging for one subject in the aversive condition. (a) Normalized time-frequency average plot of mean power modulation from the hippocampus (upper panel) time-locked to the theta trough from the amygdala (lower panel). (b) Normalized time-frequency average plot of mean power modulation from the amygdala (upper panel) time-locked to the theta trough from the hippocampus (lower panel). Outermost contour in the time frequency plot indicates statistical significance ($p < 0.01$).

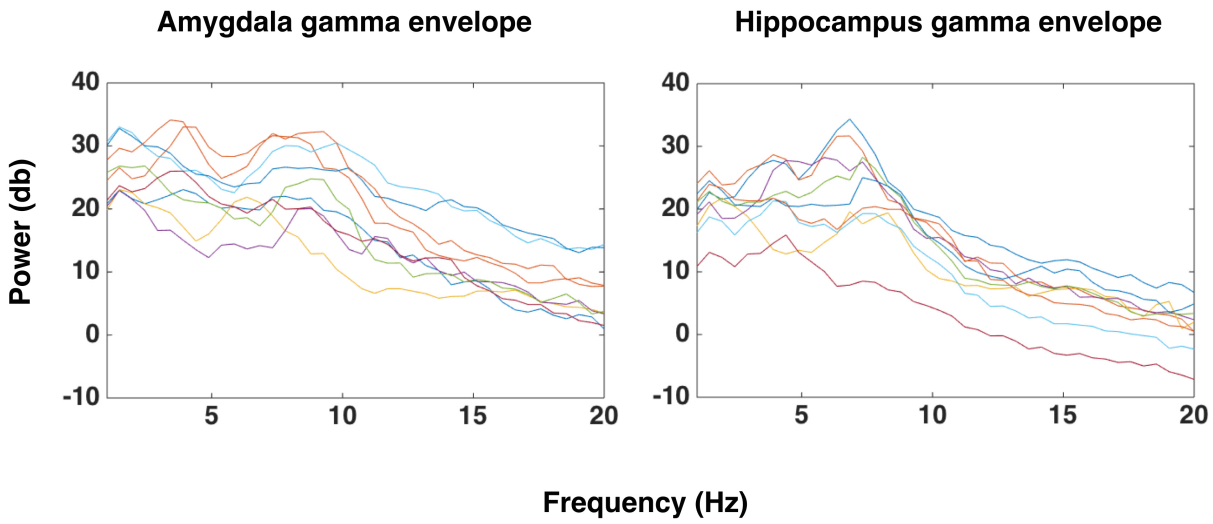

Supplementary Figure 10. Power spectral density (PSD) plots in a log-log (dB) scale for amygdala and hippocampus gamma envelope. PSD peaks around 7-8 Hz are evident across subjects in both regions. Each color line represents a single subject.

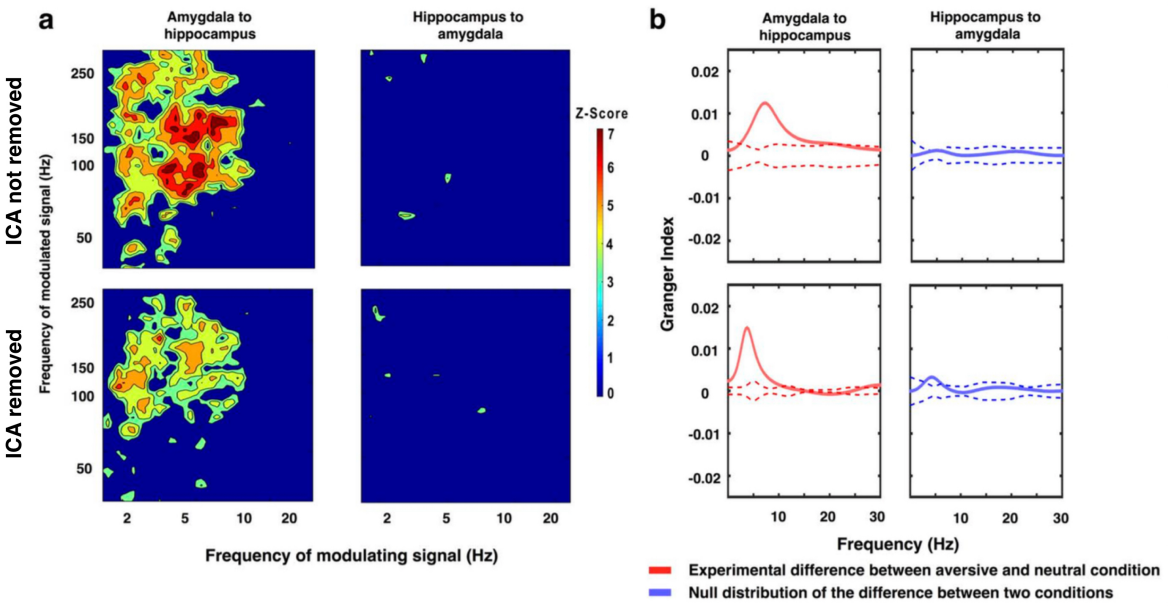

Supplementary Figure 11. Phase amplitude coupling and Granger causality with ICA correction for subject 9. Directional phase amplitude coupling (a) and Granger causality analysis (b) before and after independent component analysis (ICA)-based removal of eye movement artifacts. Significant amygdala-hippocampal directionality was evident before and after ICA-based artifact removal, demonstrating that eye movement artifact did not influence the results.

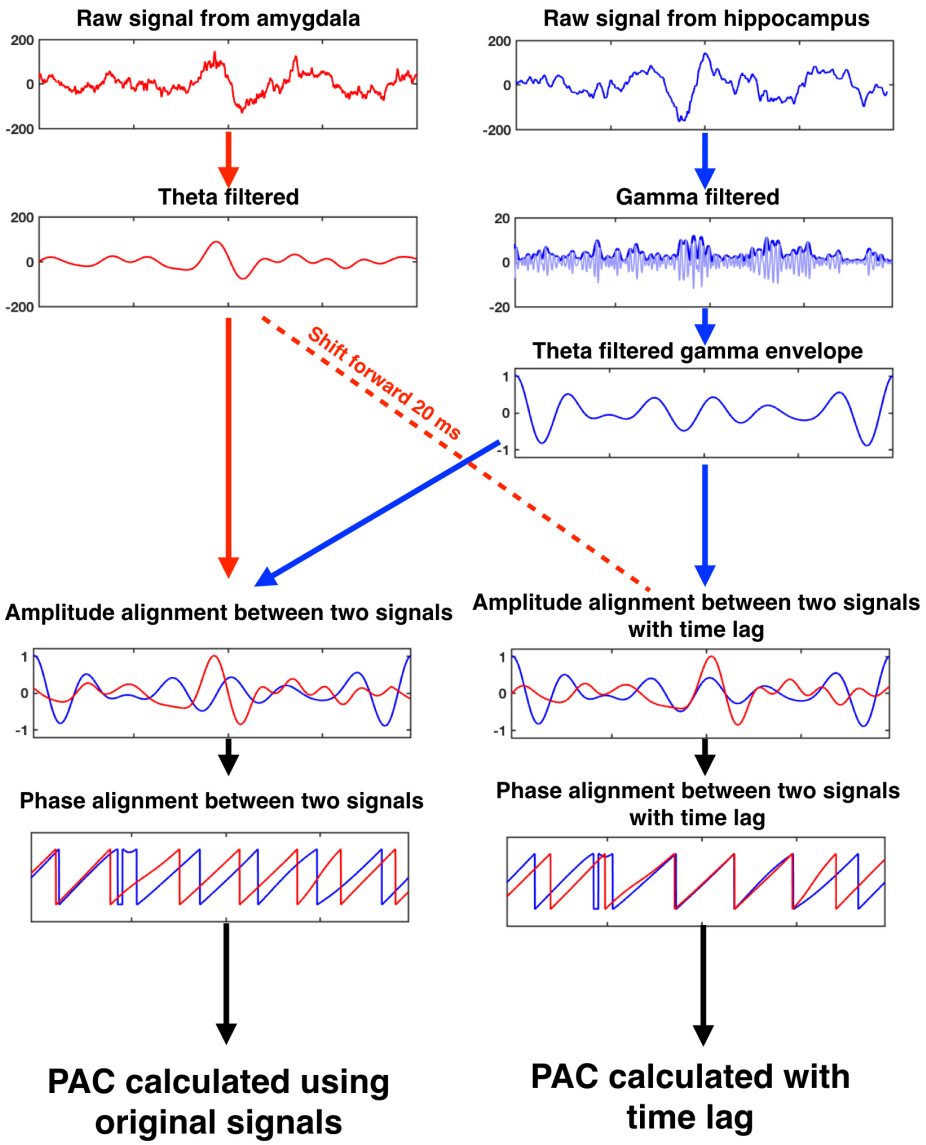

Supplementary Figure 12. Data processing schematic for calculating phase amplitude coupling (PAC) with time lag. The raw signal from the amygdala was band-pass filtered into a subject-specific theta/alpha component (5-9 Hz for the subject demonstrated here), while the raw signal from the hippocampus was band-pass filtered into high frequency gamma (70-180 Hz). We then extracted the amplitude of band-passed hippocampus high gamma and filtered this amplitude time series at the same theta/alpha band. The phase of both theta/alpha-filtered signal and the theta/alpha-filtered high gamma amplitude were extracted, and the PAC was

calculated by computing the phase-locking between these two signals. By varying the time shift between two signals, the PAC can be then presented as a function of time (Figure 2.3b).

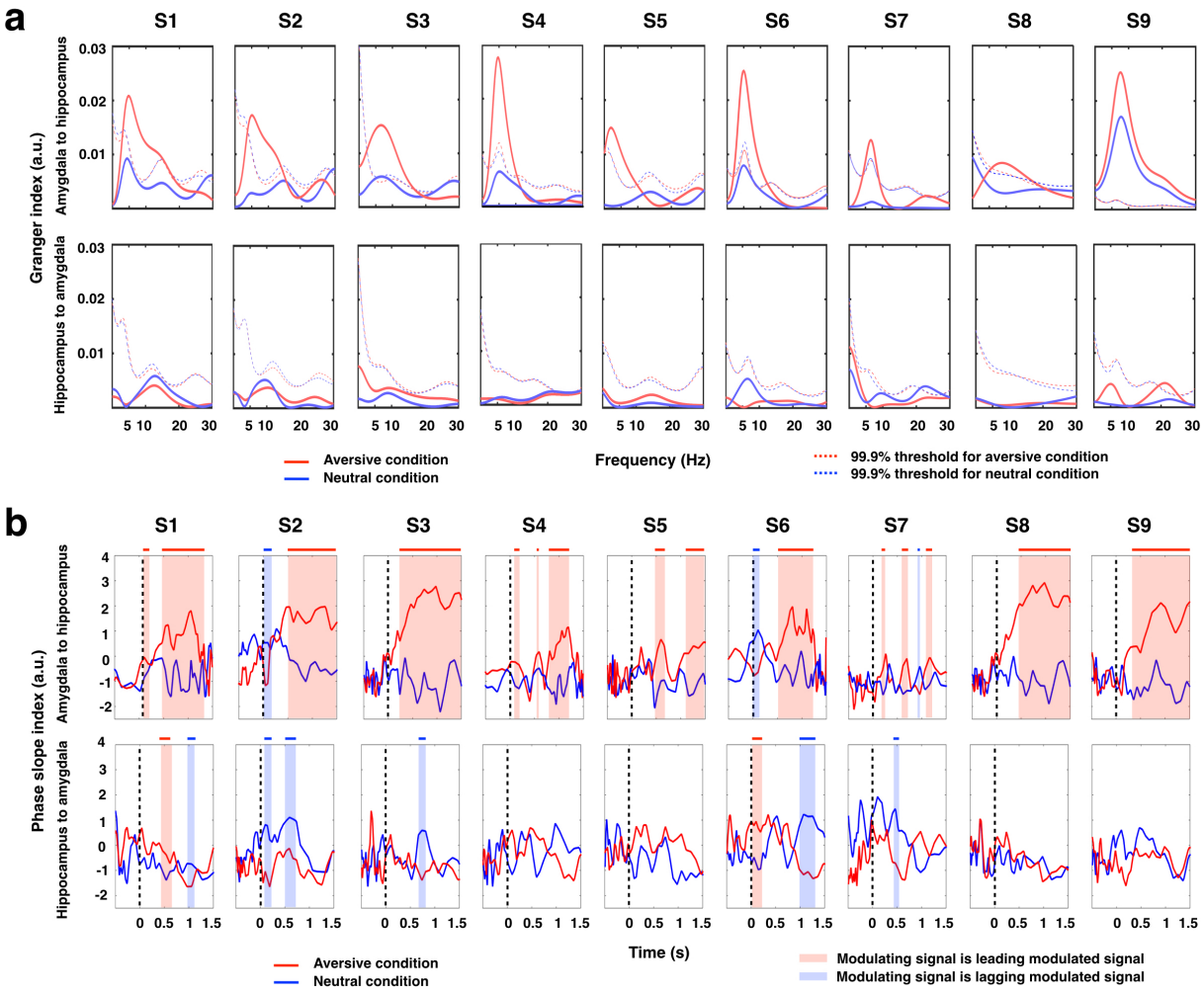

Supplementary Figure 13. Amygdala-hippocampus Granger causality and phase slope index for each subject. (a) Granger causality analyses demonstrated consistently stronger influence for the amygdala to hippocampus direction (top row) than for the hippocampus to amygdala direction (bottom row) when contrasting the aversive to the neutral condition for each subject. Solid lines are experimental data from the two conditions (red: aversive condition; blue: neutral condition). The 99.9% confidence intervals are presented as dashed lines. (b) Phase slope index (PSI) between the aversive and the neutral conditions calculated point-by-point across time using the subject specific theta band signal from the modulating channel (colored in red) and high gamma signal from the modulated channel (colored in blue) for each subject. Shaded regions denote significant differences between the two signals (all $p < 0.01$, permutation test), showing low frequency activity from the amygdala precedes hippocampus gamma for the majority of the stimuli duration.

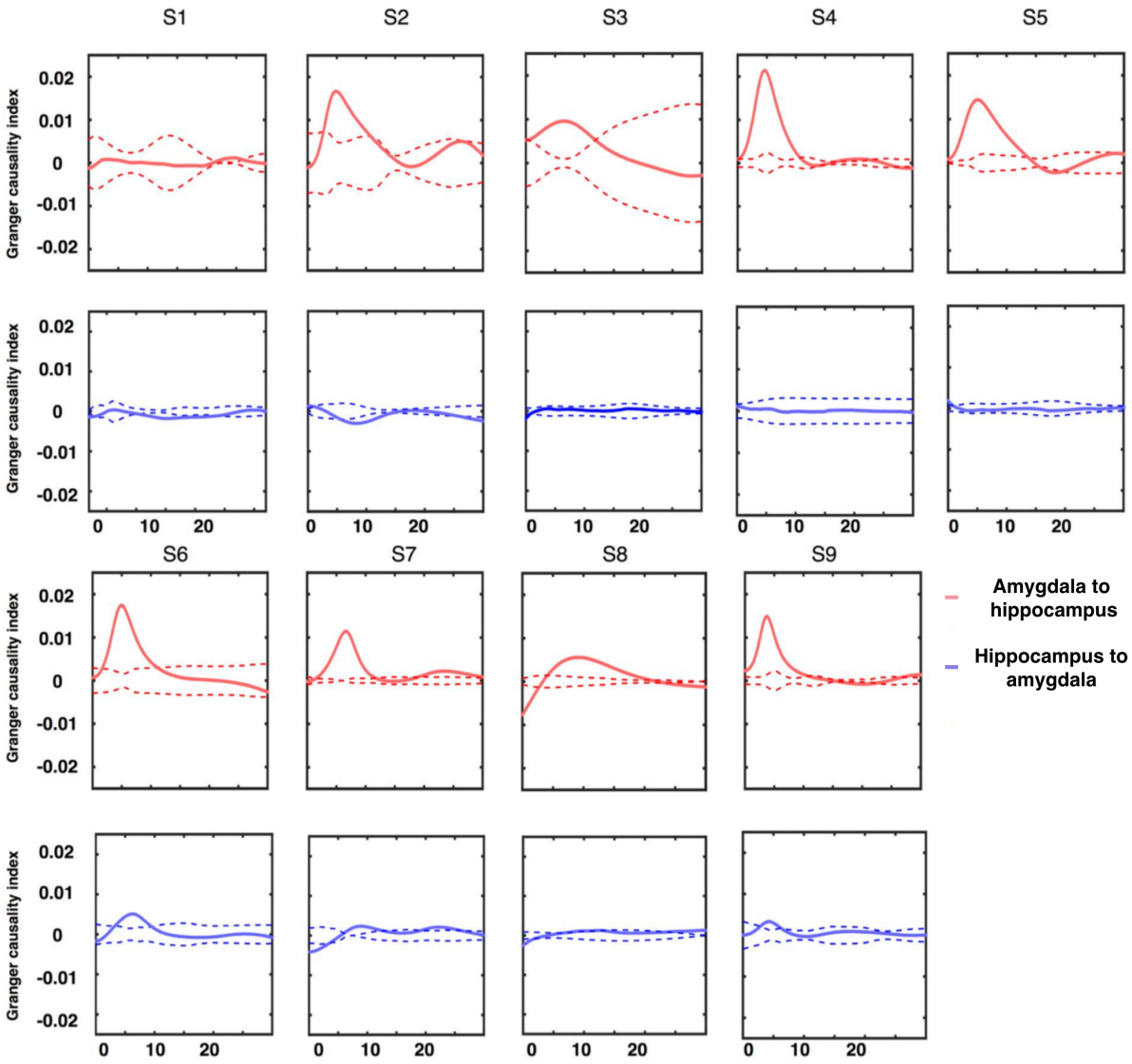

Supplementary Figure 14. Granger causality difference between aversive and neutral condition. Granger causality analyses demonstrated consistently stronger influence for the amygdala to hippocampus direction (red lines) than for the hippocampus to amygdala direction (blue lines) when contrasting the aversive to the neutral condition in all individuals except for subject 1. The solid lines represent the experimental data (the difference in Granger causality between the two conditions). The 99.9% confidence intervals for the null distribution are presented as dash lines.

APPENDIX B: Supplementary Materials for Chapter 3

Supplementary Table 1. Subject information and behavioral performance

Subject number	Gender	Age	Electrode Coverage	Epileptogenic region	Hemisphere analyzed	Accurate retrieval rate	RT* (mean + s.e.m)
1	Male	21	Bilateral	Left TLE	Right	0.754	2.89 ±0.022
2	Female	40	Bilateral	Right SMA	Right	0.786	2.55 ± 0.011
3	Female	58	Bilateral	Left TLE	Right	0.866	2.46 ± 0.007
4	Female	32	Bilateral	Right TLE	Left	0.731	2.59 ± 0.054
5	Male	24	Bilateral	Right TLE	Left	0.841	2.54 ± 0.014
6	Female	54	Bilateral	Right TLE	Left	0.783	2.51 ± 0.114
7	Male	23	Bilateral	Right TLE	Left	0.823	2.54 ± 0.022

TLE = Temporal lobe epilepsy
SMA = Supplementary motor area
s.e.m = standard error mean
*The response time are corresponding to the stimuli onset

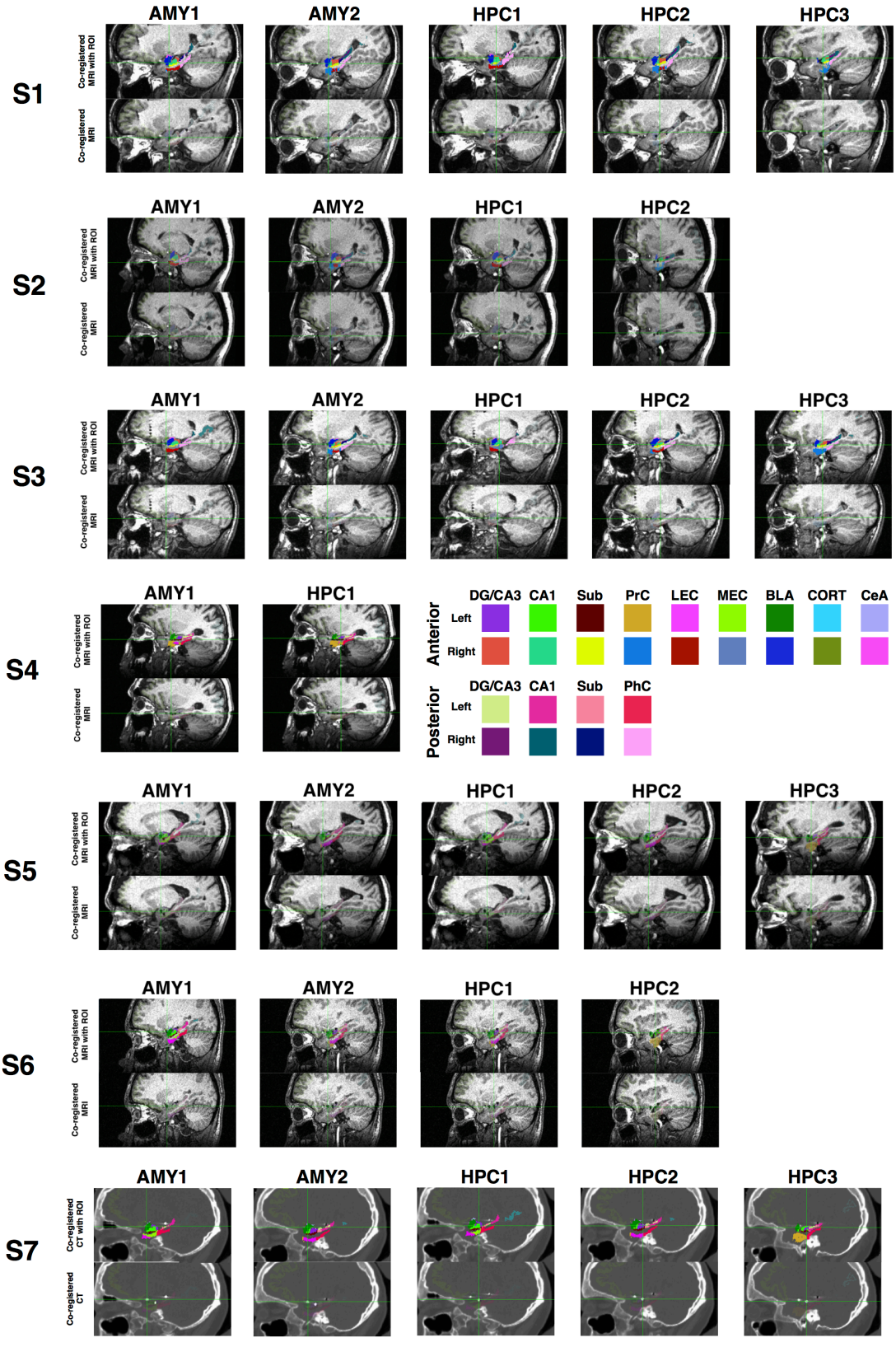
S1
AMY1
AMY2
HPC1
HPC2
HPC3
Co-registered MRI with ROI
Co-registered MRI
S2
AMY1
AMY2
HPC1
HPC2
Co-registered MRI with ROI
Co-registered MRI
S3
AMY1
AMY2
HPC1
HPC2
HPC3
Co-registered MRI with ROI
Co-registered MRI
S4
AMY1
HPC1
Co-registered MRI with ROI
Co-registered MRI
Anterior
DG/CA3 CA1 Sub PrC LEC MEC BLA CORT CeA
Left
Right
Posterior
DG/CA3 CA1 Sub PhC
Left
Right
S5
AMY1
AMY2
HPC1
HPC2
HPC3
Co-registered MRI with ROI
Co-registered MRI
S6
AMY1
AMY2
HPC1
HPC2
Co-registered MRI with ROI
Co-registered MRI
S7
AMY1
AMY2
HPC1
HPC2
HPC3
Co-registered CT with ROI
Co-registered CT

Supplementary Fig 1. Localizations of electrodes within the amygdala (AMY) and hippocampus (HPC) for all seven subjects. Post-implantation MRI (Subject 1-6) or CT (Subject 7) aligned using rigid body alignment to the pre-implantation MRI (lower panel for each subject). Translucent registered regions of interests (ROIs) were overlaid on the post-to-pre aligned MRI or CT (upper panel for each subject), including the dentate gyrus/CA3 (DG/CA3), CA1, subiculum (Sub), paraphippocampal cortex (PrC), lateral entorhinal cortex (LEC), medial entorhinal cortex (MEC), basolateral amygdala (BLA), corticosterone (CORT) and central nucleus of the amygdala (CeA). Cross hairs are centered on the electrode within the amygdala and the hippocampus.

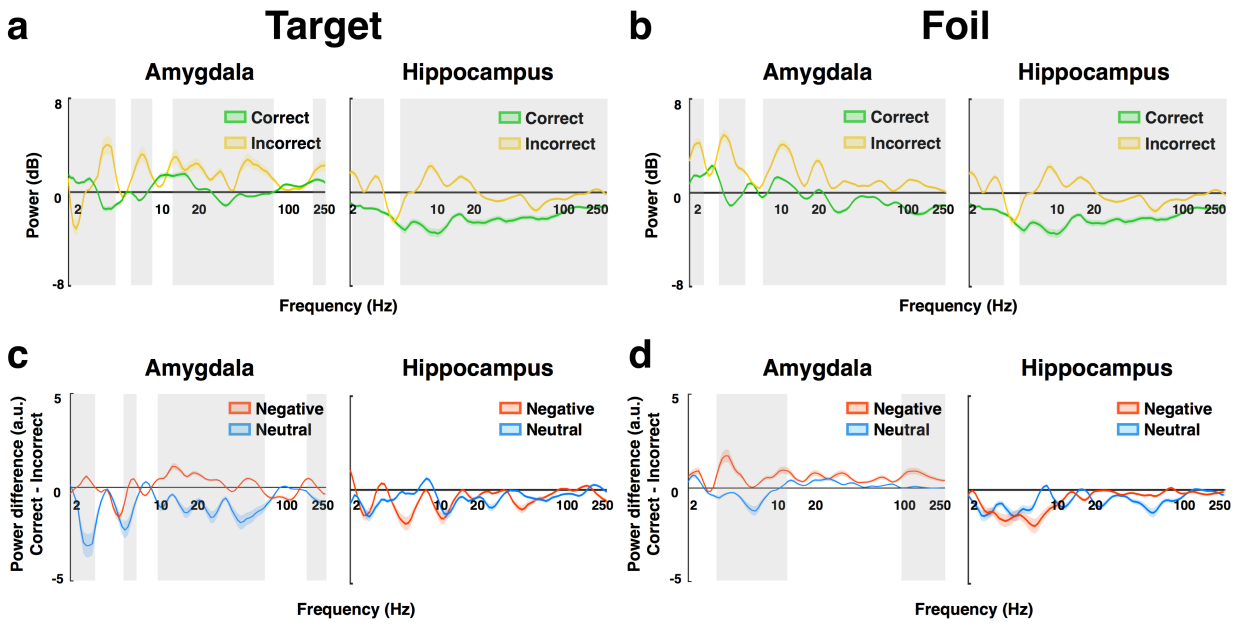

Supplementary Fig 2. Averaged power across all subjects within target and foil trials. Within the target **(a)** and the foil **(b)** condition, frequency-specific power differences were nearly absent in both the amygdala (left) and the hippocampus (right). Instead, power increases within the broader frequency range for incorrect trials compared to the correct ones has been shown in the amygdala as well as the hippocampus. (yellow lines: correct discriminations; green lines: incorrect discriminations. Color shaded area = ± s.e.m.). Gray shaded rectangles refer to significant conditional differences between correct and incorrect discrimination (t-test, $P < 0.01$). In addition, within the target **(c)** and the foil **(d)** conditions, no significant power differences (t-test, $P > 0.05$) (correct - incorrect) has been shown in the hippocampus when comparing between negative and neutral trials while the amygdala demonstrates the significant conditional difference (correct – incorrect, t-test, $P < 0.01$) at a broad frequency range. (blue lines: neutral trials; red lines: negative trials. Color shaded area = ±s.e.m.). Gray shaded rectangles represent significant conditional differences between negative and neutral trials (t-test, $P < 0.01$)

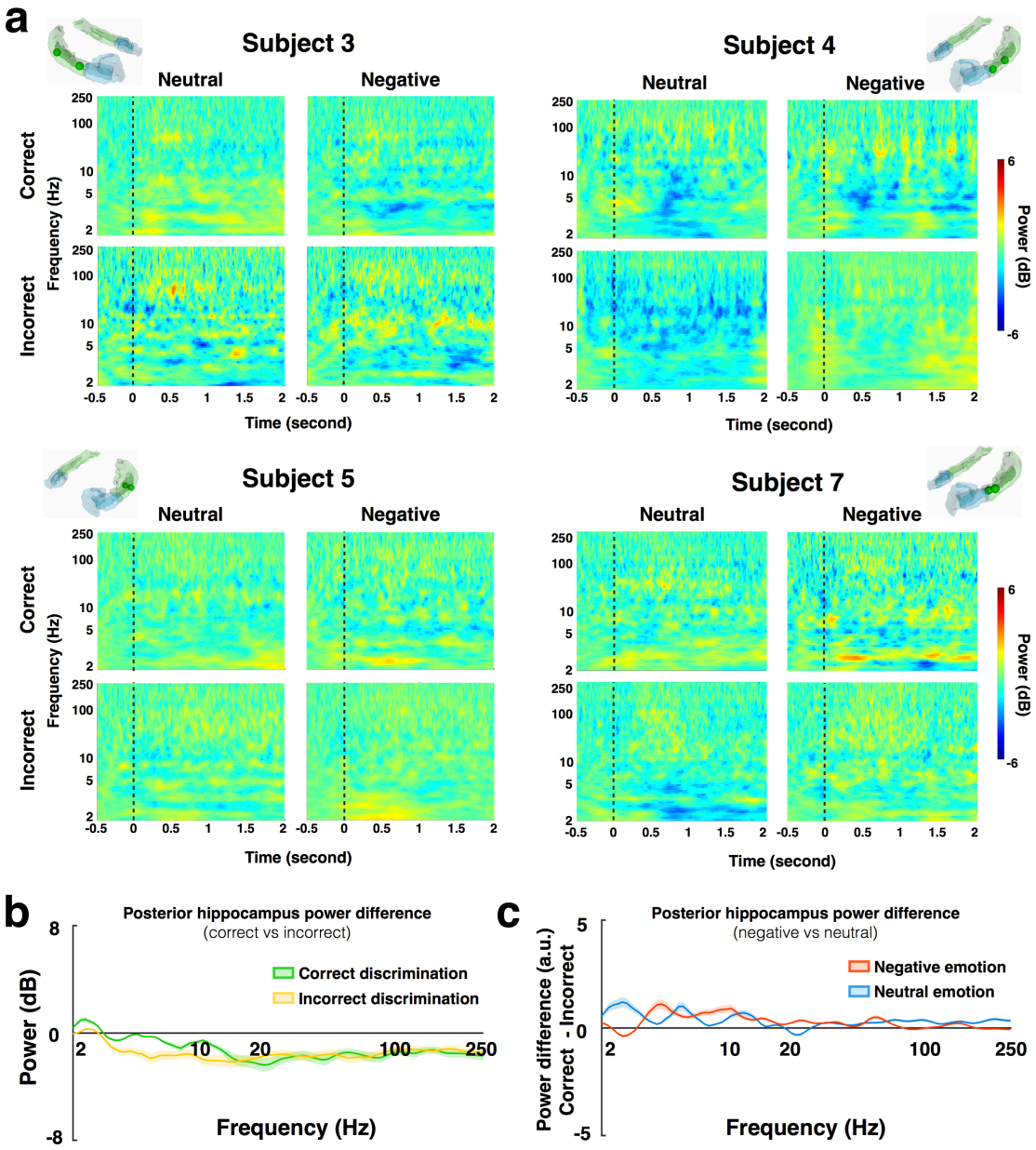

Supplementary Fig 3. Task-evoked spectrotemporal power in posterior hippocampus during emotional mnemonic discrimination. 4/7 subjects have electrodes implanted in the posterior hippocampus. **(a)** Task-induced power from 4 subjects with posterior hippocampus electrodes, normalized to the common pre-trial baseline (500-ms fixation period) and grouped based on task outcomes (correct discrimination: upper row; incorrect discrimination: lower row) and emotional valences (neutral: left column; negative: right column). Warmer colors denote task-induced power increase from the baseline while the colder colors refer to power decrease from

the baseline. Dashed black lines indicate the stimuli onsets. **(b)** Averaged power across these four subjects for correct (green) and incorrect (yellow) discriminations (color shaded area = ±s.e.m.). Positive/negative values indicate power increase/decrease from the baseline, respectively. **(c)** Averaged conditional power difference (correct– incorrect) across these four subjects for neutral (blue) and negative (red) trials (color shaded area = ±s.e.m.). Positive/negative values indicate stronger power for correct/incorrect discriminations, respectively. The 3d rendering hippocampus plots (blue: anterior hippocampus; green: posterior hippocampus) demonstrate each subject's posterior electrode locations.

APPENDIX C: Supplementary Materials for Chapter 4

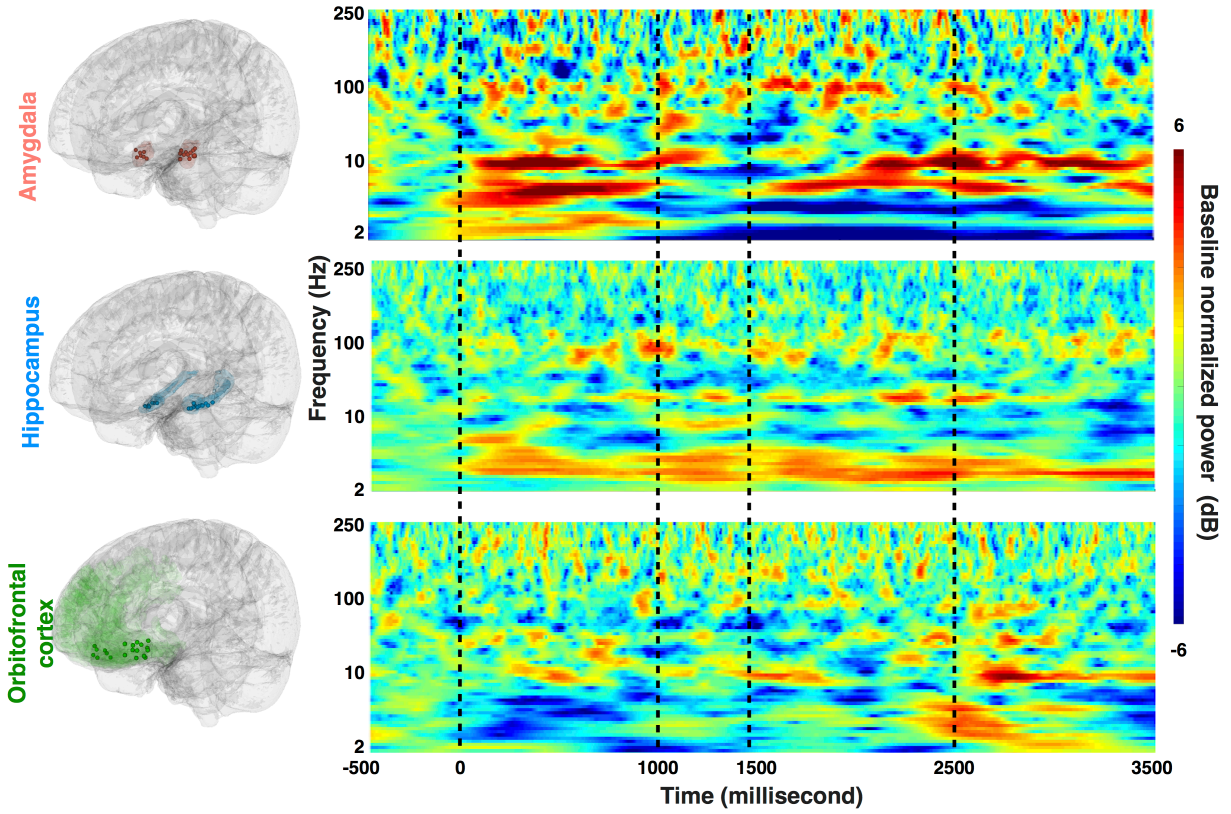

Supplementary Fig 1. Task-evoked spectrotemporal power in the amygdala, hippocampus and orbitofrontal cortex. Task-induced power normalized to the common pre-trial baseline (500-ms fixation period) and grouped based on region of interests, including the amygdala (upper panel), the hippocampus (middle panel), and the orbitofrontal cortex (lower panel). Warmer colors denote task-induced power increase from the baseline while the colder colors refer to power decrease from the baseline. Dashed black lines indicate the onsets of different task stages (context, delay, face, rate).

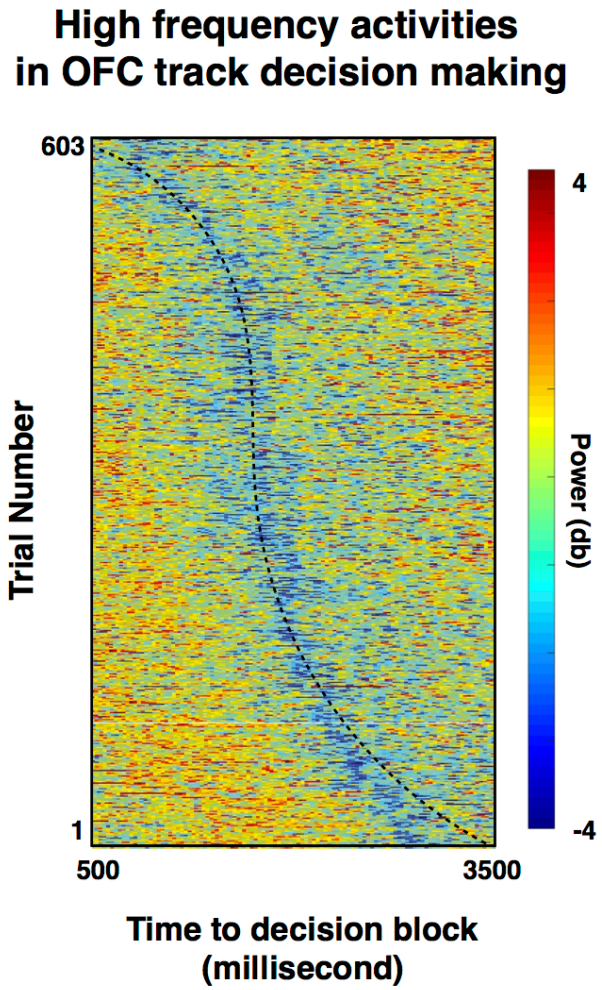

Supplementary Fig 2. Persistent high gamma activities from the orbitofrontal cortex during the rate period. The time courses of high gamma power from the orbitofrontal cortex for all the trials were stacked and sorted relative to subjects' response time. The dashed curve denotes subjects' response time (top to bottom: fast to slow response), the period on the right side of the dashed curve indicates the start of the following trial.

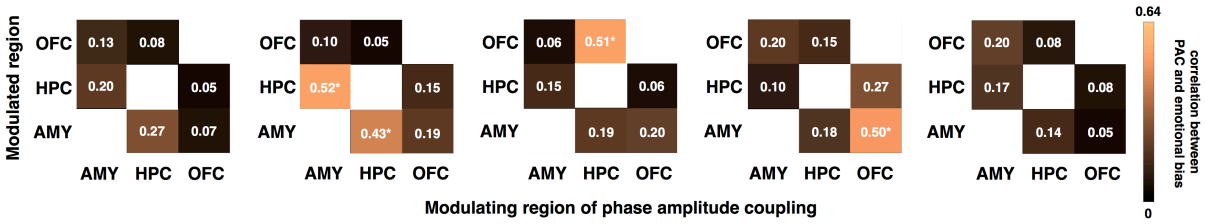

Supplementary Fig 3. Phase amplitude coupling and emotional ratings. The correlation matrix between the inter-regional phase amplitude coupling value and the contextual modulation strength for each electrode pair during five stages of the task (From left to right: Baseline, Context, Delay, Face, Rate).

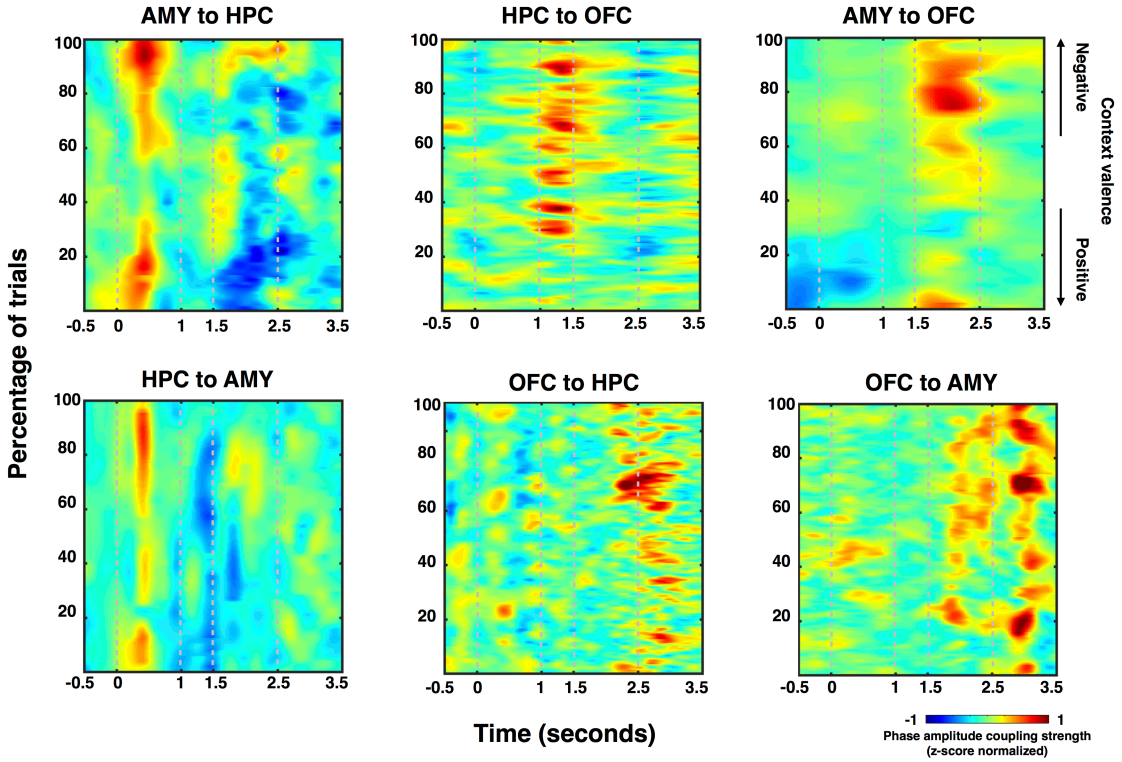

Supplementary Fig 4. Single trial stacked phase amplitude coupling corresponding. The time courses of time-resolved phase amplitude coupling from different electrode pairs were stacked trial-by-trial and sorted relative to the emotional valence of context images (top to bottom: Negative to Neutral to Positive). The dashed curve indicates different stages of the task (Baseline, Context, Delay, Face, Rate).